INFORMATION TO USERS

This manuscript has been reproduced from the microfilm master. UMI films the text directly from the original or copy submitted. Thus, some thesis and dissertation copies are in typewriter face, while others may be from any type of computer printer.

The quality of this reproduction is dependent upon the quality of the copy submitted. Broken or indistinct print, colored or poor quality illustrations and photographs, print bleedthrough, substandard margins, and improper alignment can adversely affect reproduction.

In the unlikely event that the author did not send UMI a complete manuscript and there are missing pages, these will be noted. Also, if unauthorized copyright material had to be removed, a note will indicate the deletion.

Oversize materials (e.g., maps, drawings, charts) are reproduced by sectioning the original, beginning at the upper left-hand corner and continuing from left to right in equal sections with small overlaps.

ProQuest Information and Learning
300 North Zeeb Road, Ann Arbor, MI 48106-1346 USA
800-521-0600

Université d'Ottawa • University of Ottawa

An AC Impedance Spectroscopy Study of the Freezing-Thawing Durability of Wollastonite Micro-Fibre Reinforced Cement Paste

by

Taijiro Sato

A thesis
Presented to the University of Ottawa
in partial fulfilment of the
requirements of the degree of
Master of Applied Science
in
Civil Engineering

Department of Civil Engineering
University of Ottawa
Ottawa, Canada
K1N 6N5

November, 2002

The M.A.Sc. in Civil Engineering is a joint program
with Carleton University administrated
by the Ottawa-Carleton Institute for Civil Engineering

This thesis is dedicated to my parents.

ACKNOWLEDGEMENTS

My special gratitude is deeply expressed to my supervisor, Dr. J.J. Beaudoin, Principal Research Officer at the Institute for Research in Construction, National Research Council Canada and Adjunct Professor at the Department of Civil Engineering, University of Ottawa, for his continuous advice and support on all aspects of this research.

The author would also like to thank Messrs. Gordon Chan, Jim Margeson, Bob Myers and Gary Polomark for their technical support with the laboratory work and analysis.

My appreciation also belongs to Dr. Lyndon D. Mitchell, Research Associate, at the Institute for Research in Construction, National Research Council Canada, for his helpful discussions in the course of this work.

ABSTRACT

The AC impedance spectroscopy (ACIS) is an electrochemical technique used to characterize materials in various research fields owing to its non-destructive nature. The ACIS, accordingly, appears to have a potential as a non-destructive technique to investigate the durability of cement paste. An understanding of the mechanism of frost action occurring within cement paste, a key binding component of concrete, is necessary to improve the durability of concrete with respect to freezing and thawing, particularly where the winter is severe. In addition, the research on the effectiveness of the wollastonite micro-fibres, a cost-effective naturally occurring calcium silicate, as a reinforcing material to improve the durability of cement paste is demanded due to worldwide concerns of material shortages.

Three primary objectives in this study are to further the understanding of the mechanism of frost action within cement paste subjected to freezing and thawing, to investigate the potential of the ACIS as a new technique to determine the durability of cement paste with respect to freezing and thawing and to investigate the durability of the wollastonite micro-fibre reinforced cement paste to freezing and thawing.

The ACIS elucidated and provided the further understanding of the complex microstructural behaviour and mechanism of frost action within cement paste subjected to freezing and thawing, including the difference in freezing mechanism of water in the capillary and gel pores. The investigation of the potential of the ACIS as a durability indicator was also accomplished. A comparison between the ACIS and the length change measurement of cement paste subjected to freezing and thawing ensured the effectiveness of the ACIS as a possible technique to determine the durability. Finally, the improvement of the durability of the wollastonite micro-fibre reinforced cement paste to freezing and thawing was acknowledged in some conditions. The cement paste specimens containing 10.2% wollastonite micro-fibre content by volume were more durable than those without wollastonite micro-fibre content, particularly for the higher w/c ratio.

CONTENTS

LIST OF TABLES

LIST OF FIGURES

GLOSSARY

C	capacitance, Farad
C_d	total capacitance of solid-liquid interface, Farad
C_{el}	capacitance of cement-electrode interface, Farad
C_f	capacitance of solid-liquid interface for one element, Farad
C_h	heat capacity, J/°C
c	specific heat capacity, J/°C/g
c_A	apparent specific heat capacity, J/°C/g
d	distance between two conductors, m
I	current, A
I_m	amplitude of current, A
i	current at time t, A
j	$\sqrt{-1}$
L	inductance, Henry
M	molecular weight of water, g/mole
m	mass of substance, g
N	number of elements
n	depression angle parameter
Q	electric charge, Coulomb
Q_h	molar heat of fusion, cal/mole
q	heat, J
q_p	heat required for phase transition per unit mass of substance, J/g
R	resistance, Ω
RH	relative humidity, %
R_L	resistance of liquid for one element, Ω
R_S	resistance of solid for one element, Ω
R_{el}	resistance of cement-electrode interface, Ω
R_f	resistance of solid-liquid interface for one element, Ω
R_g	gas constant, cal/mole °C
R_f	resistance at completion of freezing of water, Ω
R_i	resistance at beginning of freezing of water, Ω
R_1	total resistance of liquid, Ω
R_2	total resistance of solid-liquid interface, Ω
r_s	pore radius, Å
S	area of conductor, m^2
T	period, s
T_H	crystallization temperature of water
T_m	melting temperature of water
T_r	fusion temperature of ice crystal, °K
T_C	temperature of cement paste, °C
T_S	273 °K
t	time, s
V_C	voltage across the capacitor, V
V_L	voltage across the inductor, V
V_R	voltage across the resistor, V
V_m	amplitude of voltage, V
v	voltage at time t, V

v_i	velocity of ice crystal growth, cm/s
w_f	the actual amount of water frozen during the phase transition, $g_{water}/g_{substance}$
w_{f+40}	the actual amount of water frozen above –40°C per unit mass of substance, $g_{water}/g_{substance}$
w_{f-40}	the actual amount of water frozen below –40°C per unit mass of substance, $g_{water}/g_{substance}$
w_t	the actual amount of water thawed per unit mass of cement paste specimen, $g_{water}/g_{substance}$
Z	impedance, Ω
Z_m	amplitude of impedance, Ω
Z_1	total impedance of parallel of Rs and R_L, Ω
Z_2	total impedance of parallel of Rf and Cf, Ω
Z'	real part of impedance
Z"	imaginary part of impedance
ΔH_f	heat of fusion of water, 344.8 J/g
ΔT	temperature change, °C
ΔT_s	total supercooling, °C
ε	permittivity, Farad/m
θ	phase shift, radians
λ_R	resistance ratio
ρ_w	density of water, g/cm³
ρ_i	density of ice, g/cm³
σ_{iw}	interfacial energy between ice and water, dynes/cm
σ_{aw}	interfacial energy between air and water , dynes/cm
Φ	magnetic flux, Weber
ϕ_{dep}	depression angle, radians
ω	angular frequency, rad/s

Abbreviations

AC	alternating current
ACIS	AC impedance spectroscopy
CPE	Constant Phase Element
C-S-H	calcium silicate hydrate
DC	direct current
DSC	differential scanning calorimetry
TMA	thermomechanical analysis
C	CaO / calcium oxide (Lime)
A	Al_2O_3 / aluminum oxide (Alumina)
S	SiO_2 / silicon dioxide (Silica)
F	Fe_2O_3 / iron oxide (III)
M	MgO / magnesium oxide
H	H_2O / hydrogen oxide (Water)
N	Na_2O / sodium monoxide
K	K_2O / potassium monoxide

CHAPTER 1

INTRODUCTION AND OBJECTIVES

1.1 Introduction

It is desirable that every concrete structure withstand the damaging effects of the environment for an expected period of time. This is often referred to as the durability of concrete. Durable concrete maintains its quality and ensures the serviceability of the structure when it is exposed to the environment. Inadequate durability can lead to costly maintenance and rehabilitation of the whole structure. In countries such as Canada where the winter is severe, the freezing and thawing process can become one of the most critical problems regarding the durability of concrete. An understanding of the mechanism of frost action occurring within cement paste, a key binding component of concrete, is necessary to improve its durability with respect to freezing and thawing. The addition of micro-fibres to cement binders as reinforcing materials has been the subject of intensive research to improve the durability of cement paste. The use of the wollastonite micro-fibres, a naturally occurring calcium silicate, is of special interest particularly where a material shortage is an issue.

Even though there has been considerable research on this subject, the mechanism of frost action within cement paste is still not completely understood as it involves various phenomena occurring simultaneously. Furthermore, the current standard procedure for examining the durability of concrete with respect to freezing and thawing is a destructive method based on the limited conditions.

The AC impedance spectroscopy (ACIS) is an electrochemical technique used to characterize materials in various research fields owing to its non-destructive nature. The ACIS, accordingly, appears to have a potential as a non-destructive technique for investigating the durability of cement paste. The ACIS measures the response of current flow to an applied sinusoidal voltage perturbation as a function of frequency and provides valuable information that reflects the changes in the system due to freezing and thawing. The changes in electrical resistance of the porous materials and the nature of the solid-liquid interface in these materials are of particular interest and value.

This thesis extends the work on the ACIS initiated at the National Research Council Canada. It will discuss and demonstrate the potential of the ACIS as a new technique to investigate the durability of cement paste with respect to freezing and thawing. It will also discuss the interpretation of the microstructural behaviour and mechanism of frost action within cement paste subjected to freezing and thawing. Finally, the thesis will present the assessment of the durability of the wollastonite micro-fibre reinforced cement paste to freezing and thawing.

1.2 Overall Objectives

The three overall objectives of this thesis are as follows;

1. To further the understanding of the microstructural behaviour and mechanism of frost action within cement paste subjected to freezing and thawing
2. To investigate and demonstrate the potential of the ACIS as a new technique for determining the durability of cement paste subjected to freezing and thawing
3. To determine the durability of the wollastonite micro-fibre reinforced cement paste to freezing and thawing

1.3 Experimental Methodology

1.3.1 The Coupled ACIS-TMA Experiment

In order to investigate the potential of the ACIS and its use as a possible technique to determine the durability of cement paste to freezing and thawing, the ACIS was coupled with the Thermomechanical Analysis (TMA). The TMA measures the length change of a test specimen for the desired temperature variation of a freezing and thawing cycle and provides information that is often used as a durability indicator with respect to freezing and thawing. A comparison of the ACIS measurement with the TMA measurement provides an effectiveness of the ACIS technique as a durability indicator. A schematic description of the coupled ACIS-TMA experiment is illustrated in Fig. 1.1.

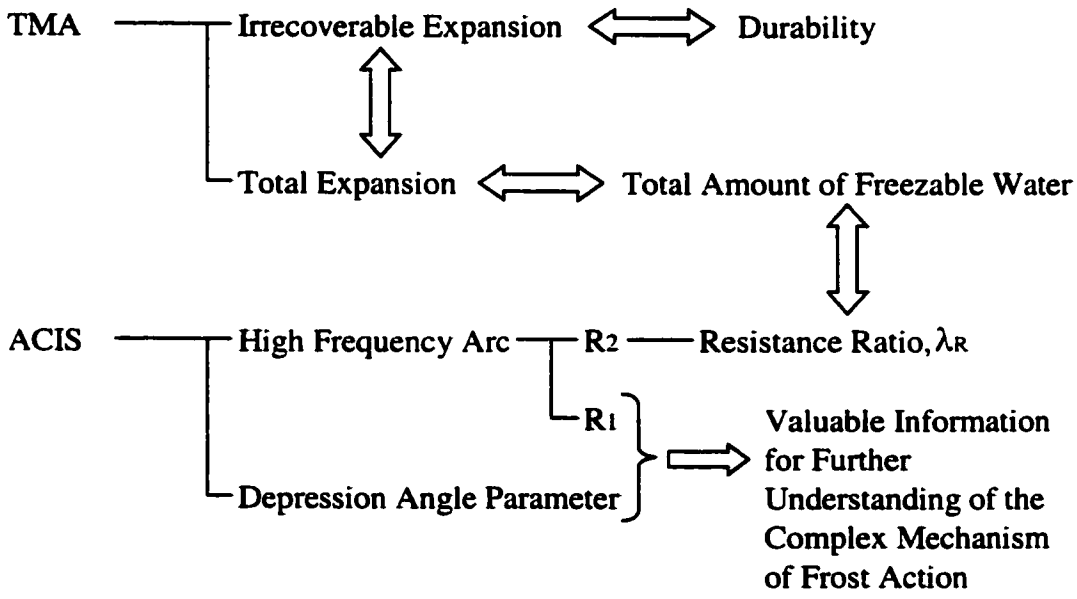

Fig. 1.1 A schematic description of the coupled ACIS-TMA experiment

The main goal of this coupled ACIS-TMA experiment is, as shown in Fig. 1.1, to link the "resistance ratio, λ_R" obtained from the ACIS measurement to the "irrecoverable expansion" obtained from the TMA measurement. This procedure provides a basis for estimating the effectiveness of the ACIS as a durability indicator. Then, the durability of the wollastonite micro-fibre reinforced cement paste to freezing and thawing was investigated using the coupled ACIS-TMA experiment. The specific objectives of the coupled ACIS-TMA experiment are as follows;

1. To investigate the relationship between the total and irrecoverable expansion, both obtained from the TMA measurement, and the durability of cement paste
2. To determine the dependence of the "resistance ratio, λ_R" obtained from the ACIS measurement with the total and irrecoverable expansion obtained from the TMA measurement
3. To further the understanding of the microstructural behaviour and mechanism of frost action within cement paste subjected to freezing and thawing through the use of the coupled ACIS-TMA experiment
4. To investigate the durability of the wollastonite micro-fibre reinforced cement paste to freezing and thawing

1.3.2 The DSC Experiment

The Differential Scanning Calorimetry (DSC) experiment was conducted to support the interpretation of phenomena observed in the coupled ACIS-TMA experiment. A heat flow of a cement paste specimen subjected to a freezing and thawing cycle measured by the DSC experiment provides valuable information on its microstructural phenomena and mechanism of frost action. The specific objectives of the DSC experiment are as follows;

1. To provide the further understanding on the microstructural phenomena and mechanism of frost action within cement paste subjected to a freezing and thawing cycle
2. To support the interpretation of phenomena observed in the coupled ACIS-TMA measurement

CHAPTER 2

BACKGROUND AND LITERATURE REVIEW

2.1 Portland Cement

2.1.1 Chemical Composition of Portland Cement

Portland cement is defined as, "a hydraulic cement produced by pulverizing clinker consisting essentially of hydraulic calcium silicates, usually containing one or more of the forms of calcium sulphate as an interground addition." (ASTM C150). Raw materials used in the manufacture of Portland cement consist mainly of four oxides: lime (CaO), silica (SiO_2), alumina (Al_2O_3) and iron oxide (Fe_2O_3). Mixtures of these oxides react with each other in a kiln, resulting in the formation of four primary compounds often regarded as the major constituents of Portland cement. They are listed in Table 2.1 with their chemical formulae and abbreviations.

Table 2.1 Main compounds of Portland cement

Constituent	Chemical Formula	Abbreviation
Tricalcium silicate	$3CaO \cdot SiO_2$	C_3S
Dicalcium silicate	$2CaO \cdot SiO_2$	C_2S
Tricalcium aluminate	$3CaO \cdot Al_2O_3$	C_3A
Tetracalcium aluminoferrite	$4CaO \cdot Al_2O_3 \cdot Fe_2O_3$	C_4AF

These four compounds account for approximately 90% of the cement mass. Gypsum (4% to 6%) and other minor compounds make up the remainder. The chemical composition of the four major

compounds present in the industrial Portland cement, however, is not exactly identical to that shown in Table 2.1. All four contain a small amount of other oxides such as MgO, Na_2O and K_2O as impurities.

2.1.2 Hydration of Portland Cement

The hydration of cement involves a number of chemical reactions that occur instantaneously and continue over a long period. Each of four main compounds, C_3S, C_2S, C_3A and C_4AF has a different reaction and function with respect to the hydration process.

2.1.2.1 C_3S and C_2S

The hydration of the calcium silicates, C_3S and C_2S, results in the formation of a calcium silicate hydrate ($3CaO \cdot SiO_2 \cdot 3H_2O$). In general, it is assumed that the approximate composition is $C_3S_2H_3$ upon the complete of hydration. It is often referred to simply as C-S-H, because the chemical composition of the calcium silicate hydrate varies widely with factors such as age, temperature and water/cement ratio. It should be noted that the notation, C-S-H, itself does not imply any particular composition or structure. The reactions of the hydration of C_3S and C_2S may be expressed approximately by the following equations. For tricalcium silicate, C_3S,

$$2(3CaO \cdot SiO_2) + 6H_2O \rightarrow 3CaO \cdot SiO_2 \cdot 3H_2O + 3Ca(OH)_2 \qquad (2.1)$$

For dicalcium silicate, C_2S,

$$2(2CaO \cdot SiO_2) + 4H_2O \rightarrow 3CaO \cdot SiO_2 \cdot 3H_2O + Ca(OH)_2 \qquad (2.2)$$

The resulting hydrate, in general, is poorly crystalline and produces a porous solid that is considered as a rigid gel.

The properties of C_3S are similar to those of Portland cement. The initial setting takes place within a few hours after the addition of water and the paste hardens rapidly. Generally, the early

strength of Portland cement is greater with an increase in the percentage of C_3S. The C_2S component, however, gains compressive strength slowly and gradually for several months. Its ultimate strength is similar to that of C_3S.

2.1.2.2 C_3A

The hydration of tricalcium aluminate, C_3A is almost instantaneous and can lead to immediate setting and stiffening of the paste, known as flash set. The immediate setting may reduce the workability of concrete mix for most construction purposes. Gypsum, $CaSO_4 \cdot 2H_2O$ is added to prevent this and to delay its setting time. The immediate reaction between C_3A and gypsum produces needle-like crystals of a high-sulphate calcium sulphoaluminate, $3CaO \cdot Al_2O_3 \cdot 3CaSO_4 \cdot 31H_2O$, referred to as ettringite. The formation of an ettringite layer on the surface of tricalcium aluminate results in a delaying effect of the immediate setting. The hydration of the calcium silicates becomes the dominant influence on the setting of cement. Ettringite continues to form while the sulphate ions are present in the solution. This generally occurs in the first 24 hours after the addition of water. Once the sulphate ions are removed, further reaction of C_3A with water converts the ettringite to the low-sulphate calcium sulphoaluminate, $3CaO \cdot Al_2O_3 \cdot CaSO_4 \cdot 12H_2O$, referred to as monosulphate.

2.1.2.3 C_4AF

C_4AF reacts with gypsum and $Ca(OH)_2$ to produce needle-like crystals of a solid solution consisting of high-sulphate sulphoaluminate and sulphoferrite phase. The hydrates fill the spaces between cement particles. A schematic description of the hydration process with respect to time is shown in Fig. 2.1 (Soroka, 1979).

A dormant period, caused by the formation of a thin layer of ettringite on the C_3A, lasts about one or two hours. Hydration products in this period are mainly $Ca(OH)_2$ and ettringite. At the end of the dormant period, the C-S-H gel starts to form and fill in the spaces. As the volume of solids increases, the porosity of the paste decreases as shown by the dotted line at the top of Fig. 2.1.

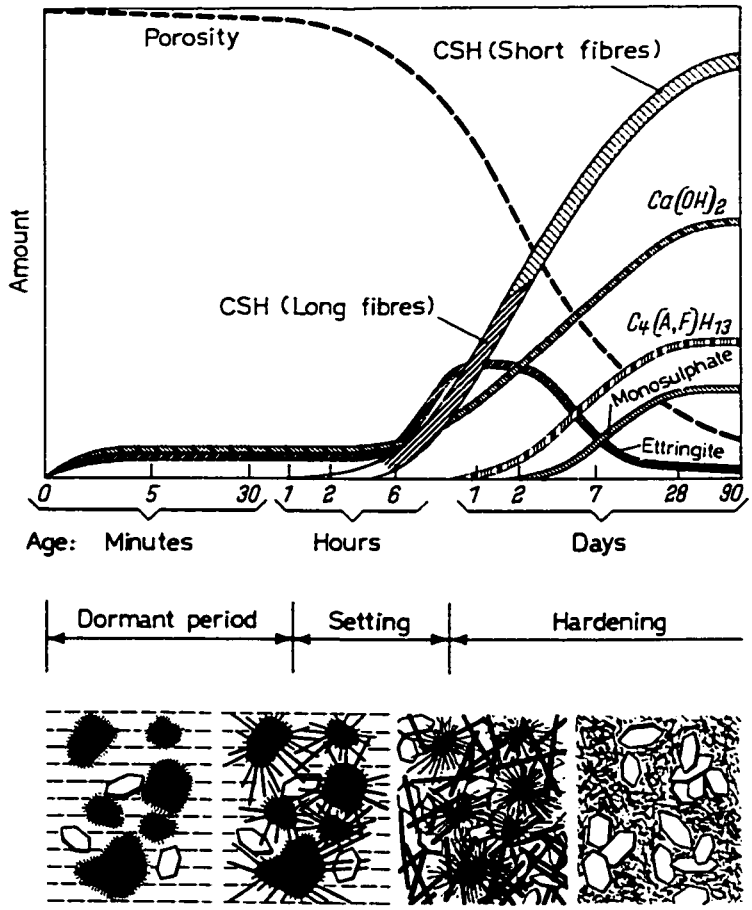

Fig. 2.1 *A schematic description of the hydration and structure development of cement paste*

2.1.3 Pore Structure of Hydrated Portland Cement Paste

2.1.3.1 Capillary and Gel Pores

Properties of hydrated cement paste are often determined by its physical structure rather than its chemical composition. Fresh cement paste is a plastic network of small gel particles which are mainly hydrates of the calcium silicate with some aluminates and ferrites. There are water-filled spaces between those particles called capillary pores and the water in the capillary pores is called capillary water. There exists water-filled spaces in the gel itself, called gel pores and the water in the gel pores is called gel water. Figure 2.2 shows the simplified diagram of paste structure with both capillary and gel pores (Powers, 1958). Solid dots represent gel particles; interstitial spaces are gel pores; spaces marked with "C" are capillary pores. The size of gel pores is not to scale.

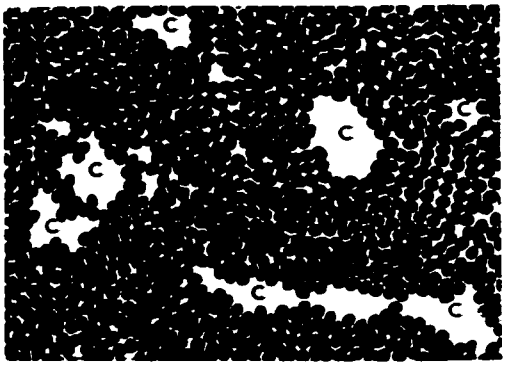

Fig. 2.2 Simplified diagram of paste structure with capillary and gel pores

The size of gel pores is approximately 1 nm to 10 nm and that of capillary pores is 10 nm to 100 nm. The gel pores are formed interstitially because of the colloidal characteristic of the C-S-H gel particles. The capillary pores are the remnants of the original water-filled spaces that have not become filled with gel. Therefore, capillary porosity decreases as the hydration takes place. The capillary porosity, at any stage of hydration, depends on the proportion of water to the amount of unhydrated cement.

2.1.3.2 State of Water in Hydrated Cement Paste

Water exists in cement paste in various forms. Four different types of water present in cement paste have been described (Neville, 1995). These can be grouped into two categories, evaporable water and non-evaporable water as shown in Fig. 2.3.

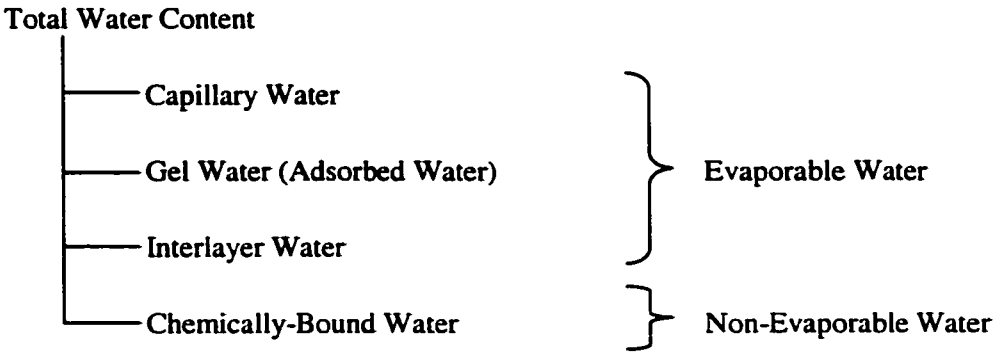

Fig. 2.3 Different types of water present in cement paste

The evaporable water is defined as the water which evaporates upon drying at a temperature of 105°C. Evaporable water includes capillary water, adsorbed water and interlayer water. Capillary water is free water which is present in capillary pores where the surface forces associated with the gel particles of the paste does not interfere. Gel water, on the other hand, is the water held by the surface forces of the gel particles since the gel pores are small. It is sometimes referred to as adsorbed water. Interlayer water, introduced by Feldman and Sereda (1968), is the water held in the layered structure of the C-S-H gel particles. Figure 2.4 diagrammatically shows how water is physically adsorbed and intercalated between the layers of the C-S-H gel particles.

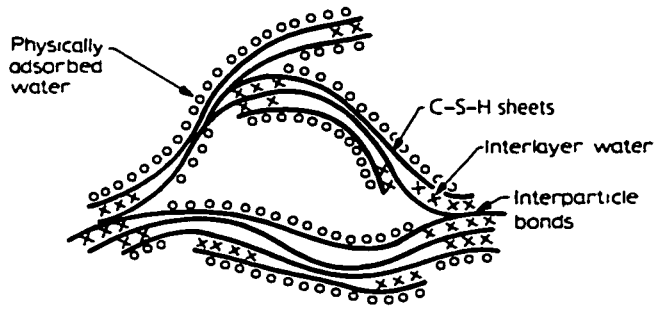

Fig. 2.4 Microstructure of the C-S-H gel particles

The non-evaporable water is the water which can be removed by drying over a very high temperature range, usually from 105°C to 1050°C. The non-evaporable water in cement paste is considered to be the chemically-bound water. The chemically-bound water is the water which is chemically combined in the hydrated cement compounds. The amount of non-evaporable water, therefore, increases as hydration proceeds.

2.2 Wollastonite Micro-Fibres and Micro-Fibre Reinforced Cement Paste

2.2.1 Introduction

The study of micro-fibre reinforced cement paste has been intensified in recent years, owing to the dramatic improvement of the brittle behaviour and relatively low tensile strength of concrete.

Fibres added to concrete provide a means of arresting the crack growth and increasing the tensile strength (Beaudoin, 1982). Reinforcing materials are often made of steel, glass and polymer. However, because of worldwide concerns of energy and material shortages, the use of natural and mineral fibre reinforcing materials has been the subject of intensive research. The potential of wollastonite micro-fibres, a naturally occurring calcium silicate, has therefore attracted the attention as an effective reinforcement in a Portland cement-based matrix. The use of wollastonite micro-fibres has been also studied as a primary replacement of asbestos in fibre reinforced concrete. The hazardous characteristics of asbestos have been a worldwide concern.

2.2.2 Mineral Characteristics of Wollastonite

Wollastonite is a naturally occurring calcium silicate, $CaO \cdot SiO_2$, and is generally available in the shape of acicular particles of mixed particle size for commercial applications. A Scanning Electron Microscope (SEM) photomicrograph of wollastonite micro-fibres is shown in Fig. 2.5. The transverse dimension of the individual particle can vary from about 10 to 100 μm and the length can vary from about 0.05 mm to 2.0 mm (Low and Beaudoin, 1993). It forms from the interaction of limestone that contains calcite, $CaCO_3$, and silica, SiO_2, at a high temperature, usually in hot magmas. The reaction can be expressed as follows:

$$\underset{\text{Silica}}{SiO_2} + \underset{\text{Calcite}}{CaCO_3} \Rightarrow \underset{\text{Wollastonite}}{CaO \cdot SiO_2} + \underset{\text{Carbon Dioxide}}{CO_2} \qquad (2.3)$$

The density of wollastonite is 2840 kg/m³. Its temperature coefficient of linear expansion is 11.8×10^{-6} 1/°C. Wollastonite exists in two forms, β-$CaO \cdot SiO_2$ and α-$CaO \cdot SiO_2$. The β-$CaO \cdot SiO_2$ is wollastonite which occurs in nature. The mineral wollastonite is stable up to 1150°C. The α-$CaO \cdot SiO_2$ is a form of wollastonite which is stable between 1150°C and 1540°C and is termed pseudowollastonite. It does not occur in nature but has often been found in melts and slags. In this thesis, the term "wollastonite" refers to the mineral wollastonite, β-$CaO \cdot SiO_2$, unless otherwise noted.

The history of the industrial use of wollastonite micro-fibres is rather short. No appearance in the industrial market occurred until 1950. However, wollastonite made some impact on the industrial

market, when it was discovered that the addition of wollastonite micro-fibres improved the properties and increased the strength of a tile. Since then, research has been continuously carried out in the ceramic industry and other industries including plastics, asbestos products, metallurgy and paints. In 1999, the total amount of wollastonite utilized worldwide was estimated to be between 575,000 t and 625,000 t. The major deposits are located at New York and California, U.S.; Quebec, Canada; China; Mexico and Finland. The percentage of wollastonite use in various industries is as follows: plastics (37%), ceramics (28%), metallurgy (10%), paints (10%), friction products (9%) and miscellaneous (6%). (Virta, 1999).

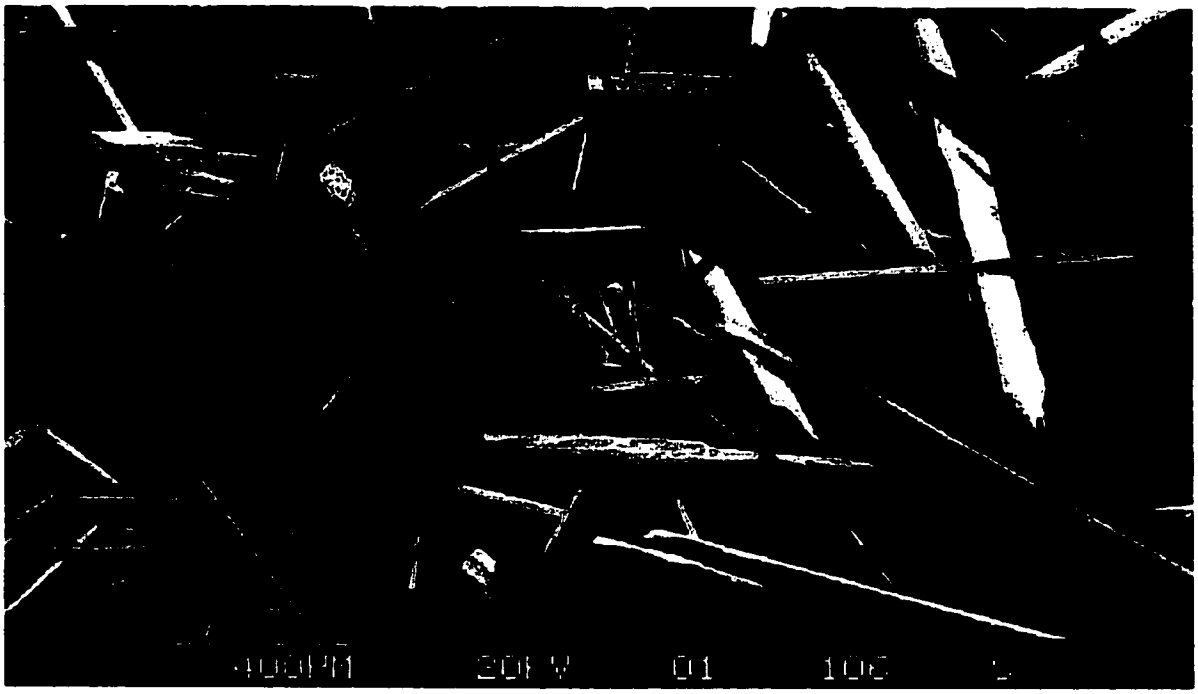

Fig .2.5 SEM photomicrograph of wollastonite micro-fibres

2.2.3 Wollastonite Micro-Fibre Reinforced Cement Paste and its Properties

In addition to addressing environmental concerns, the use of wollastonite micro-fibres as a reinforcing material in cement products may be more cost-effective than the use of steel or carbon fibres. Therefore, systematic investigations of the potential use of wollastonite micro-fibres as a reinforcing material have been conducted by Low and Beaudoin (1992, 1993 and 1994). The primary objective was to determine the effect of various factors affecting the properties of wollastonite micro-fibre reinforced cement paste.

2.2.3.1 Flexural Strength and Toughness

The flexural strength of wollastonite micro-fibre reinforced cement paste with various amounts of wollastonite and hydration periods was determined using a three-point loading method. Figure 2.6 shows the flexural strength versus the wollastonite content by volume (Low and Beaudoin, 1992). The flexural strength of the wollastonite micro-fibre reinforced cement paste was observed to vary from 10 MPa to 23 MPa based on the wollastonite content and the hydration period. The hydration period does not appear to significantly affect the flexural strength. A relatively linear increase in the flexural strength with wollastonite content, however, can be observed for levels of reinforcement between 2% and 11.5% by volume. A wollastonite content greater than 11.5% results in a slight reduction of flexural strength. This behaviour can be observed at any stage of hydration.

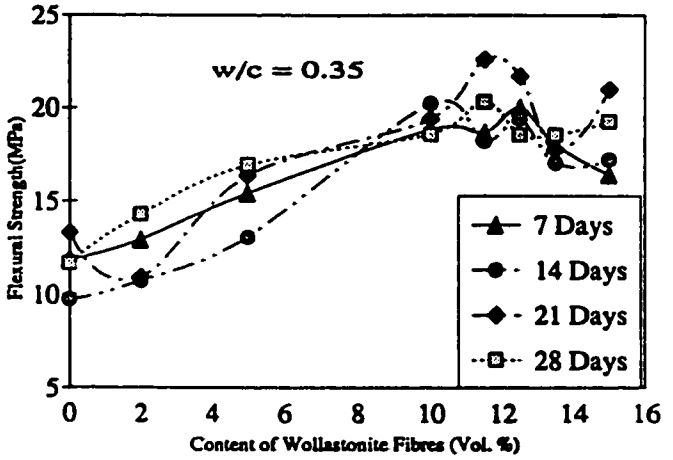

Fig. 2.6 Flexural strength of wollastonite micro-fibre reinforced cement pastes versus content of wollastonite micro-fibres

In addition to the flexural strength, one of the primary reasons to add fibres to concrete is to improve its energy-absorbing capacity, or its flexural toughness. Low and Beaudoin (1994) investigated the effect, on the flexural toughness, of wollastonite micro-fibre addition to cement paste with different contents of silica fume. The flexural toughness was estimated from the area under the load-deflection curve. The relative toughness, defined as the ratio of the toughness of the composites specimen to that of the basic matrix, is a meaningful index. Figure 2.7 is a plot of the relative toughness of the wollastonite micro-fibre reinforced cement pastes with silica fume. Although the effect of wollastonite micro-fibre reinforcement was significantly enhanced by the increase in silica fume content, the wollastonite micro-fibre addition to the plain cement paste itself increases its flexural toughness.

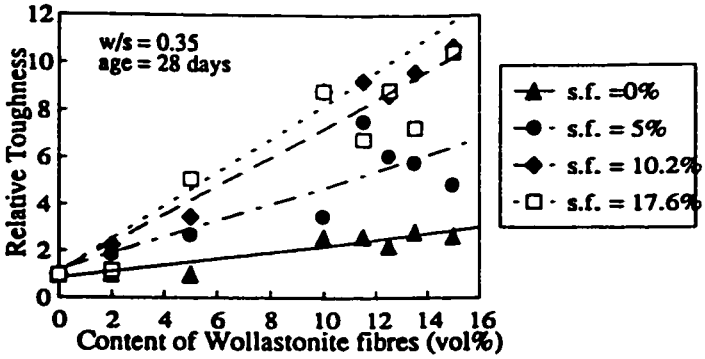

Fig. 2.7 Relative Toughness of wollastonite micro-fibre reinforced cement pastes versus wollastonite micro-fibre content

2.2.3.2 Porosity and Pore Size Distribution

Gu et al. (1993) characterized the porosity and pore size distribution of wollastonite micro-fibre reinforced cement paste by mercury intrusion porosimetry. Table 2.2 provides the total porosity values of cement pastes of w/c ratio 0.35 with different amounts of wollastonite micro-fibres hydrated for 1 day and 21 days. It is noted that the porosity of cement paste with 0% wollastonite is lower than that of all other wollastonite micro-fibre reinforced cement pastes for 1 day hydration. It is however higher for the 21 days hydration. Gu et al. (1993) argue that the transition zone at the interface contributes more significantly to porosity at early hydration times. The interface becomes dense at later ages. Its contribution to porosity is then much less significant.

Table 2.2. Total porosity of wollastonite micro-fibre reinforced cement pastes determined by mercury intrusion porosimetry

Hydration Period	Wollastonite Content: %			
	0	5	10	15
1 day	31.50%	32.48%	34.14%	33.32%
21 days	24.79%	22.81%	23.28%	22.21%

The pore size distribution of cement pastes hydrated for 21 days with different amounts of wollastonite micro-fibres is shown in Fig. 2.8. The addition of wollastonite micro-fibres does not affect the pore size distribution of cement paste significantly for the pore size range between 0.01 μm and 0.1 μm. However, it does affect the pore size distribution in the pore size range greater

than 0.1 μm. The cement paste with 15% wollastonite content seems to have higher percentage of pores greater than 0.1 μm, while the cement paste with no wollastonite content does not contain a high percentage of pores greater than 0.1 μm.

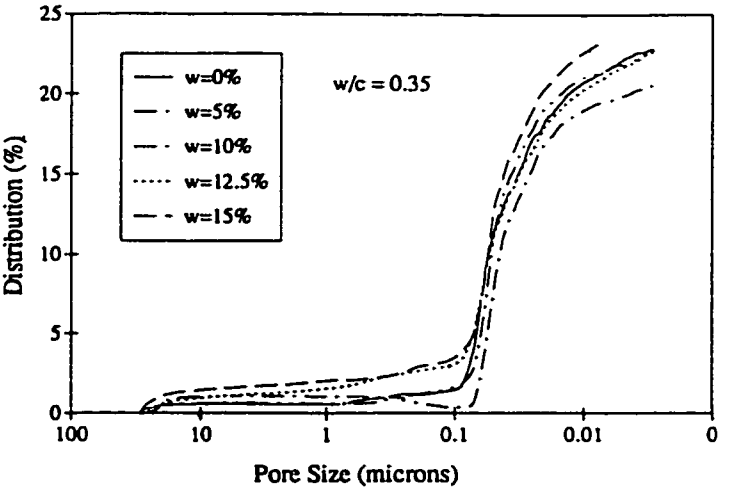

Fig. 2.8 Pore size distribution of wollastonite micro-fibre reinforced cement pastes

2.3 Frost Action

2.3.1 Introduction

Durability of cement paste exposed to different conditions has been studied extensively. It is of special interest for the Canadian construction. The resistivity of cement paste exposed to freezing and thawing conditions in cold climates is one of the major factors that determines the service-life of concrete. An understanding of the mechanism of frost action within cement paste is necessary to improve its durability under freezing and thawing conditions. However, it is still not completely understood as the complex mechanism of frost action involves various phenomena that occur simultaneously.

2.3.2 Mechanism of Frost Action

Water expands 9% in volume when it freezes. The water in the pores of cement paste also expands its volume when the cement paste is subjected to freezing. When the pressure associated with this volume expansion, known as a hydraulic pressure, exceeds the tensile strength of the cement paste, it creates the damage. This is the basic cause of freezing and thawing damage of cement paste. However, there are two phenomena which occur simultaneously and greatly affect the mechanism of frost action. These two phenomena are the depression of freezing and melting temperature of pore water and the migration of water within cement paste during the freezing and thawing.

2.3.2.1 Depression of Freezing and Melting Temperature

Pure water freezes at 0°C at 1 atmospheric pressure and melts at the same temperature. However, the water in a porous material, such as cement paste, does not freeze at a normal freezing temperature, but remains as a supercooled water until the nucleation of ice initiates at a much lower temperature. This depression of freezing temperature of the pore water becomes greater as the pore size decreases. Helmuth (1960), based on Kelvin's equation, developed the following equation to obtain the depression of freezing temperature with respect to the pore size;

$$T_r = T_S \exp\left(-\frac{2\sigma_{iw} M}{r_S Q_h \rho_i}\right) \tag{2.4}$$

where T_r = fusion temperature of ice crystal, °K

T_S = 273°K

σ_{iw} = interfacial energy between ice and water, dynes/cm

M = molecular weight of water, g/mole

r_S = pore radius, Å

Q_h = molar heat of fusion, cal/mole

ρ_i = density of ice, g/cm^3

There are several approaches suggested in different studies to calculate the depression of freezing temperature in terms of pore size. Higuchi (1968) modified Eq. (2.4) by using the surface energy of water instead of interfacial energy between ice and water and using the density of water instead of that of ice. Figure 2.9 (Kou and Kamada, 1975) summarizes the published data relating freezing temperature depression as a function of pore size obtained by different methods.

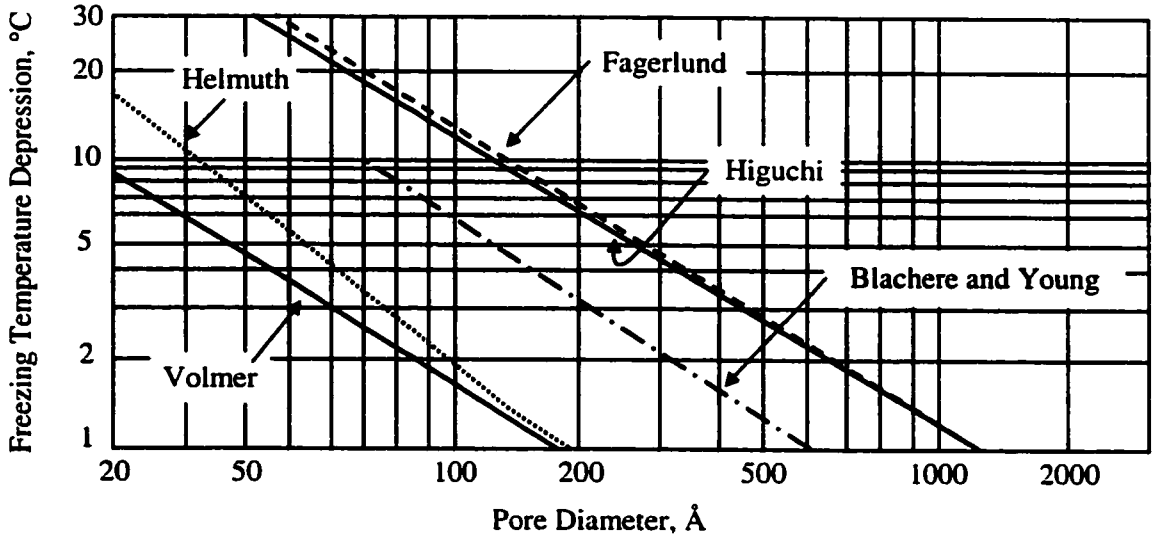

Fig. 2.9 Freezing temperature depression obtained by various methods

The diagram shown in Fig. 2.10 is a well-known phase diagram of water. The boundary curve A – D represents the temperature when the liquid phase changes to the solid phase at different values of pressure. This curve is, however, obtained based on the melting temperature, while the freezing temperature can sometimes be much lower than the melting temperature; the water can be highly supercooled without any crystallization of ice. Figure 2.11 illustrates the crystallization temperature of highly supercooled water as a function of pressure obtained by Kanno et al (1975). T_H and T_m represent the crystallization temperature and melting temperature, respectively. The lowest crystallization temperature was measured as –92°C at the pressure of 2000 bar and even at very low pressure, the water can be supercooled to –40°C. There is a large difference between freezing temperature and melting temperature caused by the supercooled water.

Similarly, a relatively large difference between freezing and melting temperature of pore water can be observed when a cement paste specimen is subjected to a freezing and thawing cycle. Helmuth(1960) suggests that the supercooled water in the pores of cement paste only freezes at temperatures corresponding to the formation of stable ice crystals. Once the supercooled water

freezes, it does not melt until the temperature corresponding to the size of each particular frozen capillary is reached. Accordingly this temperature is higher than freezing temperature.

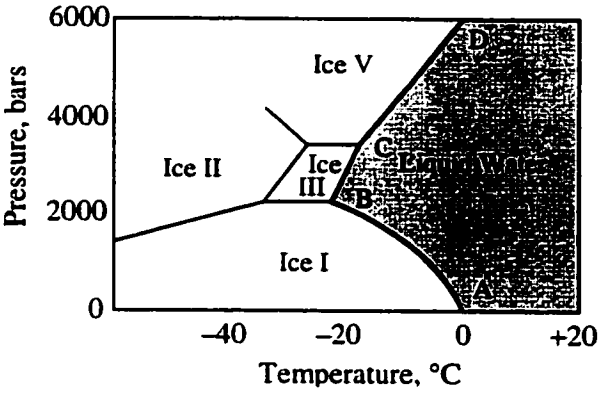

Fig. 2.10 Phase diagram of water

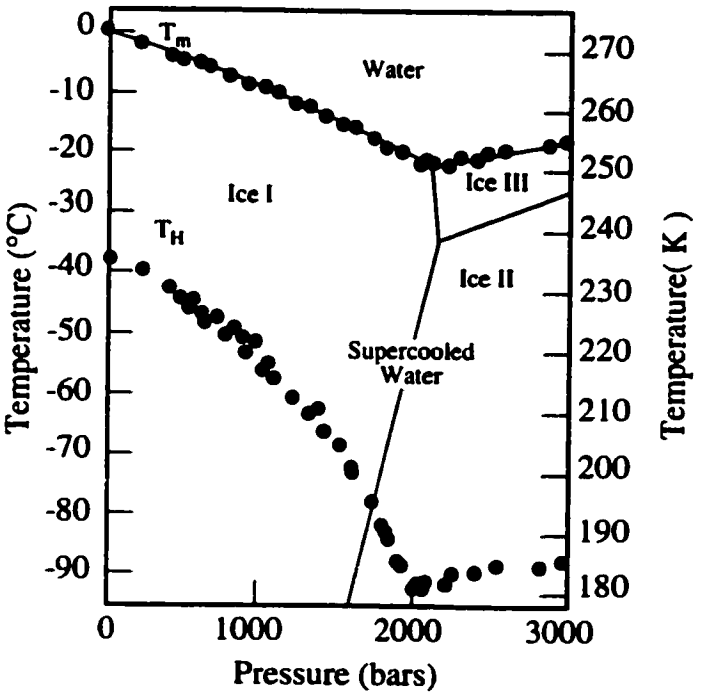

Fig. 2.11 Crystallization temperature of highly supercooled water as a function of pressure

2.3.2.2 Migration of Water

In addition to the depression of freezing and melting temperature, the migration of water throughout the network of the pores is an integral part of the mechanism of frost action within cement paste. There are two main theories, the hydraulic pressure theory in which water migrates from where freezing occurs and the thermodynamic theory in which water migrates toward where freezing occurs. The hydraulic pressure is basically caused by the 9% volume expansion of freezing water, however, the mechanism of frost action will be discussed in terms of migration of water.

The hydraulic pressure theory is based on the migration of water from where the formation of ice occurs. This concept was first introduced by Powers (1945) and modified by Powers and Helmuth (1953). Figure 2.12 is a similar diagram to Fig. 2.2 which shows the paste structure with capillary and gel pores (Powers and Helmuth, 1953).

Fig. 2.12 Paste structure with capillary and gel pores

As described previously, the formation of ice within the pores is dependent on the pore size and nucleation of ice crystals becomes more difficult as pore size decreases. Freezing initiates in larger capillary pores marked "C" in Fig. 2.12. When the water in the capillary pores freezes, the volume of water plus ice will exceed the original capacity of the pore, owing to the fact that freezing of water results in about 9% increase in volume. Therefore as the water in the pores freezes, the pores must expel the excess water into the nearest escape boundary. This is usually an air void located in this case at the left in Fig. 2.12. The process of excess water being expelled from the pores generates a so-called hydraulic pressure which puts the surrounding solid under stress. If the stress is lower than the tensile strength of the solid, an elastic volume change takes

place. If the stress is higher than the tensile strength of solid, irrecoverable volume change occurs and results in permanent damage such as cracking.

Thermodynamic theory is based on the migration of water toward where the freezing occurs. In other words, when the water in the capillary pores freezes, the unfrozen water in the surrounding gel pores migrates toward the capillary pores. It is noted that the water in the surrounding gel pores, which are smaller than capillary pores, freezes at much lower temperature. Therefore, as freezing initiates in the capillary pores, the water in the gel pores remains as a supercooled water. This leads to a thermodynamic disequilibrium between the ice in the capillary pores and the supercooled water in the surrounding gel pores. The free energy of the supercooled water becomes higher than that of the ice. Then the difference in vapour pressure becomes significant. As a result, the gel water migrates into the capillary pores, the ice crystals grow and the pore matrix expands. This theory was first introduced by Powers and Helmuth (1953) and described in terms of the diffusion of gel water.

This is similar to the description provided by Litvan. Litvan (1972) describes this migration of the gel water into the capillary pores in terms of the decreasing relative humidity over the supercooled water. Relative humidity is defined as the ratio of the water vapour pressure present at a certain temperature to the saturated water vapour pressure at the same temperature. In this case, relative humidity is the ratio of the vapour pressure of bulk ice that can form in an air void or boundary void at the temperature below the triple point to the vapour pressure of supercooled water in the gel pore. For the same temperature, the vapour pressure of the ice is lower than that of the supercooled water, and as the temperature decreases below the freezing point, the difference between the vapour pressure of the ice and that of the supercooled water increases. Figure 2.13 shows how the relative humidity decreases with decrease in the temperature.

With the decrease in relative humidity over the supercooled water, due to an increase in difference between the vapour pressure of the ice and that of the supercooled water, the supercooled water in the gel pores migrates into the capillary pores where the vapour pressure is lower than that in the gel pores. The difference in the damage mechanism described by Litvan to that of Powers and Helmuth is that the transport or migration of water itself is destructive. The Litvan mechanism does not have to involve the formation of ice as a direct cause of damage.

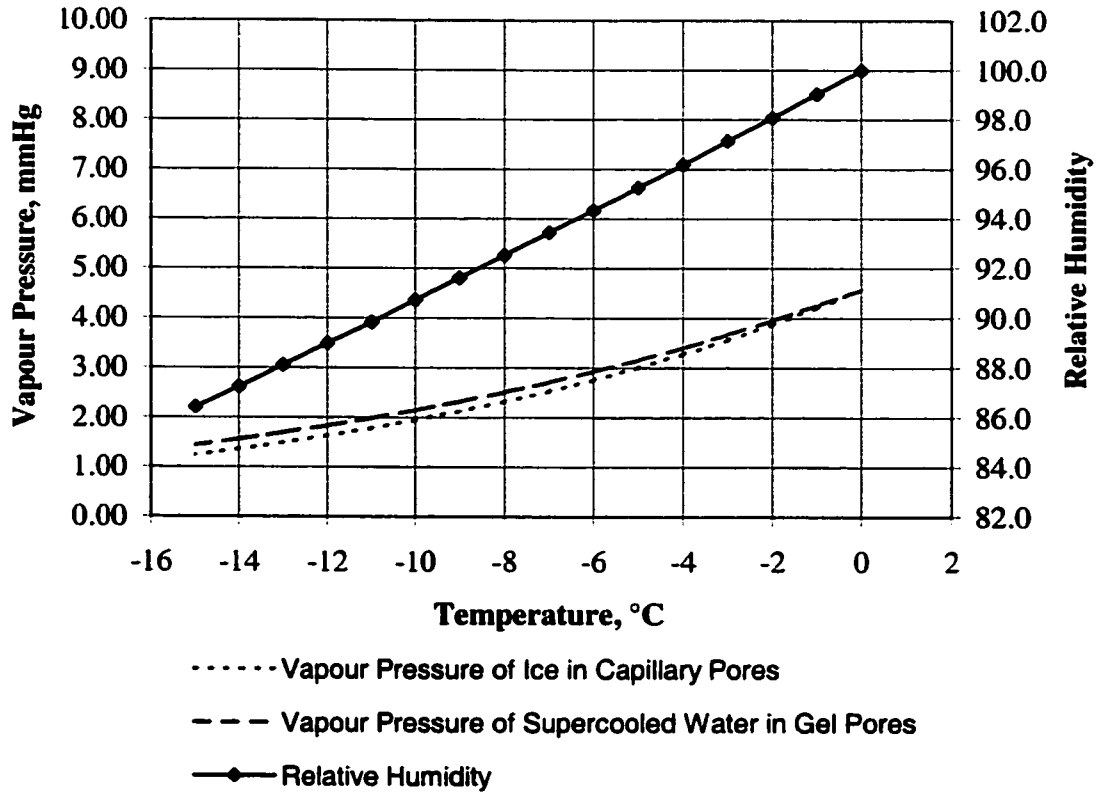

Fig. 2.13 Relative humidity as a function of temperature

Powers and Helmuth (1953) also proposed the osmotic pressure which forces the gel water to migrate into the capillary pores. Water in the capillary pores generally contains several soluble substances, such as alkalies, chlorides and calcium hydroxide. Water containing soluble substances freezes at lower temperature than pure water; the higher the concentration, the lower is the freezing temperature. This causes local increases in the concentration of the unfrozen portion of the solution in the capillary pores, creating the osmotic pressure which impels unfrozen water in the surrounding gel pores to diffuse into the solution of the frozen parts of the capillary pores. Powers et al. (1954) investigated the effect of osmotic pressure generated by a change in alkali concentration and concluded that its effect on freezing and thawing of cement paste was small. It might become a major problem, however, when the osmotic pressure is generated by salt concentration, usually originated from de-icing agents used to improve driving conditions in winter. An intensive study for the effect of de-icing agents on freezing of cement paste was conducted by Litvan (1975). The heavy usage of de-icing agents results in a serious damage which is known as salt scaling.

The hydraulic pressure theory was thought to be the dominant cause of frost action. This theory is based on the movement of water from where freezing occurs, because the freezing of water is accompanied by a 9% increase in volume. However, the thermodynamic theory became as dominant as the hydraulic pressure theory, since the same kind of destruction was observed even for the cement pastes saturated with organic liquids that contract on freezing. Beaudoin and MacInnis (1974) observed the dilation of benzene saturated cement paste subjected to freezing. Litvan (1972) saturated porous silica glass with organic liquids and also obtained the results which showed an expansion. These results indicate that hydraulic pressure caused by the 9% increase in volume is not the only cause of dilation of cement paste subjected to freezing.

2.3.3 Effect of Micro-Fibre Reinforcement on the Frost Action

There are only a few studies conducted to examine the effect of micro-fibre addition on cement paste or concrete subjected to freezing and thawing. Balaguru and Ramakrishnan (1986) conducted an extensive study on freeze-thaw durability of fibre reinforced concrete using ASTM Procedure C666 and indicated that the behaviour of fibre-reinforced concrete was similar to that of plain concrete. Beaudoin (1990) states that the freezing and thawing durability of steel fibre reinforced concrete does not appear to be adversely affected by the fibres, since the freezing and thawing durability of non-air-entrained concrete is similar to that of steel fibre reinforced concrete. Kobayashi (1983) reports that air-entrained steel fibre reinforced concrete has a better durability than air-entrained concrete without steel fibre reinforcement. Fibres act as crack-bridging elements so that they increase the crack tolerance of the C-S-H matrix.

2.3.4 Other Factors Affecting the Frost Action

2.3.4.1 Water/Cement Ratio

Water/cement ratio (w/c ratio) is one of the most important factors affecting the frost action of cement paste. It determines not only the total porosity, but also the permeability of cement paste. Figure 2.14 shows the length change of 100% saturated cement pastes subjected to freezing and thawing (Litvan, 1972). The higher the w/c ratio, the greater is the irrecoverable dilation. This is because there is a greater amount of water to freeze in cement paste for the higher w/c ratio.

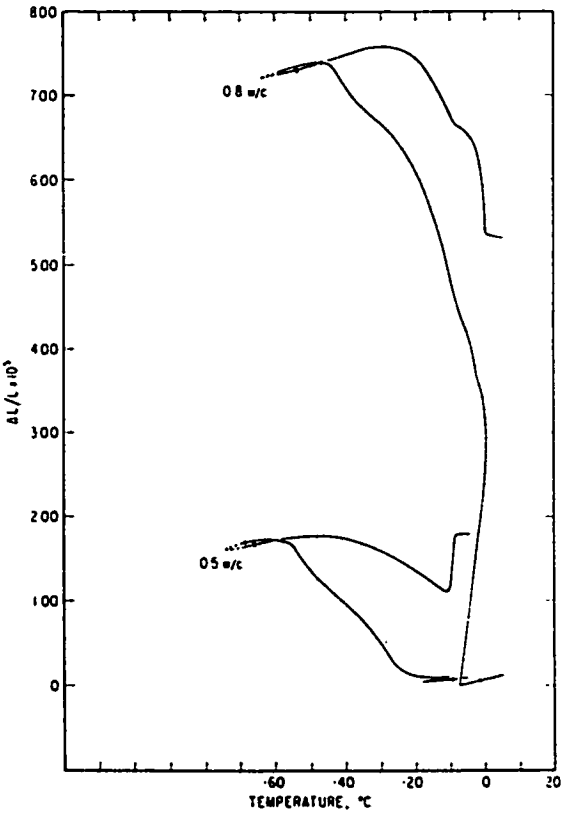

Fig. 2.14 Length change of 100% saturated cement pastes of w/c ratio 0.5 and 0.8

2.3.4.2 Degree of Saturation and Relative Humidity

The degree of saturation of cement paste is also one of the main factors controlling the frost action. There is a critical value of degree of saturation at which cement paste is likely to dilate when exposed to low temperature. Since the freezing of water results in 9% increase in volume, theoretically no dilation should occur by the hydraulic pressure, if the degree of saturation of cement paste is lower than approximately 92%.

Cement paste, fully saturated, remains in the same condition only if the 100% relative humidity is maintained. As the relative humidity decreases, however, the degree of saturation, hence the moisture content in the pores also decreases. The relationship between the relative humidity and the pore size can be obtained from Kelvin's equation as follows;

$$r_S = \frac{2\sigma_{aw} M}{\rho_w R_g T_C \ln RH} \qquad (2.5)$$

where r_S = pore radius, Å

σ_{aw} = interfacial energy between air and water, dynes/cm

M = molecular weight of water, g/mole

ρ_w = density of water, g/cm³

R_g = gas constant, cal/mole °C

Tc = temperature of cement paste, °C

RH = relative humidity

The pore radius obtained by Kelvin's equation with respect to different values of relative humidity is shown in Table 2.3. It indicates that, for instance, if the relative humidity is 80%, the pores whose radius is larger than 50 Å do not contain water and the pores whose radius is smaller than that are fully saturated.

Table 2.3 "Saturation" pore radius estimated from Kelvin's equation at various values of relative humidity

Relative Humidity RH, %	Pore Radius rs, Å	Relative Humidity RH, %	Pore Radius rs, Å
100	∞	70	31
98	550	60	22
95	217	50	16
90	105	40	12
80	50	30	9

The length change of cement pastes subjected to freezing and thawing after equilibration at 84% relative humidity is shown in Fig. 2.15 (Litvan, 1972). There is no dilation indicated when the pastes were equilibrated at 84% relative humidity. Saturated cement pastes exhibit irrecoverable dilation when subjected to the same freezing and thawing cycle as shown previously in Fig. 2.14. It should be noted that, for the cement paste equilibrated at 84% relative humidity, the effect of w/c ratio is not as significant as it is for the 100% saturated cement paste. The dilation indicated for cement paste of w/c ratio 0.50 is approximately the same as the one of w/c ratio 0.80, at 84% relative humidity, Fig. 2.15.

2.3.4.3 Air Content

The presence of air in cement paste is as important as the presence of water. Entrained air is the air intentionally mixed with cement paste to protect it from frost damage. Air entrainment im-

proves the resistance of cement paste to freezing and thawing. Figure 2.16 shows the length change of cement pastes with 16% air entrainment and with no air entrainment subjected to a freezing and thawing cycle (Powers, 1958). It clearly indicates that the cement paste with no air entrainment results in the irrecoverable dilation while the length change of the cement paste with 16% air entrainment is completely reversible. Regarding the entrained air, not only the total air content itself, but also the size of air bubbles and spacing between them are important. Powers (1949 and 1954) determined the effects of the size and the spacing of air bubbles.

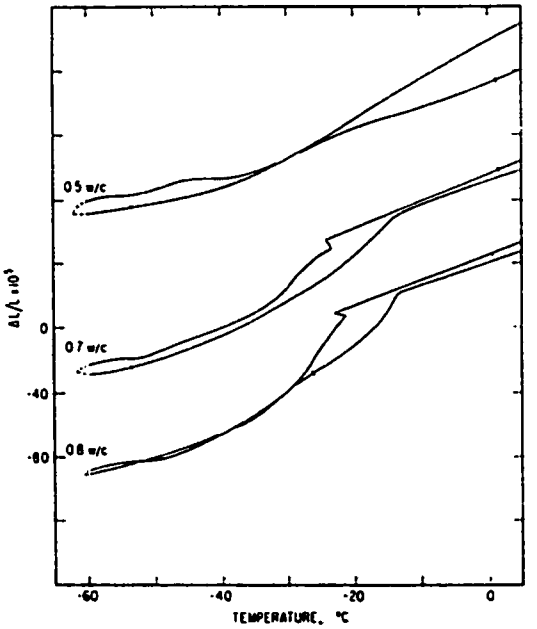

Fig. 2.15 Length change during a freezing and thawing of cement pastes after equilibration at 84% relative humidity

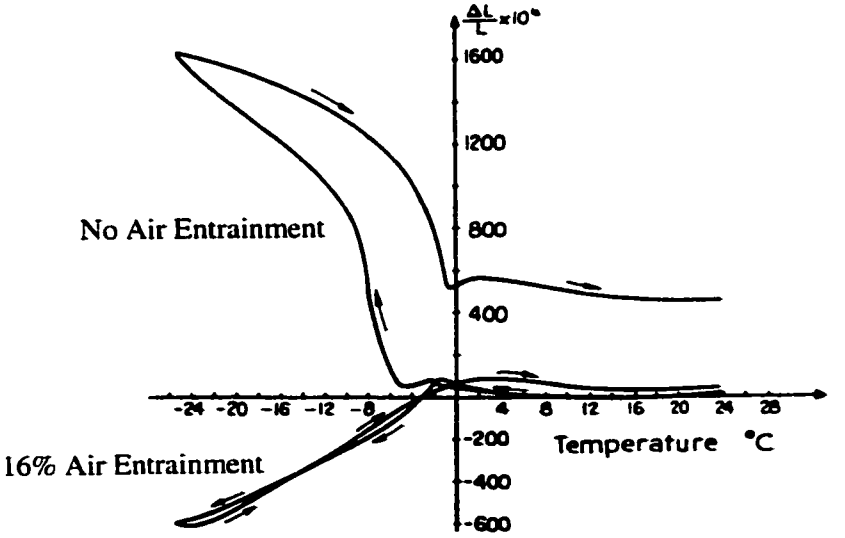

Fig. 2.16 Length change of cement pastes with and without air entrainment

2.3.4.4 Rate of Freezing

Rate of freezing is an external factor which affects the frost action of cement paste. In the field, the rate of freezing does not vary dramatically. However, a high rate of freezing can cause much more severe damage than a low rate of freezing. Powers and Helmuth (1953) describe the rate of freezing as one of the most important factors which control the hydraulic pressure. Length change of cement pastes subjected to different rates of freezing is shown in Fig. 2.17. It demonstrates that the higher the rate of freezing, the greater is the dilation. Lowering the rate of freezing gives cement paste a chance to desiccate during the freezing and thawing cycle. In other words, the degree of saturation is reduced. This could be one of the reasons that the cement paste does not dilate as much when subjected to lower rates of freezing.

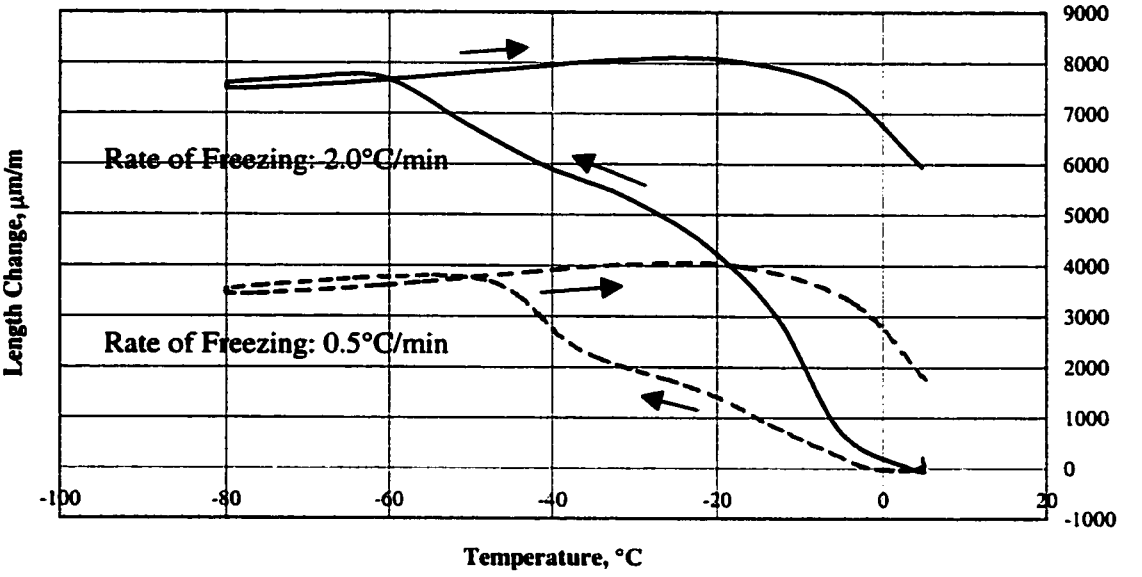

Fig. 2.17 Length change of cement pastes subjected to various freezing rates

2.3.4.5 Applied Load

In most cases, concrete structures in service are under a certain applied load. Those in cold climates are subjected to freezing and thawing at the same time. Therefore, it is important to understand the effect of applied load to the freezing and thawing resistance. Zhou et al. (1994) have conducted the research on the effect of an external flexural load on the frost resistance of air-entrained and non-air-entrained concrete with and without silica fume. They concluded that the load had no effect on the air-entrained material, but increased significantly the damage to the non-air-entrained concrete. Further investigation, however, is required to confirm these conclusions.

2.4 AC Impedance Spectroscopy (ACIS)

2.4.1 Introduction

Electrochemical measurements are widely used to characterize materials in various research fields, such as corrosion, surface treatment and battery testing. Among a number of electrochemical techniques, AC impedance spectroscopy (ACIS) has become a dominant technique in recent years. The basic theory of impedance spectroscopy involves the measurement of a signal resulting from an applied perturbation, or the external driving force. For example, when an electrical potential or perturbation is applied to a certain material, a resulting current flows through it. The ratio of the applied potential to the current is observed.

If a direct current (DC) technique is used, an applied potential is constant, and the ratio of the applied potential to the current is the resistance of the material. If an alternating current (AC) technique is used, the applied potential is variable, and the ratio is measured as the impedance of the material. The DC technique has been widely used. However it requires a relatively large perturbation and is not particularly effective when it is applied to low conductive media. Accordingly the AC technique has become more dominant, since only a small perturbation is required even for low conductive media. The ACIS is gaining wider application owing to its advantages: rapid and accurate data acquisition, continuous measurement and the attractiveness of a non-destructive process.

2.4.2 Basic Theory of ACIS

2.4.2.1 Alternating Current

There are two types of electrical sources; a direct current (DC) source and alternating current (AC) source. With the DC source, a current flows continuously in one direction and its magnitude remains constant. With an AC source, however, the current alternates its flow direction and its magnitude varies with respect to time in a sinusoidal manner as illustrated in Fig. 2.18.

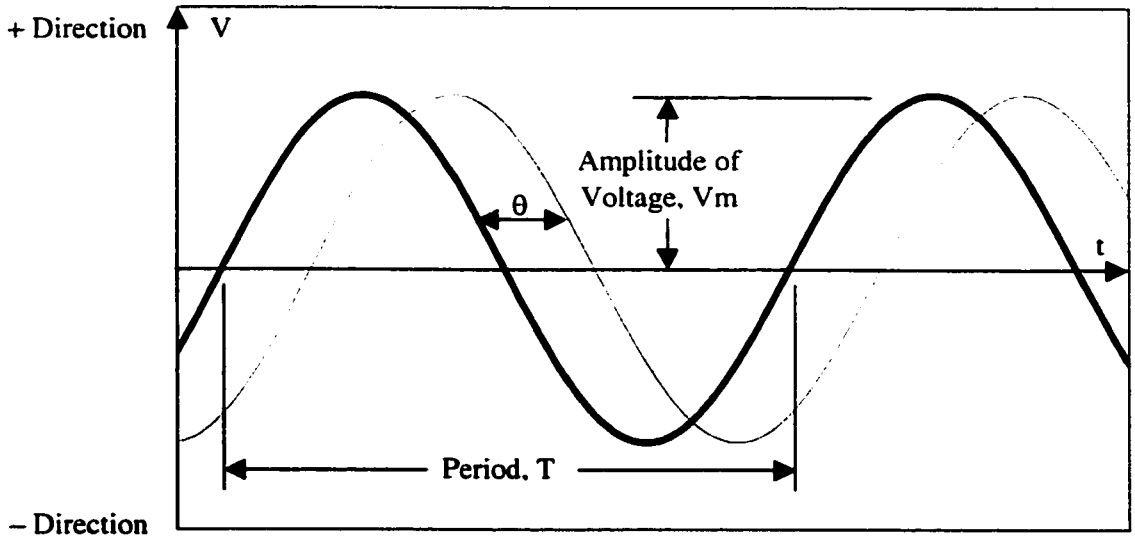

Fig. 2.18 Sinusoidal behaviour of the alternating current

Figure 2.18 depicts how the alternating current changes direction with time. The sinusoidal behaviour of the alternating current can be expressed as follows:

$$v(t) = V_m \sin(\omega t + \theta) \tag{2.6}$$

where v = voltage at time t, V

V_m = amplitude of voltage, V

t = time, s

ω = angular frequency, rad/s

θ = phase shift, radians

Angular frequency, ω can be expressed as $\omega = 2\pi / T$, where T is the period as shown in Fig. 2.18.

2.4.2.2 Resistance, Capacitance and Inductance

The three basic properties in the AC circuit are the resistance, capacitance and inductance. Resistance is a property of the material that determines its ability to oppose the current. Capacitance is the property of the material that measures its ability to store an electric charge. Inductance is the property of the material related to its capability of generating an electromagnetic field. Figure 2.19 summarizes the terminology regarding the AC circuit.

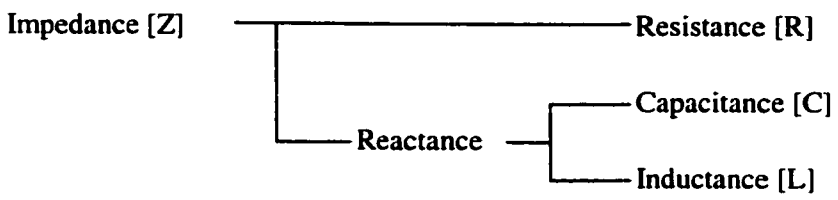

Fig. 2.19 Summary of terminology regarding the AC Circuit

Reactance is the total opposite of capacitance and inductance. The relationship between the impedance and the other three properties will be discussed later. It should be noted that the resistor, capacitor and inductor are devices that the impart resistance, capacitance and inductance to an electric circuit respectively. Figure 2.20 is a graphic representation of a resistor, capacitor and inductor.

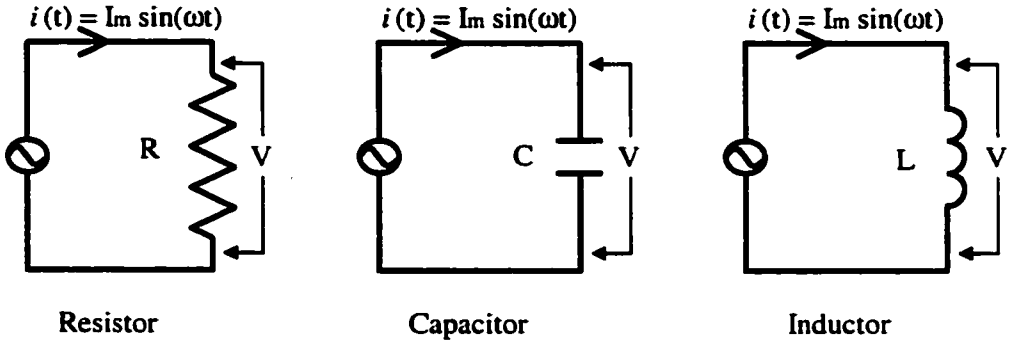

Fig. 2.20 A graphic representation of a resistor, capacitor and inductor

Resistance, R is a property of the material that determines its ability to oppose a flow of electricity; it dissipates electrical energy as heat. The unit of resistance is ohms, Ω. One ohm is defined as the resistance through which a potential difference of one volt will produce a current of one ampere. The Ohm's law can be applied to the alternating current circuit as well as the direct current circuit and states that the electric current flowing through a given resistor is equal to the applied voltage divided by the resistance or;

$$I = \frac{V}{R} \tag{2.7}$$

where I = electrical current, A

R = resistance, Ω

When the AC current flows through a resistor, the expression for the voltage drop across the resistor is similar to the one for the current. The AC current is sinusoidal as a function of time and can be expressed as follows;

$$i(t) = I_m \sin(\omega t) \tag{2.8}$$

where i = current at time t, A

I_m = amplitude of current, A

Substituting Eq. (2.8) into Eq. (2.7) and rewriting in terms of voltage;

$$v(t) = R\, I = R\, I_m \sin(\omega t) \tag{2.9}$$

Equation (2.9) shows that, when the sinusoidal current, $I_m \sin(\omega t)$ flows through the resistor, R, the voltage across the resistor has the amplitude magnified by R with no phase shift as shown in Fig. 2.21.

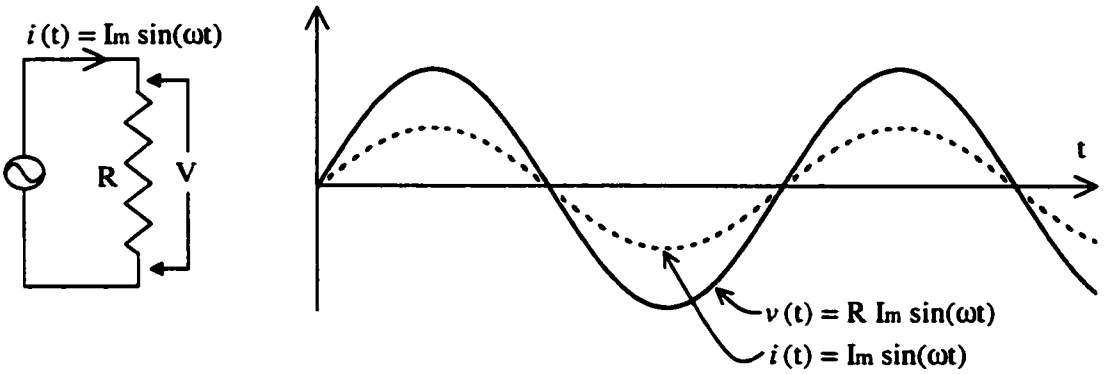

Fig. 2.21 Description of voltage when current flows through the resistor

A resistor basically has the same behaviour in an AC circuit as in a DC circuit. Capacitance and inductance, on the other hand, have unique properties in the AC circuit.

As mentioned before, capacitance is an ability to store the electric charge and expressed as the ratio of stored charge to the voltage or;

$$C = \frac{Q}{V} \tag{2.10}$$

where C = capacitance, Farad

Q = electric charge, Coulomb

The relationship between voltage and current for capacitance can be obtained by defining the current in terms of charge. The current is the rate of change in charge with respect to time and can be expressed as follows;

$$i(t) = \frac{dQ(t)}{dt} \tag{2.11}$$

From Eqs. (2.10) and (2.11),

$$i(t) = \frac{dQ(t)}{dt} = C\,\frac{dV(t)}{dt} \tag{2.12}$$

A structure of a simple capacitor is shown in Fig. 2.22. It consists of two conductors (e.g., metal plates) separated by a dielectric, that is a non-conductive material, such as a vacuum or water.

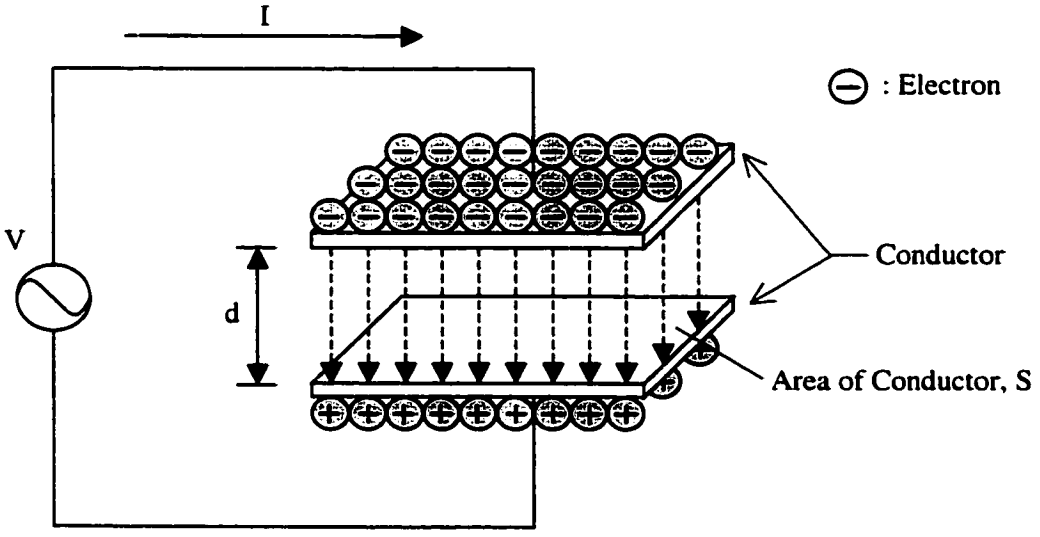

Fig. 2.22 Structure of capacitor

Capacitance is also dependent on the geometry of the capacitor, and it can be obtained as follows;

$$C = \varepsilon \frac{S}{d} \tag{2.13}$$

where ε = permittivity, Farad/m

S = area of conductor, m^2

d = distance between two conductors, m

When the DC voltage is applied to the capacitor, the current charges the plates of the capacitor, but does not flow through the capacitor itself, because of the gap between the two plates. When the AC voltage is applied to the capacitor, however, the current flows in the sinusoidal manner similar to the applied voltage, although there is a phase shift between the current and voltage as shown in Fig. 2.23.

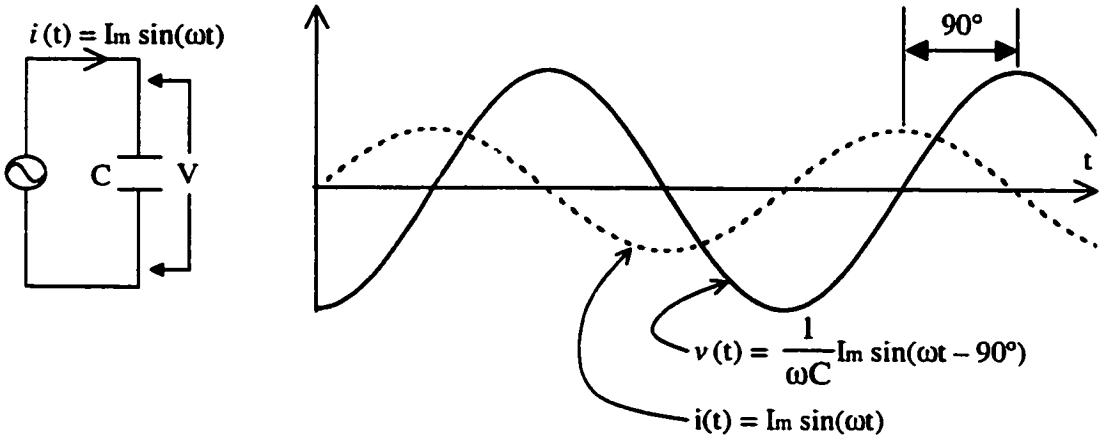

Fig. 2.23 Description of voltage when current flows through the capacitor

As shown in Fig. 2.21, the voltage and current for the resistor are said to be in phase, which means the peak values of the voltage and current occur at the same time. For the capacitor, however, the current has its peak value 90° before the voltage, which means that the current leads the voltage by 90°. This can be mathematically justified. Rewriting Eq. (2.12) in terms of voltage;

$$v(t) = \frac{1}{C} \int i(t)dt \tag{2.14}$$

Assuming the current $i(t) = I_m \sin(\omega t)$, Eq. (2.14) gives;

$$v(t) = \frac{1}{C}\int \{I_m \sin(\omega t)\}\, dt \tag{2.15}$$

$$= \frac{I_m}{\omega C}\{-\cos(\omega t)\} \tag{2.16}$$

$$= \frac{I_m}{\omega C}\sin(\omega t - 90°) \tag{2.17}$$

Equation (2.17) indicates that, when the sinusoidal current, $I_m \sin(\omega t)$ flows through the capacitor, C, the voltage across the capacitor has the amplitude magnified by $I_m/\omega C$ with 90° phase shift as shown in Fig. 2.23.

Inductance is a measurement of the electromagnetic induction of an electric component. Electromagnetic induction is the production of an electromotive force in a conductor as a result of a changing magnetic field. When the current, I flows through the inductor, its inductance can be determined as follows;

$$L = \frac{\Phi}{I} \tag{2.18}$$

where L = inductance, Henry

Φ = magnetic flux, Weber

The voltage between the two ends of inductor is proportional to the change in current with respect to time, and its coefficient is the inductance. In other words;

$$V = L\frac{dI}{dT} \tag{2.19}$$

The property of an inductor is opposite to that of capacitor. When the inductor is subjected to the DC voltage, the current easily flows, whereas the current does not flow when the capacitor is subjected to the DC voltage. When an AC voltage is applied to the inductor, the current flows in a sinusoidal manner. There is also a time difference between the peak values of voltage and current. As indicated in Fig. 2.24, although the current leads the voltage by 90° for the capacitor, the current has its peak value 90° after the voltage for the inductor, which means that the current lags the voltage by 90°.

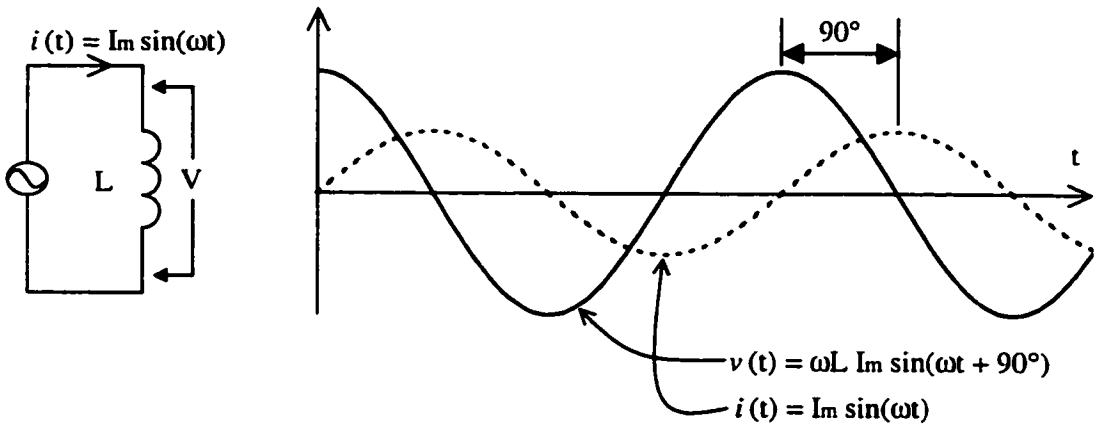

Fig. 2.24 Description of voltage when current flows through the inductor

This also can be shown mathematically. When the current $i(t) = I_m \sin(\omega t)$ flows through the inductor, Eq. (2.19) gives;

$$v(t) = L \frac{d\{I_m \sin(\omega t)\}}{dT} \tag{2.20}$$

$$= \omega L\, I_m \cos(\omega t) \tag{2.21}$$

$$= \omega L\, I_m \sin(\omega t + 90°) \tag{2.22}$$

Equation (2.22) justifies that, when the sinusoidal current, $I_m \sin(\omega t)$ flows through the inductor, L, the resulting sinusoidal voltage has the amplitude magnified by ωL with 90° phase shift as shown in Fig. 2.24.

Now substituting $i(t) = I_m \sin(\omega t)$ back into Eqs. (2.9), (2.17) and (2.22), they become;

Resistance, R	$V = R \cdot I$	(2.23)
Capacitance, C	$V = \frac{-j}{\omega C} \cdot I$	(2.24)
Inductance, L	$V = j\omega L \cdot I$	(2.25)

The symbol "j" in Eq. (2.25) denotes that the current lags the voltage by 90° and "$-j$" in Eq. (2.24) means that the current leads the voltage by 90°. The source of this symbol will be discussed in the next section. As the equations above show, the three components R, $-j/\omega C$ and

$j\omega L$ in Eqs. in (2.23), (2.24) and (2.25) respectively indicate the ability to oppose a current flow when the voltage, V is applied. They are termed an "Impedance, Z" and can be expressed as follows;

$$V = Z \cdot I \tag{2.26}$$

where Z = Impedance, Ω

Also Table 2.4 summarizes the properties of impedance.

Table 2.4 Properties of impedance

	Resistance, R	Capacitance, C	Inductance, L
Magnitude	R	$1/\omega C$	ωL
Phase Shift (I to V)	0°	− 90°	+ 90°
Impedance, Z	R	$-j/\omega C$	$j\omega L$

2.4.2.3 Complex Representation

One of the most well-known AC circuits is the series circuit containing an inductor, resistor and capacitor (LRC circuit). Figure 2.25 diagrammatically shows the typical LRC circuit with the applied AC voltage of $v(t) = V_m \sin(\omega t)$. Analyzing the AC impedance spectroscopy, ACIS of this circuit utilizes the summation of the voltage drops around the circuit.

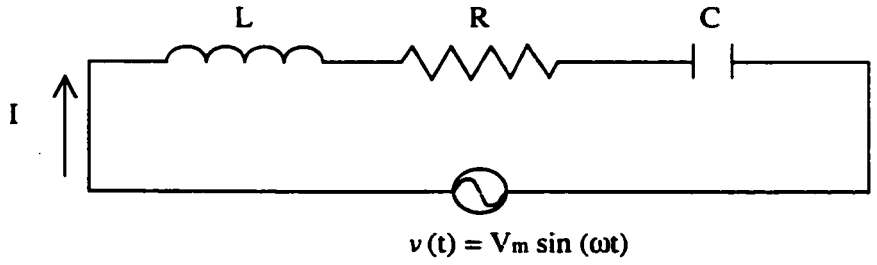

Fig. 2.25 A typical LRC circuit

According to Eqs. (2.7), (2.10) and (2.19),

$$v(t) = V_m \sin(\omega t) = V_L + V_R + V_C \tag{2.27}$$

$$= L\frac{dI}{dT} + IR + \frac{Q}{C} \tag{2.28}$$

where V_L = voltage across the inductor

V_R = voltage across the resistor

V_C = voltage across the capacitor

Substituting $i(t) = \frac{dQ}{dt}$, Eq. (2.28) becomes,

$$L\frac{d^2Q}{dt^2} + R\frac{dQ}{dt} + \frac{Q}{C} = V_m \sin(\omega t) \tag{2.29}$$

Analysis of the ACIS by solving the above differential equation may lead to complicated mathematical operations as this typical and simple example of the LRC circuit describes. However, for a given frequency, ω, it is much easier to represent the ACIS by just two variables, the amplitude and phase shift. For this purpose, the concept of complex representation can be introduced. The advantage of using the complex number originates from its unique property of representing and manipulating two variables as a single quantity. In fact, the complex number can be represented in a two-dimensional display called the complex plane. Equations for the current $i(t) = I_m \sin(\omega t)$ and the resulting voltage $v(t) = V_m \sin(\omega t + \theta)$, can be expressed by the complex variable in a polar form respectively as follows;

$$i(t) = I_m \sin(\omega t) \implies I = I_m e^{j\omega t} \tag{2.30}$$

$$v(t) = V_m \sin(\omega t + \theta) \implies V = V_m e^{j(\omega t + \theta)} \tag{2.31}$$

where $j = \sqrt{-1}$

Then, the impedance, Z can be expressed by the complex variable in the polar form by rearranging Eq. (2.26),

$$Z = \frac{V}{I} = \frac{V_m e^{j(\omega t + \theta)}}{I_m e^{j\omega t}} = \frac{V_m}{I_m} e^{j\theta} \tag{2.32}$$

$$= Z_m e^{j\theta} \tag{2.33}$$

where $Z_m = \frac{V_m}{I_m}, \Omega$

The complex variable shown in Eq. (2.33) can be expressed in the complex plane as presented in Fig. 2.26(a).

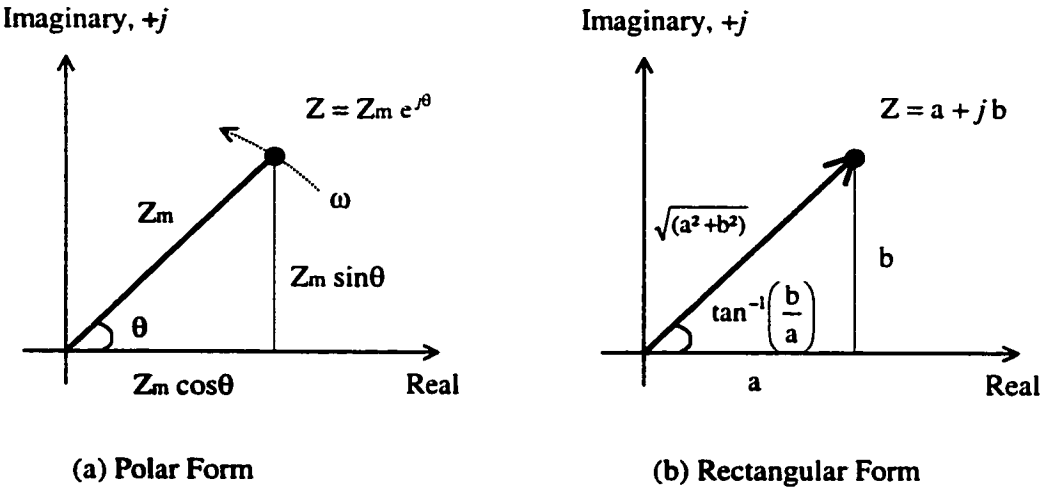

Fig. 2.26 Complex variable in polar and rectangular form

The complex variable in a polar form is convertible to the one in a rectangular form using the Euler's formula,

$$e^{\pm j\theta} = \cos\theta \pm j \sin\theta \tag{2.34}$$

Then, Eq. (2.33) becomes,

$$Z = Z_m e^{j\theta} \tag{2.35}$$

$$= Z_m (\cos\theta + j \sin\theta) \tag{2.36}$$

$$= a + jb \tag{2.37}$$

where $a = Z_m \cos\theta = Z'$

$b = Z_m \sin\theta = Z''$

Figure 2.26 (b) shows the graphic representation of a complex variable in the rectangular form. A complex variable on the complex plane can also be treated as a vector, since it denotes both magnitude and direction. Comparing Figs. 2.26 (a) and (b), it can be seen that the complex variable in a polar form can be converted to the one in a rectangular form. Z_m and θ can be calculated as

$\sqrt{(a^2+b^2)}$ and $\tan^{-1}(b/a)$, respectively. Variables a and b in Eq. (2.37) are often denoted as Z' and Z", respectively.

As mentioned previously, the symbol "*j*" has been introduced as the square-root of negative one, and it is used to denote an imaginary part in a complex number. There is a unique behaviour of "*j*" on the complex plane. It is that, on the complex plane, multiplying a complex variable by "*j*" rotates it 90° counterclockwise and 90° clockwise if it is multiplied by "$-j$". Figure 2.27 shows a vector "$\vec{A}$" on the +X axis. This vector $\vec{A}$ is referred to as a complex variable of $Z = A + j \times 0$, in other words, it only has a real number "A". Multiplying this vector by j leads to $j\vec{A}$ which is on the $+j$ axis. It means that the vector $\vec{A}$ has rotated counterclockwise by 90°. Similarly, if $j\vec{A}$ is multiplied by j once more, it becomes $-\vec{A}$ and rotates counterclockwise by 90°. Likewise, if $\vec{A}$ is multiplied by j twice more, it goes back on the +X axis. Also if the vector $\vec{A}$ on the +X axis is multiplied by the $-j$, it rotates clockwise by 90° and so on.

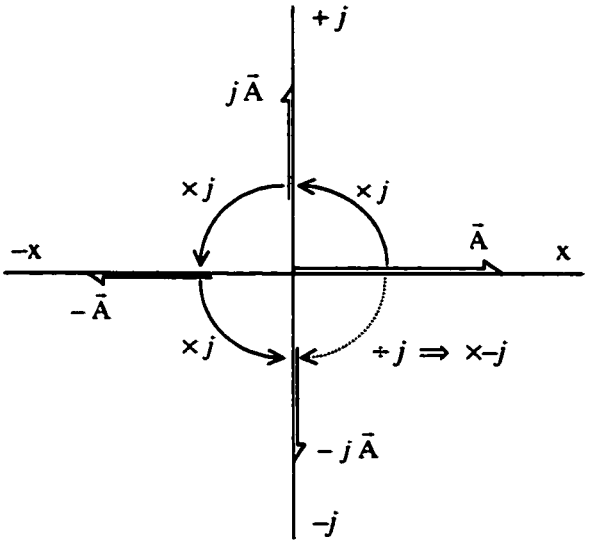

Fig. 2.27 A vector $\vec{A}$ and "j"

This behaviour can also be observed for the capacitance and inductance in the complex plane. In general electrochemistry, it can be confusing, but the positive Y axis is often set as the $-j$ axis. Equation (2.24) shows the relationship between voltage, current and capacitance and Fig. 2.28 (a) depicts it graphically. Recalling Eq. (2.24);

$$V = \frac{-j}{\omega C} \cdot I \tag{2.38}$$

In Fig. 2.28 (a), a vector of current, $\bar{I}$ is on the +X axis. Since the voltage, V is the product of current, I, $1/\omega C$ and $-j$ as shown in Eq. (2.38), a vector of voltage, $\bar{V}$ should be on the $-j$ axis after multiplication by $-j$ and its magnitude is $I/\omega C$. Once again, the positive Y axis in Fig. 2.28 (a) is set as the $-j$ axis, so that multiplying the vector by $-j$ rotates it 90° counterclockwise. Figure 2.28 (a) clearly shows that, for the capacitance, the current leads the voltage by 90° as explained before. Similarly, the same behaviour can be observed for the inductance. Recalling Eq. (2.25);

$$V = j\omega L \cdot I \tag{2.39}$$

Equation (2.39) is illustrated in Fig. 2.28 (b). Since the voltage, V is the product of current, I, ωL and $+j$ as shown in Eq. (2.39), a vector of voltage, $\bar{V}$ should be on the $+j$ axis after multiplied by $+j$ and its magnitude is ωLI. As graphically shown, for the inductance, the current lags the voltage by 90°.

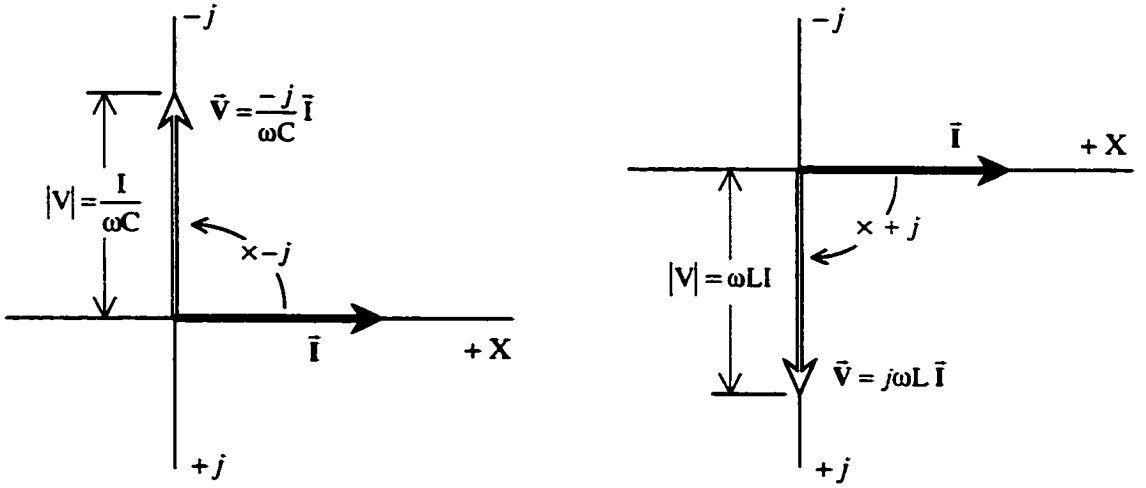

Fig. 2.28 Description of capacitance and inductance in the complex plane

2.4.3 ACIS and Cement Paste

2.4.3.1 The High Frequency Arc

The ACIS describes the response of current flow with respect to an applied sinusoidal voltage perturbation as a function of frequency. It can be represented in the complex plane. The graph in Fig. 2.29 shows a typical ACIS plot in the complex plane as frequency changes when the sinusoidal voltage is applied to a cement paste specimen through the electrodes.

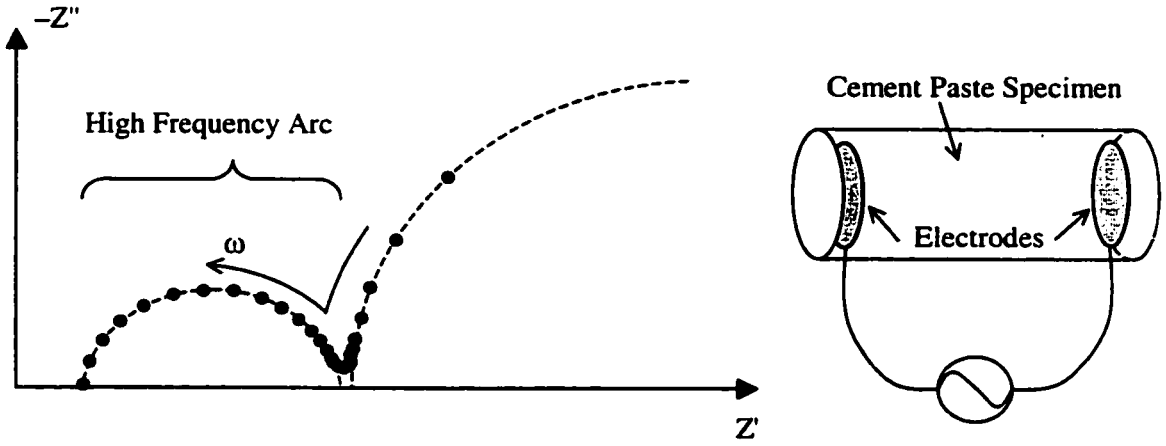

Fig. 2.29 A typical ACIS plot in the complex plane

The graph contains a semicircle on the left hand side and a part of another semicircle on the right hand side. Since the frequency increases from right to left, the semicircle on the left hand side is known as the high frequency arc, and the part of semicircle on the right hand side is the low frequency arc. In a study of cement paste using the ACIS technique, the high frequency arc is the important part to be investigated. The reason will be explained in the following section.

2.4.3.2 Equivalent Circuit

In order to analyze the resulting ACIS measurement taken from a certain material, the concept of an equivalent circuit must be introduced. The equivalent circuit is a method for modelling the resulting ACIS measurement by a combination of resistors, capacitors and inductors. In other words, an electric circuit with a combination of those three basic components should be modelled so that the impedance of the equivalent electric circuit fits the resulting ACIS measurement.

If a sinusoidal voltage is applied across a pure resistor of magnitude R, then the magnitude of the impedance, $|Z|$ is R and the phase shift is 0° as shown in Fig. 2.30 (a). If the sinusoidal voltage is applied across a pure capacitor, the magnitude of impedance is now dependent on the frequency, according to $|Z| = 1/\omega C$ and the phase shift is –90° as shown in Fig. 2.30 (b).

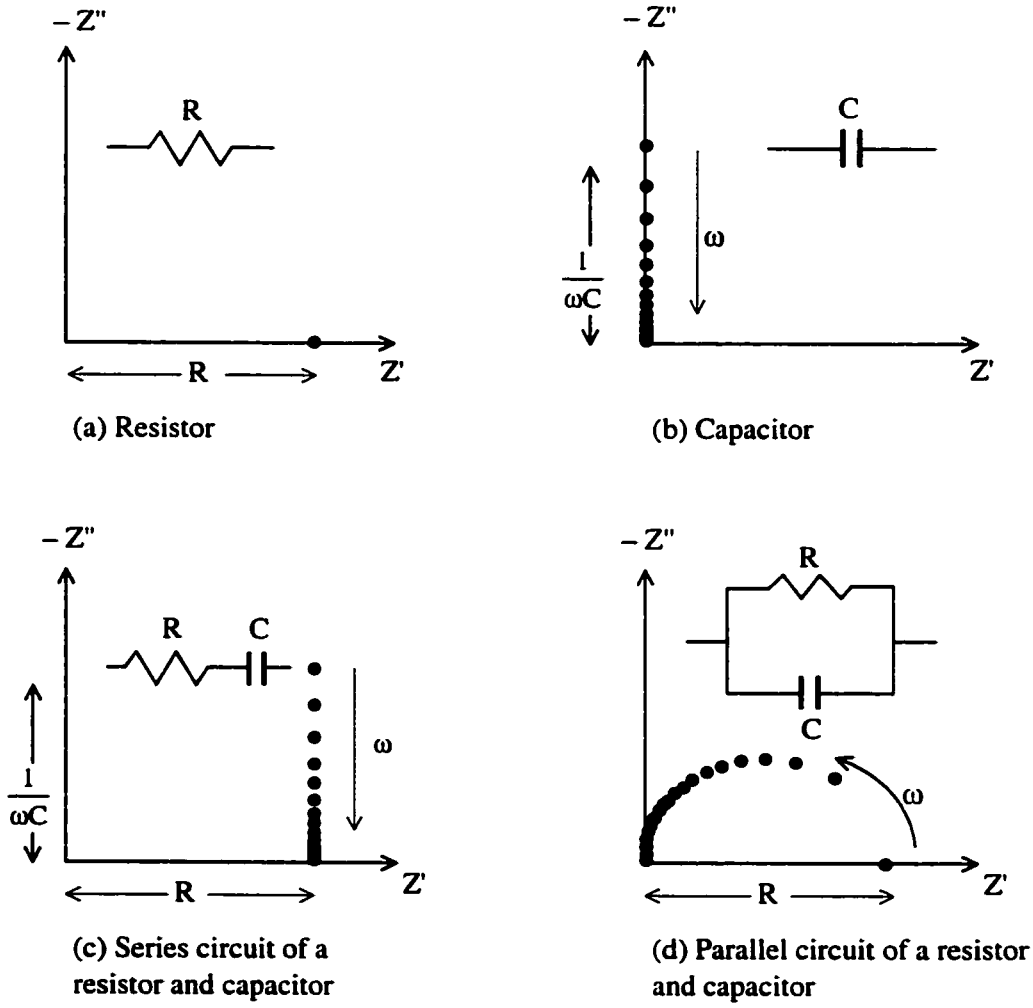

Fig. 2.30 Description of various combination of resistor and capacitor

While the impedance of a resistor is constant for all frequencies, that of a capacitor decreases as the frequency increases. If the equivalent circuit is modelled to contain a resistor and capacitor in series or in parallel, the resulting impedance can be expressed as shown in Figs. 2.30 (c) and (d), respectively. The impedance of the resistor and capacitor in series can be graphically deduced from Figs. 2.30 (a) and (b). However, the impedance of the resistor and capacitor in parallel results in the semicircle with diameter, R.

Xie et al.(1993) developed the following physical and mathematical interpretation of an equivalent circuit for the saturated cement paste. Considering the saturated cement paste specimen under the applied voltage, the specimen was modelled as an electric circuit consisting of N electric elements connected in series as shown in Figs. 2.31 (a) and (b). The elements have the same physical properties and consist of three sub-elements, solid, bulk liquid and solid-liquid interface normal to the electric field. Figure 2.31 (c) illustrates the detailed representation of the solid-liquid interface. As shown, the ionic composition and microstructure of the solid-liquid interface is different from that of bulk liquid owing to the surface adsorption of the solid. Xie et al. (1993) suggested that, under an AC signal, the separation of opposite charges in the solid and solid-liquid interface results in capacitance behaviour and it can be modelled by the equivalent circuit as shown in Fig. 2.31 (d). R_S and R_L represent the electrical resistance of solid-liquid respectively, and R_f and C_f represent the electrical resistance and capacitance of solid and liquid interface, respectively. Finally the equivalent circuit for the whole specimen is a summation of N elements as shown in Fig. 2.31 (e).

The mathematical interpretation of the equivalent circuit shown in Fig. 2.31 (e) was developed by Xie et al. (1993). The total impedance, Z, of the specimen can be calculated as follows;

$$Z = Z_1 + Z_2 \tag{2.40}$$

where Z_1 = total impedance of parallel circuit component containing R_S and R_L

Z_2 = total impedance of parallel circuit component containing R_f and C_f

The total impedance of the parallel R_S and R_L circuit component can be obtained by;

$$Z_1 = \sum_{i=1}^{N} \left(\frac{1}{\frac{1}{R_S} + \frac{1}{R_L}} \right)_i \tag{2.41}$$

Since $R_S >> R_L$, Eq. (2.41) becomes;

$$Z_1 = \sum_{i=1}^{N} (R_L)_i = NR_L \tag{2.42}$$

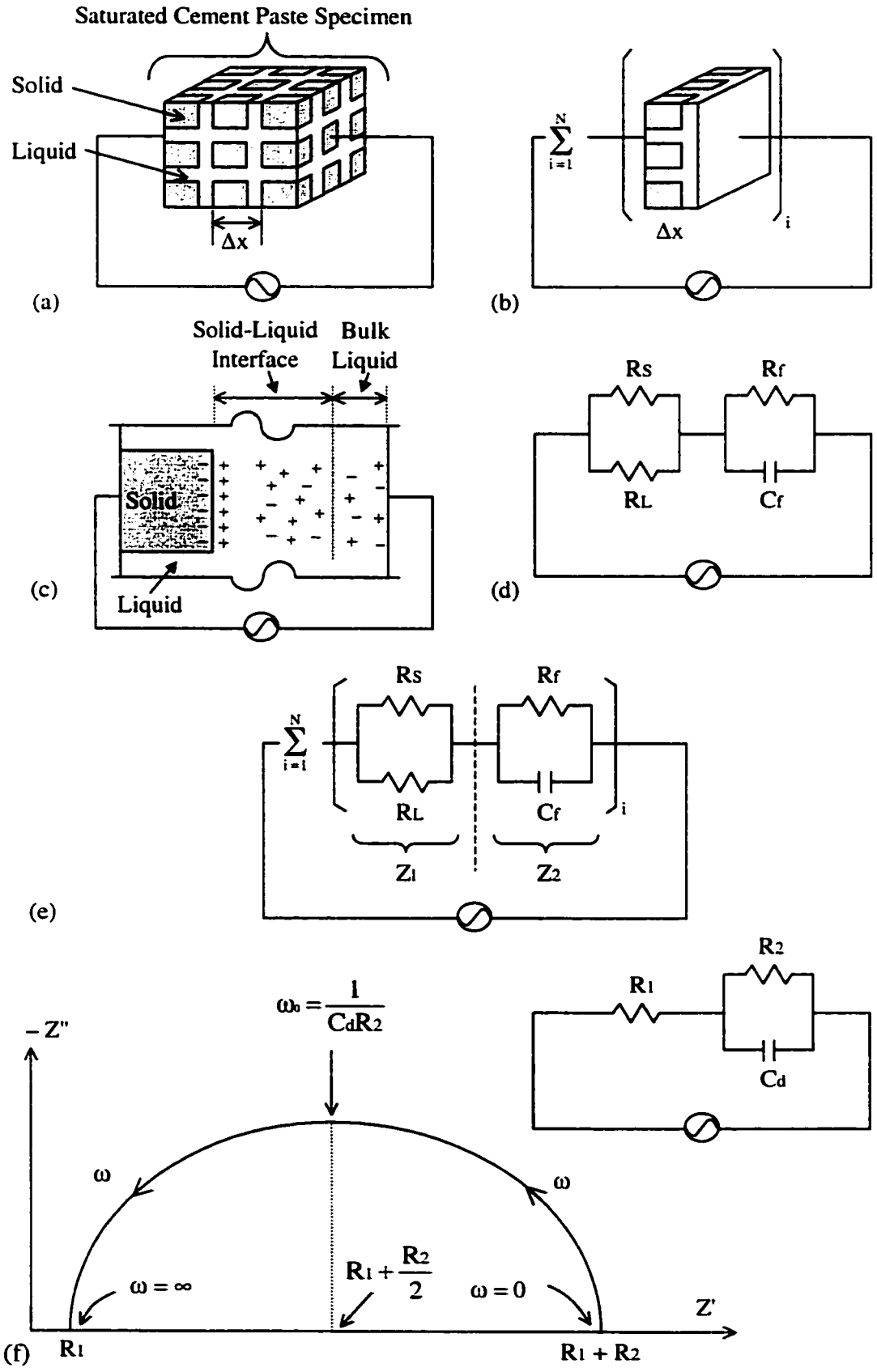

Fig. 2.31 Model of cement paste specimen as an electric circuit

Z_2, on the other hand, is the total impedance of the parallel circuit of R_f and C_f and can be obtained by;

$$Z_2 = \sum_{i=1}^{N} \left(\frac{1}{\frac{1}{R_f} + j\omega C_f} \right)_i \tag{2.43}$$

$$= \sum_{i=1}^{N} \left(\frac{R_f}{1+(\omega C_f R_f)^2} - j\frac{\omega C_f R_f^{\,2}}{1+(\omega C_f R_f)^2} \right)_i \tag{2.44}$$

$$= \frac{NR_f}{1+(\omega C_f R_f)^2} - j\frac{N\omega C_f R_f^{\,2}}{1+(\omega C_f R_f)^2} \tag{2.45}$$

Substituting Eqs. (2.42) and (2.45) into Eq. (2.40) gives;

$$Z = Z_1 + Z_2 = N R_L + \frac{NR_f}{1+(\omega C_f R_f)^2} - j\frac{N\omega C_f R_f^{\,2}}{1+(\omega C_f R_f)^2} \tag{2.46}$$

Letting $R_1 = NR_L$, $R_2 = NR_f$ and $C_d = C_f/N$, Eq. (2.46) becomes;

$$Z = R_1 + \frac{R_2}{1+(\omega C_d R_2)^2} - j\frac{\omega C_d R_2^{\,2}}{1+(\omega C_d R_2)^2} \tag{2.47}$$

If $Z' = R_1 + \frac{R_2}{1+(\omega C_d R_2)^2}$ and $Z'' = \frac{\omega C_d R_2^{\,2}}{1+(\omega C_d R_2)^2}$, the following equation can be obtained;

$$\left(Z' - \left(R_1 + \frac{R_2}{2}\right)\right)^2 + (Z'')^2 = \left(\frac{R_2}{2}\right)^2 \tag{2.48}$$

Equation (2.48) is the equation of a semicircle with radius $R_2/2$ and centre $(R_1 + R_2/2, 0)$ in the complex plane as shown in Fig. 2.31 (f). Now, since the sinusoidal voltage is applied through the electrodes, the model developed in Fig. 2.31 can be modified as illustrated in Figs. 2.32 (a) and

(b). Figure 2.32 (c) illustrates the equivalent circuit when the electrode was taken into consideration.

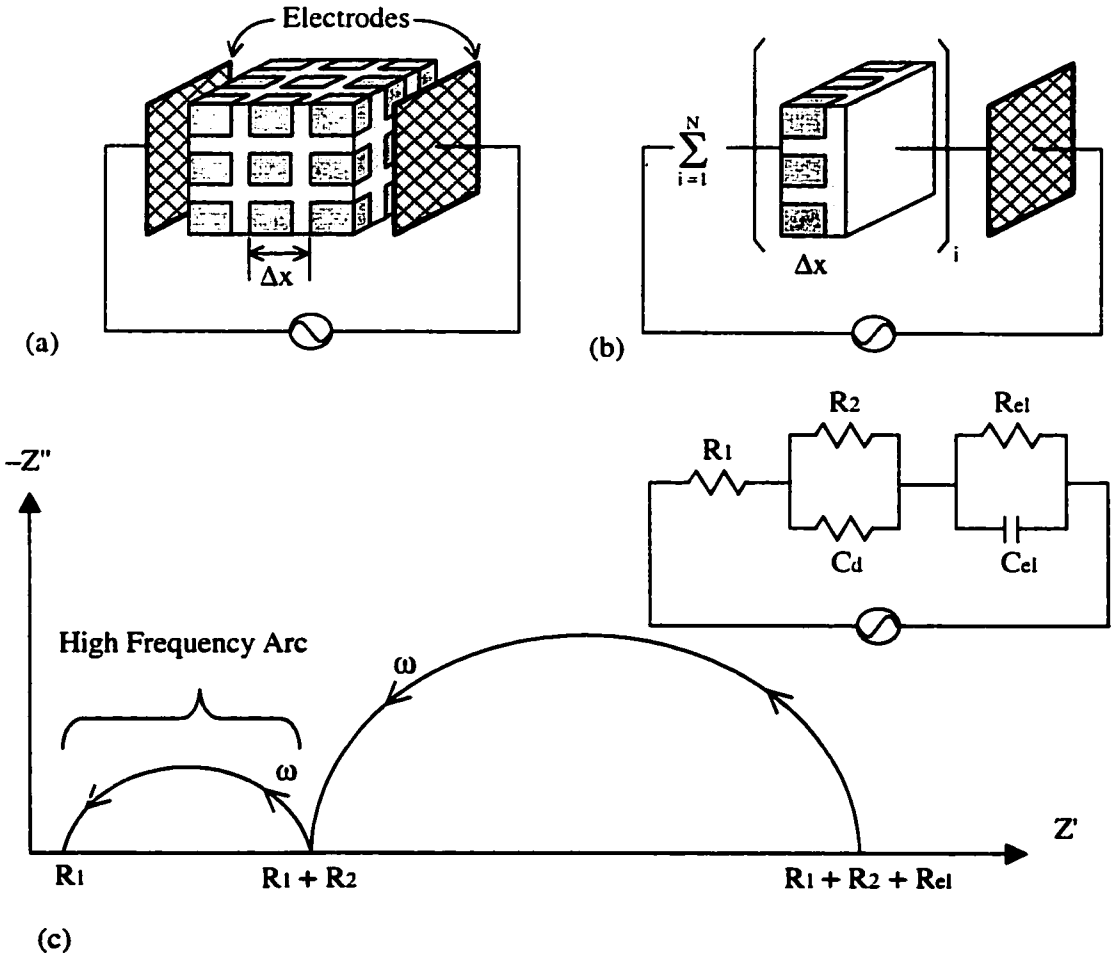

Fig. 2.32 Modified model of cement paste specimen as an electric circuit

As the solid-liquid interface results in capacitance behaviour, the cement-electrode interface also results in capacitance behaviour. Therefore, another capacitor, C_{el}, as well as a resistor, R_{el}, were added where R_{el} and C_{el} represent the electrical resistance and capacitance of the cement paste-electrode interface, respectively. This equivalent circuit includes the low frequency semicircle on the right hand side, accounting for the cement paste-electrode effect and the semicircle on the left hand side, the high frequency arc, modelling the behaviour of the cement paste itself. This is the reason that the high frequency arc becomes more important than the low frequency arc when employing the ACIS measurement. Since, in most cases, the high frequency arc is the main characteristic to be investigated, the equivalent circuit shown in Fig. 2.31 (f) is the well-known circuit

used to model the ACIS measurement for the cement paste. This equivalent circuit can be mathematically expressed by substituting Eqs. (2.42) and (2.43) into Eq. (2.40);

$$Z = NR_L + \left(\frac{1}{\frac{1}{NR_f} + j\omega \frac{C_f}{N}} \right) \tag{2.49}$$

Since $R_1 = NR_L$, $R_2 = NR_f$ and $C_d = C_f/N$, Eq. (2.49) becomes;

$$Z = R_1 + \left(\frac{1}{\frac{1}{R_2} + j\omega C_d} \right) \tag{2.50}$$

At high frequencies, the capacitance, C_d, conducts readily leaving only the effect of the resistance, R_1. As the frequency decreases, the conduction of C_d becomes less and the response of R_2 increases. As the frequency approaches zero, the capacitor ceases to conduct and the impedance becomes a function of R_1 and R_2.

2.4.3.3 The Depression Angle Parameter

As illustrated in Fig. 2.31 (f), the equivalent circuit models the ideal semicircle. However, the semicircle obtained from the ACIS measurement is, in most cases, inclined and its centre is depressed below the real axis by a depression angle, ϕ_{dep} as shown in Fig. 2.33.

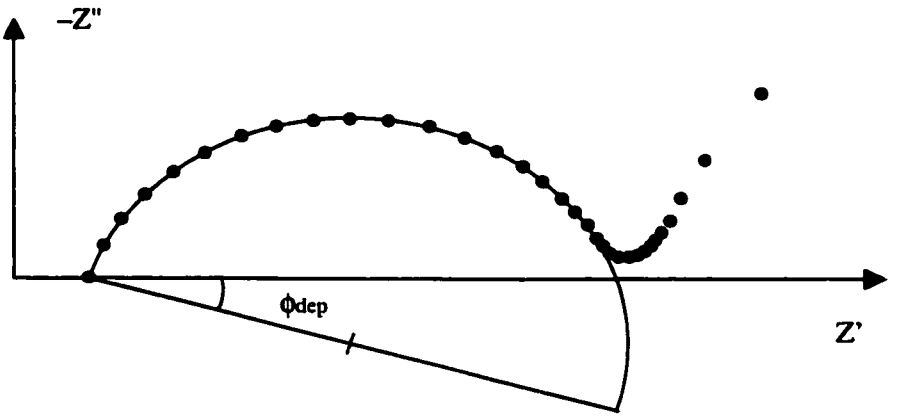

Fig. 2.33 ACIS plot and its depression angle

In order to model and represent the depression of the semicircle, the concept of the depression angle parameter and constant phase element (CPE) can be introduced. The depression angle parameter, n, can be defined as follows;

$$n = 1 - \frac{2}{\pi}\ \phi_{dep} \tag{2.51}$$

where n = depression angle parameter

ϕ_{dep} = depression angle, radians

The CPE is the circuit element used to model the capacitor with the phase shift less than 90°, that is, the depression of the semicircle, and its impedance can be defined as follows;

$$Z = \frac{1}{C(j\omega)^n} \tag{2.52}$$

For the ideal semicircle, that is, n = 1.0, the impedance of CPE becomes $1/j\omega C$ with a 90° phase shift. When n is less than 1.0, the phase shift can be determined as $n \times 90°$.

In general electrochemistry, the depression of the semicircle is said to be influenced by the heterogeneity and roughness of an interface. As the interface becomes more heterogeneous and rough, the depression angle, ϕ_{dep} increases and therefore the depression angle parameter decreases. Conversely, when the interface becomes less heterogeneous and rough, the depression angle, ϕ_{dep} decreases and therefore the depression angle parameter approaches 1.00. McCarter and Brousseau (1990) suggested that the depression angle parameter of cement paste is influenced by a spread of relaxation times, and Gu et al. (1994) extended this idea and discussed the pore size distribution of cement paste as one of the possible influences on the depression angle parameter. The explanation is that the dipoles of ions inside the micropores orient themselves to follow the applied AC signal. Then the time for the orientation of ions, that is, relaxation time, appears to be affected by the geometry of the pores and surface chemistry of the solid. The differences of ion-ion interaction between large and small pores are expected to result in differences in relaxation times. This indicates that a large depression angle can correspond to a spread of relaxation times inherent in porous materials containing a broad pore size distribution. Perron and Beaudoin (2002) applied this dependence of the depression angle parameter on the pore size distribution to explain ice formation within cement paste subjected to a freezing and thawing cycle.

2.5 Differential Scanning Calorimetry (DSC)

2.5.1 Introduction

The differential scanning calorimeter (DSC) is a device used to measure heat flow associated with phase transitions as a function of temperature and time. It has been widely used, in various fields, to investigate the phase transitions of the substance as well as to determine its heat capacity. Beddoe and Setzer (1988) conducted the DSC experiments to investigate the phase transitions of cement paste subjected to freezing and thawing cycles. Extensive studies using the DSC were conducted by Bager and Sellevold (1986 and 1987) for the cement pastes cured in various environments and subjected to freezing and thawing cycles.

2.5.2 Basic Theory of DSC

2.5.2.1 Heat of Fusion and Specific Heat Capacity

When the heat is absorbed by a substance, its temperature increases; the temperature decreases when the heat is released from the substance. The relation between the heat absorbed or released and the associated temperature changes can be obtained by introducing the heat capacity as follows;

$$q = C_h \Delta T \tag{2.53}$$

$$= c\, m\, \Delta T \tag{2.54}$$

where q = heat, J

C_h = heat capacity, J/°C

ΔT = temperature change, °C

c = specific heat capacity, J/°C/g

m = mass of substance, g

The heat capacity of a substance, C_h in Eq. (2.53), is the amount of heat required to change its temperature by one degree and the specific heat capacity, c in Eq. (2.54), is therefore the amount of heat required to change its temperature by one degree per unit mass of substance. For example,

the specific heat capacity of ice is 2.049 J/°C/g, which means that 2.049 J of heat is required to raise the temperature by one degree per gram of ice. When the temperature reaches the melting point of water, the water changes its phase from solid to liquid. There is no change in temperature during this phase transition, however the heat required to accomplish the phase transition is much greater than the specific heat capacity. The heat needed to convert unit mass of a substance from solid to liquid is often referred to as heat of fusion, denoted as ΔH_f, and the heat of fusion of water is approximately 344.8 J/g. When the melting is completed, a further addition of heat is required to raise the temperature of the water based on the specific heat capacity of liquid water, that is 4.186 J/°C/g. Figure 2.34 summarizes the relation between the heat and the temperature of water. The specific heat capacity of ice and liquid water represent the slopes of the heat and temperature graph.

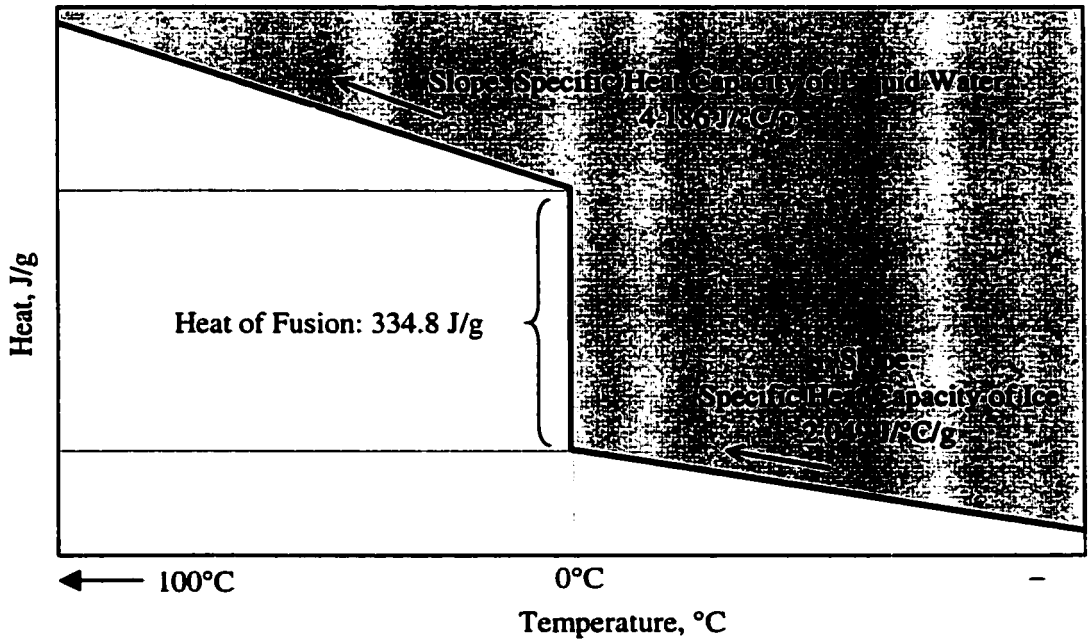

Fig. 2.34 Relation between the heat absorbed or released and the temperature of water

2.5.2.2 Apparent Specific Heat Capacity

The DSC measures the heat flow at a constant rate of temperature change. This is the heat absorbed or released for a given time interval, or dq/dt. Then, as the rate of temperature change dT/dt, is constant, the measured heat flow is converted to the heat for a given temperature interval per unit mass. This is referred to as an apparent specific heat capacity and is determined as follows;

$$c_A = \frac{\frac{dq}{dt}}{\frac{dT}{dt} \cdot m} \tag{2.55}$$

$$= \frac{dq}{dT} \cdot \frac{1}{m} \tag{2.56}$$

where c_A = apparent specific heat capacity, J/°C/g

The reason for the term "apparent" is owing to the heterogeneity of cement paste during the freezing and thawing process, consisting of ice and supercooled water which have different values of specific heat capacity. Since the heat required for the phase transitions is relatively large, the phase transitions appear as peaks in the plot of the apparent specific heat capacity versus temperature. Figure 2.35 is a typical plot, obtained from the DSC measurement, of the apparent specific heat capacity versus temperature for a cement paste specimen subjected to a freezing and thawing cycle. The apparent specific heat capacity remains constant as the temperature decreases, since the rate of heat released from cement paste is constant. As soon as a part of the pore water in the cement paste specimen starts freezing, a large amount of heat is released without a temperature change, resulting in a peak as shown in Fig. 2.35; the remaining pore water remains supercooled.

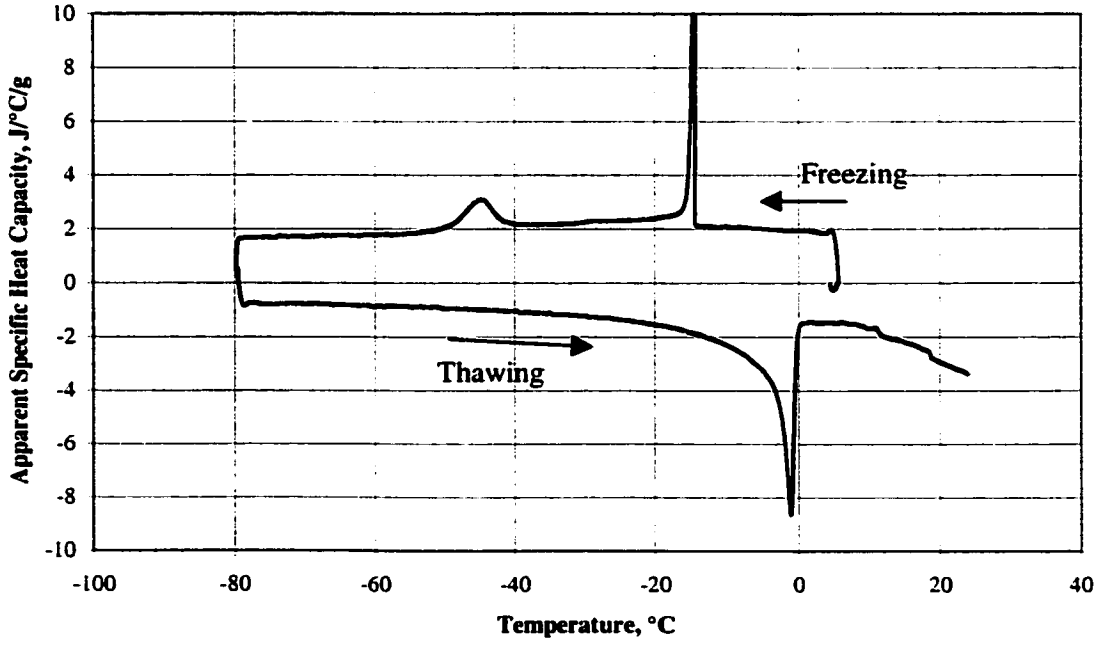

Fig. 2.35 A typical DSC plot of cement paste subjected to a freezing and thawing cycle

The area under this peak with a linear baseline in the plot of the apparent specific heat capacity versus temperature is the amount of heat released per unit mass of cement paste owing to the phase transition. It can be expressed mathematically as follows;

$$q_P = \int_T c_A dT = \frac{1}{m}\int_T \frac{dq}{dT} dT \tag{2.57}$$

where q_P = heat required for phase transition per unit mass of a substance, J/g

The actual amount of water frozen during the phase transition per unit mass of substance, wf can then be calculated from q_P as follows;

$$wf = \frac{q_P}{\Delta H_f} \tag{2.58}$$

where wf = the actual amount of water frozen during the phase transition, $g_{water}/g_{substance}$

ΔHf = heat of fusion of water, 344.8 J/g

The unit of wf is defined as $g_{water}/g_{substance}$ to indicate that the wf is the actual amount of water frozen per unit mass of cement paste specimen for a comparison purpose.

CHAPTER 3

EXPERIMENTAL

3.1 Introduction

Two basic experiments were employed; the AC impedance Spectroscopy (ACIS) coupled with the thermomechanical analysis (TMA), and the differential scanning calorimetry (DSC). The coupled ACIS-TMA experiment was designed to investigate the potential of the ACIS measurement, whereas the DSC experiment was designed to support the interpretation of phenomena observed in the coupled ACIS-TMA experiment. In this chapter, the experimental procedure and the specimen preparation method for the coupled ACIS-TMA and DSC experiments will be discussed.

3.2 The coupled ACIS-TMA Experiment

3.2.1 Experimental Setup

One of the main objectives was to investigate the potential of the ACIS measurement as a possible technique for determining the durability of cement paste to freezing and thawing. The ACIS was coupled with the TMA, since a comparison of these two measurements provides the effec-

tiveness of the ACIS measurement and its independent use as a durability indicator. The ACIS measures the response of the current flow with respect to an applied sinusoidal voltage, while the TMA simultaneously measures the length change with respect to temperature variation. A graphic illustration of the coupled ACIS-TMA experiment and a detailed sectional description of a temperature control chamber are provided in Figs. 3.1 (a) and (b) respectively.

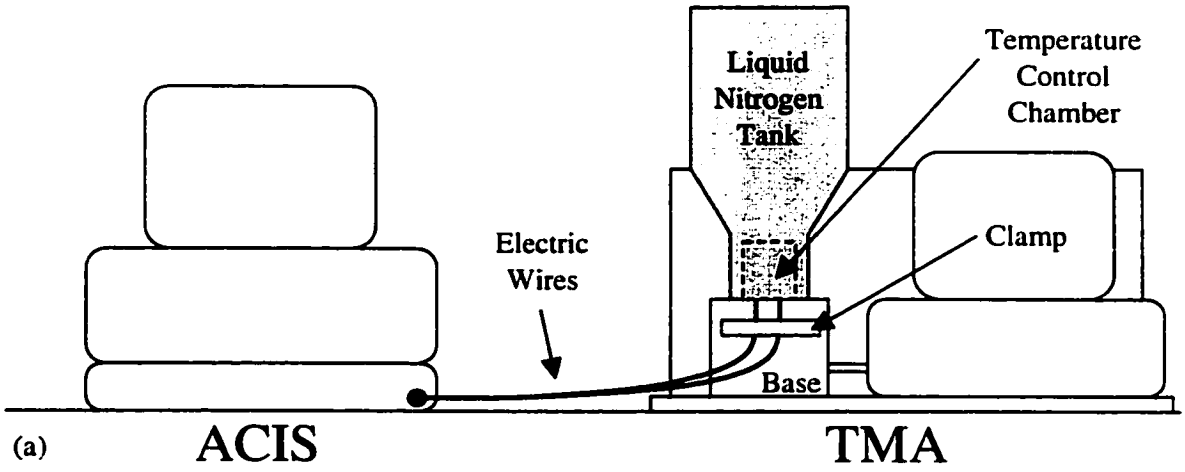

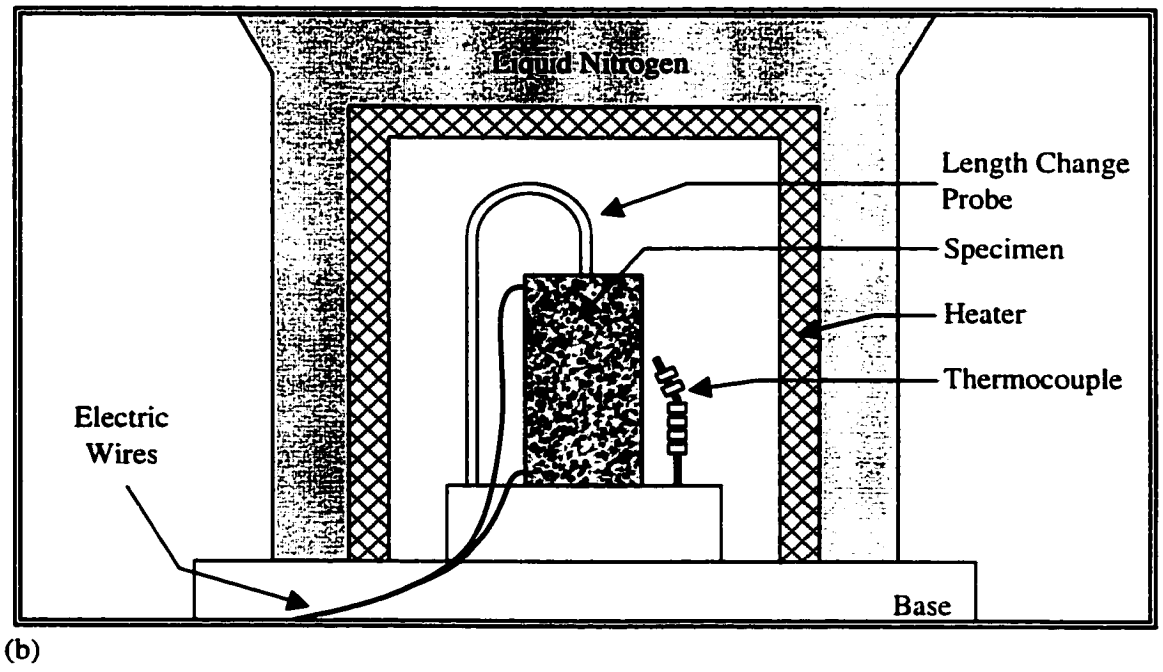

Fig. 3.1 (a) A graphic illustration of the coupled ACIS-TMA experiment and (b) A detailed sectional description of temperature control chamber

A liquid nitrogen tank and a heater mounted inside allow the temperature in the chamber to be controlled at the desired value and rate of change. The temperature in the chamber was monitored by a thermocouple installed next to a specimen as shown in Fig. 3.1 (b). The length change of the specimen was detected through the movement of the length change probe. Electric wires were soldered onto the electrodes cast in the specimen. The electric wires led from the temperature control chamber to connect with the ACIS data acquisition system. They were also clamped to the base of the temperature control chamber in order to avoid pulling down the specimen by their own mass.

The programmed temperature variation during the experiment was based on the air temperature of the chamber measured by the thermocouple installed next to the specimen. The difference between the air temperature and the temperature within the specimen was one of the concerns and was investigated by installing a cast-in thermocouple into the specimen to measure the temperature within the specimen. Figure 3.2 shows the air temperature measured by the TMA thermocouple and the specimen temperature measured by the cast-in thermocouple. The temperature difference of approximately 3°C – 5°C can be observed; however, the analysis of the experiments was conducted based on the air temperature of the chamber because of the following two reasons: the exact definition of the specimen temperature is rather ambiguous because a cement paste specimen itself consists of the C-S-H gel, water and ice; the air temperature surrounding the cement paste specimen would be practical upon the application of the ACIS technique in the field.

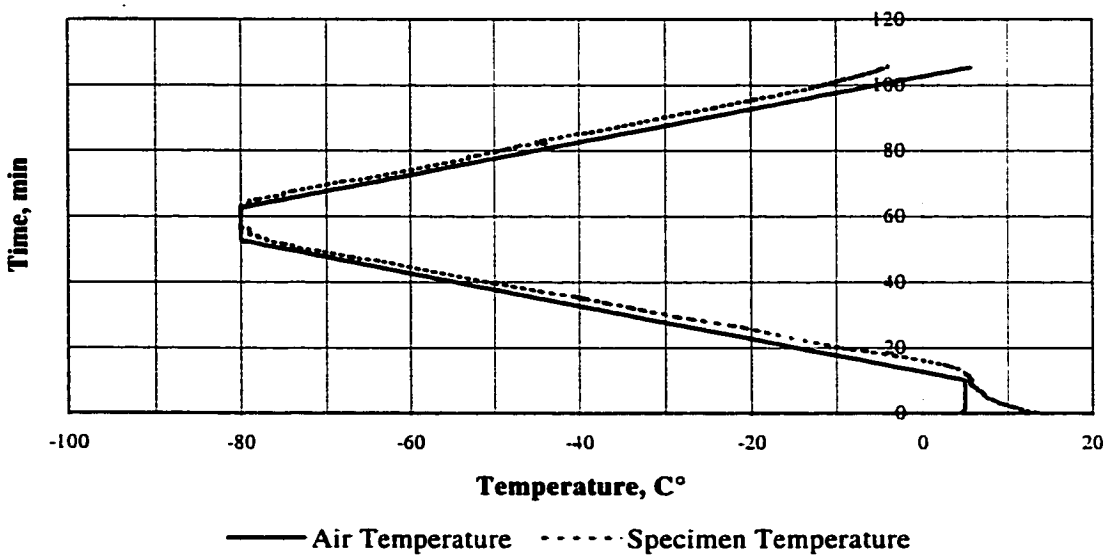

Fig. 3.2 An air temperature-time curve measured by the TMA thermocouple and a specimen temperature-time curve using a cast-in specimen thermocouple

The ACIS measurement was obtained using the Solartron SI 1260 Impedance / Gain-Phase Analyzer and was fit to the equivalent circuits using the ZView software. The TA Instruments Thermomechanical Analyzer 2940 was used to obtain the TMA measurement.

3.2.2 Experimental Procedure

The information for the desired temperature variation was input into the TMA computer, so that no additional operation was required during a freezing and thawing cycle once the experiment was initiated. The temperature variation of the freezing and thawing cycle was input as follows;

1. Equilibrate the chamber at +5°C
2. Hold isothermal condition at +5°C for 10 minutes
3. Decrease the temperature by 2°C/min to –80°C
4. Hold isothermal condition at –80°C for 10 minutes
5. Increase the temperature by 2°C/min to +20°C

After equilibrating the temperature of the chamber at +5°C, the temperature is held for 10 minutes to compensate for the difference between the temperature within the specimen and air temperature measured by the thermocouple. The temperature gradient of 2°C/min was chosen to avoid the substantial evaporation of moisture from the specimen. The rate was also chosen so as not to exceed a test time of 2 hours due to the maximum capacity of the liquid nitrogen tank. The temperature was lowered to –80°C, so that all the freezable water within a cement paste specimen would freeze. The raw TMA data were collected every 2 seconds.

The data acquisition for the ACIS measurement was initiated when the temperature in the chamber was equilibrated at +5°C. The raw data were taken every 74 seconds within a frequency range of 100 Hz – 5 MHz. The data were then fit to the equivalent circuits to obtain the high frequency arc and the depression angle parameter. Figure 3.3 is a plot of selected ACIS measurements at different values of temperature during the freezing process.

The specimen was surface-dried before loading, and its mass was measured before and after the experiment to monitor any evaporation of moisture from the specimen during the experiment. The values of the percentage loss of moisture of the specimen were in the range of 0.05% – 3.06%; which indicates no significant loss of moisture during the experiment.

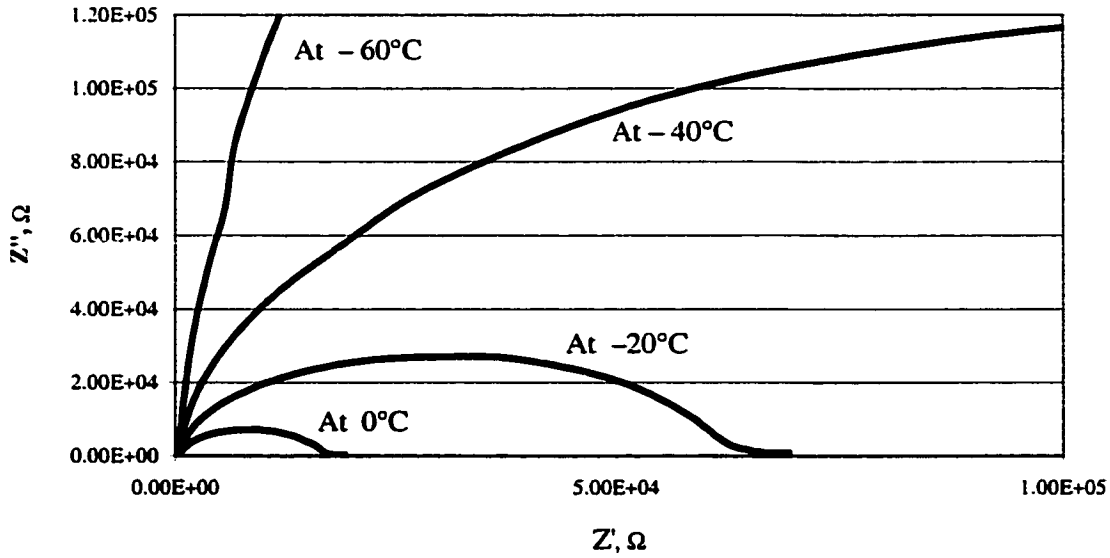

Fig. 3.3 ACIS measurements at different values of temperature

3.2.3 Materials and Specimen Preparation

The specimens were prepared to study the effect of three variables: w/c ratio, degree of hydration and wollastonite micro-fibre reinforcement. The specimens were prepared for w/c ratio 0.35, 0.40, 0.50 and 0.60 and were hydrated for 1, 3, 7 and 28 days. The variation of the wollastonite content was 0%, 5.1%, 8.1% and 10.2% by volume. Therefore, the test matrix comprised 64 different specimen conditions in total as listed in Table 3.1. The materials used for the experiment were Type 10 Portland cement supplied by Lafarge, Paris, France and the commercially available NYAD 'G' grade wollastonite micro-fibres obtained from NYCO Minerals, Inc., Willsboro, N.Y., USA.

As mentioned previously, the specimens were designed to facilitate the coupling of the ACIS measurement with the TMA measurement. The specimens were cylindrical, 9.64 mm in diameter and 19.05 mm in length as illustrated in Fig. 3.4 (a). Two stainless steel electrodes, on which electric wires were soldered, were cast into the end of each specimen. A plastic tube mould was used to prepare the specimen. It was slit at each end in order to install the two electrodes before casting a cement mix, Fig. 3.4 (b). The cement mix was prepared by a hand-made mixer and the mixing duration was one minute. The cement mix was then cast in three steps. The mould was

vibrated after each step to remove any air bubbles within the cement mix. Finally the specimen was capped and stored in a saturated calcium hydroxide solution. The specimen was demoulded the day following the casting and cured in the saturated calcium hydroxide solution for the desired hydration period.

Table 3.1 Test matrix for the cement paste specimens

Wollastonite Content, %	0															
w/c Ratio	0.35				0.40				0.50				0.60			
Hydration Period [d]	1	3	7	28	1	3	7	28	1	3	7	28	1	3	7	28
Wollastonite Content, %	5.1															
w/c Ratio	0.35				0.40				0.50				0.60			
Hydration Period [d]	1	3	7	28	1	3	7	28	1	3	7	28	1	3	7	28
Wollastonite Content, %	8.1															
w/c Ratio	0.35				0.40				0.50				0.60			
Hydration Period [d]	1	3	7	28	1	3	7	28	1	3	7	28	1	3	7	28
Wollastonite Content, %	10.2															
w/c Ratio	0.35				0.40				0.50				0.60			
Hydration Period [d]	1	3	7	28	1	3	7	28	1	3	7	28	1	3	7	28

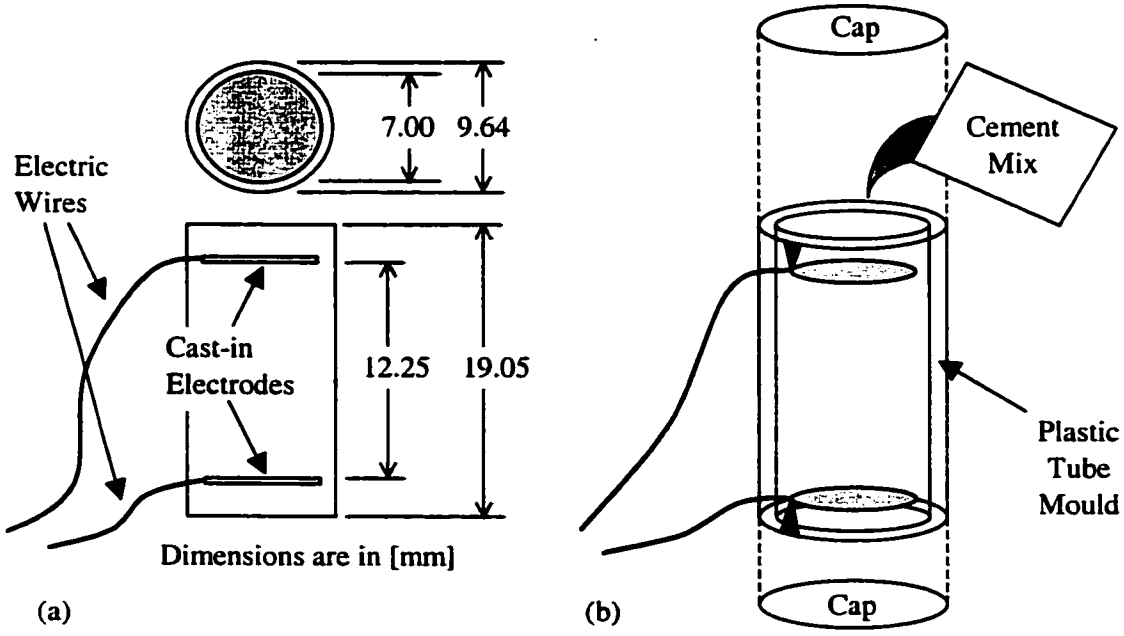

Fig. 3.4 Specimen configuration and preparation: (a) Specimen configuration and (b) Specimen preparation details

3.3 The DSC Experiment

3.3.1 Experimental Setup

The DSC experiment was designed to support the interpretation of phenomena observed in the coupled ACIS-TMA experiment. The DSC is a device to measure heat flow into or out of a substance as a function of temperature and time for the desired temperature variation. A schematic of the DSC experiment and a detailed description of the test chamber are illustrated in Figs. 3.5 (a) and (b) respectively. The DSC is operated with a computer that controls the temperature variation inside the test chamber of the DSC. There are two pans in the DSC test chamber: the sample pan, holds a specimen to be tested; the reference pan, is left empty, as illustrated in Fig. 3.5 (b). The pan itself is aluminum. The capable range of the temperature variation is approximately from −180°C to 600°C. The base on which each pan is located possesses a heater and thermocouple underneath. The heater and surrounding liquid nitrogen allow the two pans in the test chamber to follow the programmed temperature variation. For instance, if the temperature was set to be lowered from −10°C to −40°C in 10 minutes, the heater needs to compensate for the cooling effect of the liquid nitrogen surrounding the test chamber. The DSC measures the difference in heat generated from each heater to follow the temperature variation. The TA Instruments Differential Scanning Calorimetry 2910 was used to obtain the DSC measurement.

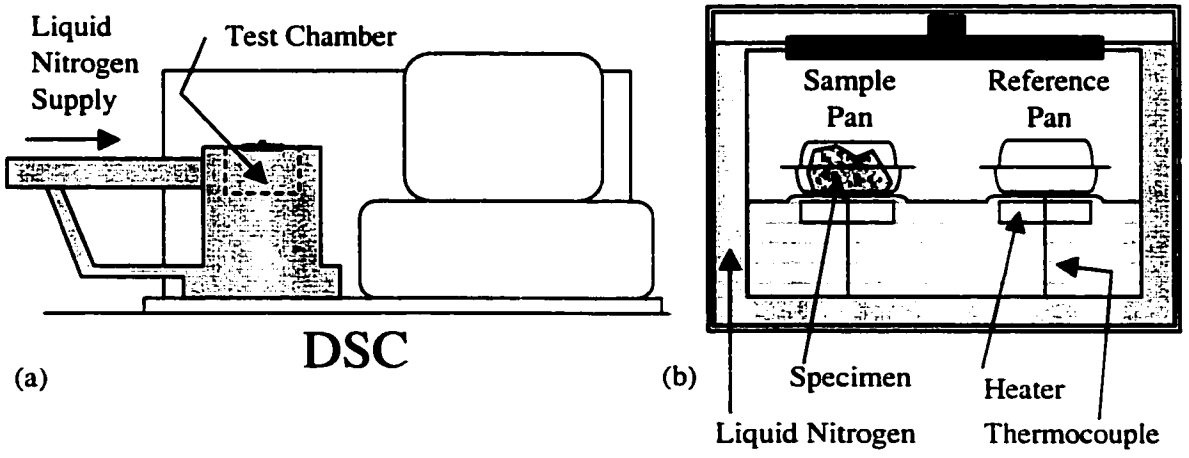

Fig. 3.5 (a) A schematic of the DSC experiment and (b) A detailed sectional description of the DSC test chamber

3.3.2 Experimental Procedure

The programmed temperature variation of the freezing and thawing cycle for the DSC experiment was set to be identical to the one for the coupled ACIS-TMA experiment.

1. Equilibrate the chamber at +5°C
2. Hold isothermal condition at +5°C for 10 minutes
3. Decrease the temperature by 2°C/min to –80°C
4. Hold isothermal condition at –80°C for 10 minutes
5. Increase the temperature by 2°C/min to +20°C

The pans were sealed with a manual compressor. Therefore there was less risk of losing moisture from the sample pan in the test chamber of the DSC experiment, Fig. 3.5 (b). The maximum capacity of the liquid nitrogen supply was much greater than the one for the coupled ACIS-TMA experiment. However, the temperature gradient of 2°C/min was chosen in order to be consistent with the coupled ACIS-TMA experiment. The raw DSC data were collected every 2 seconds.

A total mass of approximately 15 mg of the crushed specimen was sealed into the sample pan with the manual compressor. The reference pan was also sealed with the compressor and it was left empty. The mass of the sample pan was recorded before and after the experiment to monitor the loss of sample moisture from the pan. The values of the percentage loss of moisture from the sample pan were in the range of 0.04% – 2.59%; which indicates no significant loss of moisture during the experiment.

3.3.3 Materials and Specimen Preparation

The specimens were prepared to determine the effect of three variables: w/c ratio, degree of hydration and wollastonite micro-fibre reinforcement. They were identical to the ones prepared for the coupled ACIS-TMA experiment as listed in Table 3.1. The materials used for the specimens were from the same sources as used for the coupled ACIS-TMA experiment, i.e., the Type 10 Portland cement and the NYAD 'G' grade wollastonite micro-fibres. The specimen preparation method was exactly the same as the one for the coupled ACIS-TMA experiment except no electrodes were installed for the DSC experiment. The specimen was cured in the saturated calcium hydroxide solution for the desired hydration period, then crushed into small pieces and placed into the sealed sample pan.

CHAPTER 4

RESULTS AND DISCUSSION:

The Coupled ACIS-TMA Experiment

4.1 Introduction

The main objective of the coupled ACIS-TMA experiment was to investigate the potential of the ACIS measurement and its use to determine the durability of cement paste on freezing and thawing. The coupled ACIS-TMA experiment was designed to establish a possible relationship between the ACIS measurement and the TMA measurement. The TMA measurement provides the length change of a tested specimen subjected to freezing and thawing and is often used as a durability indicator. The schematic description of the ACIS-TMA experiment is shown in Fig. 1.1. The durability of the wollastonite micro-fibre reinforced cement paste with respect to freezing and thawing was also investigated applying the ACIS-TMA experiment. As mentioned previously, the coupled ACIS-TMA experiment focused on the cement paste specimens with variable wollastonite content, w/c ratio and degree of hydration. The test matrix is summarized in Table 3.1.

This chapter will discuss the results of the coupled ACIS-TMA experiment in three stages. First, a typical coupled ACIS-TMA measurement of one of the cement paste specimens will be chosen and its microstructural behaviour and mechanism of frost action occurring within the specimen will be interpreted in detail. Then, the coupled ACIS-TMA measurements obtained for the cement paste specimens will be compared in terms of w/c ratio and degree of hydration and the re-

lationship between the ACIS and TMA measurements will be established to investigate the potential of the ACIS measurement to determine the durability of cement paste on freezing and thawing. Finally, the durability of the wollastonite micro-fibre reinforced cement paste with respect to freezing and thawing will be discussed in terms of the results from the coupled ACIS-TMA measurements.

4.2 Microstructural Behaviour and Mechanism of Frost Action of Cement Paste Subjected to a Freezing and Thawing Cycle

4.2.1 TMA

The TMA is a very informative measurement; it provides the length change of cement paste subjected to a freezing and thawing cycle. The TMA measurement yields two important parameters: one is the total expansion and the other is the irrecoverable expansion. The total expansion reflects the total amount of water frozen in a cement paste specimen during a single freezing and thawing cycle. The irrecoverable expansion is the residual deformation after the single freezing and thawing cycle, which is often referred to as a durability indicator. The TMA measurement provides not only these two parameters, but also significant information enabling the interpretation of the microstructural mechanism of frost action of the cement paste specimen.

Figure 4.1 is a typical plot of length change versus temperature obtained from the TMA measurement for a cement paste specimen of w/c ratio 0.50 at 7 days hydration subjected to a freezing and thawing cycle. The temperature variation of the freezing and thawing cycle is described in Chapter 3. In this thesis, "the freezing and thawing cycle" refers to the same temperature variation, unless otherwise noted. In Fig. 4.1, the freezing process is described in the steps, A to F; the thawing process in the steps, F to H. Figures 4.2 (a) through (e) illustrate how ice formation takes place in a cement paste specimen during the freezing and thawing cycle. The letters A – E correspond to those in Fig. 4.1. Saturated capillary pores and the C-S-H gel are represented as shown in Fig. 4.2 (a). It should be noted that there are saturated gel pores within the C-S-H gel. As mentioned in Chapter 2, the mechanism of frost action is complex and various phenomena occur si-

multaneously. However, a possible explanation for each section of the graph in Fig 4.1 is as follows;

Freezing section of Fig. 4.1:

A ~ B: A cement paste has a positive coefficient of thermal expansion like most engineering materials. Accordingly the specimen contracts as the temperature decreases. The specimen continues to contract until point B in Fig. 4.1, approximately at –7°C, indicating that the water in the specimen remains unfrozen even below the normal freezing temperature of water. The depression of the freezing point has occurred.

B ~ C: A sudden expansion occurs between point B and C. This indicates that the initial freezing has occurred in the relatively large capillary pores (50 – 100 nm) of the specimen. This is illustrated in Fig. 4.2 (b). The nucleation of ice (ice nuclei are denoted as black dots) is initiated at one point in the capillary pores; ice crystals then grow until they reach the pore wall. The water is pushed out of the capillary pores generating a hydraulic pressure; ice formation results in a 9% increase in volume. The growth of ice crystals in the supercooled water is extremely rapid. The velocity of ice crystal growth in the supercooled water simulated in a glass capillary tube conducted by Hilling and Turnbull (1956) can be estimated as follows;

$$v_i = 0.16\,(\Delta T_S)^{1.7} \tag{4.1}$$

where v_i = velocity of ice crystal growth, cm/s

ΔT_S = total supercooling, °C

If the ΔT_S is 7°C, the velocity of ice crystal growth would be 4.4 cm/s. The velocity of ice crystal growth depends mainly on the pore size, since the water in the smaller pores experiences a greater degree of supercooling.

C ~ D: The specimen continues to expand as the temperature decreases further. The ice crystals in the large capillary pores continue to increase their volume and the ice nucleation occurs simultaneously in the relatively smaller capillary pores (10 – 50 nm), Fig. 4.2 (c). It is necessary to note that the expansion is caused also by the migration of water itself and it becomes more obvious when the temperature is held constant. Figure 4.3, taken from Powers and Helmuth (1953), illustrates the length change of cement paste when the temperature was lowered to –21.3°C and held constant. As soon as the cooling is ceased and

the temperature is held constant, the nucleation of ice ceases as well. However, the supercooled water in the gel pores migrates into the capillary pores and causes the expansion.

D ~ E: The water in most of the capillary pores has frozen when the temperature reaches point D. The water in the gel pores remains supercooled as illustrated in Fig. 4.2 (d). There is a slight increase in the rate of expansion between point D and E, as shown in Fig. 4.1. Recalling the phase diagram of water in Fig. 2.11, water can become supercooled to –40°C without any ice nucleation at a relatively low pressure. Then as the temperature decreases further in the cement paste specimen and the water becomes more supercooled, the pressure increases as well. This indicates that the freezing of water in most capillary pores is completed at –40°C and as the temperature decreases further, the water in the gel pores starts to freeze and generates the higher pressure. This causes the higher rate of expansion as observed in Fig. 4.1. At point E, the freezing of the water in most of the gel pores has completed, Fig. 4.2 (e). It should be noted that there is a portion of water including the gel water that has never frozen during the entire freezing process.

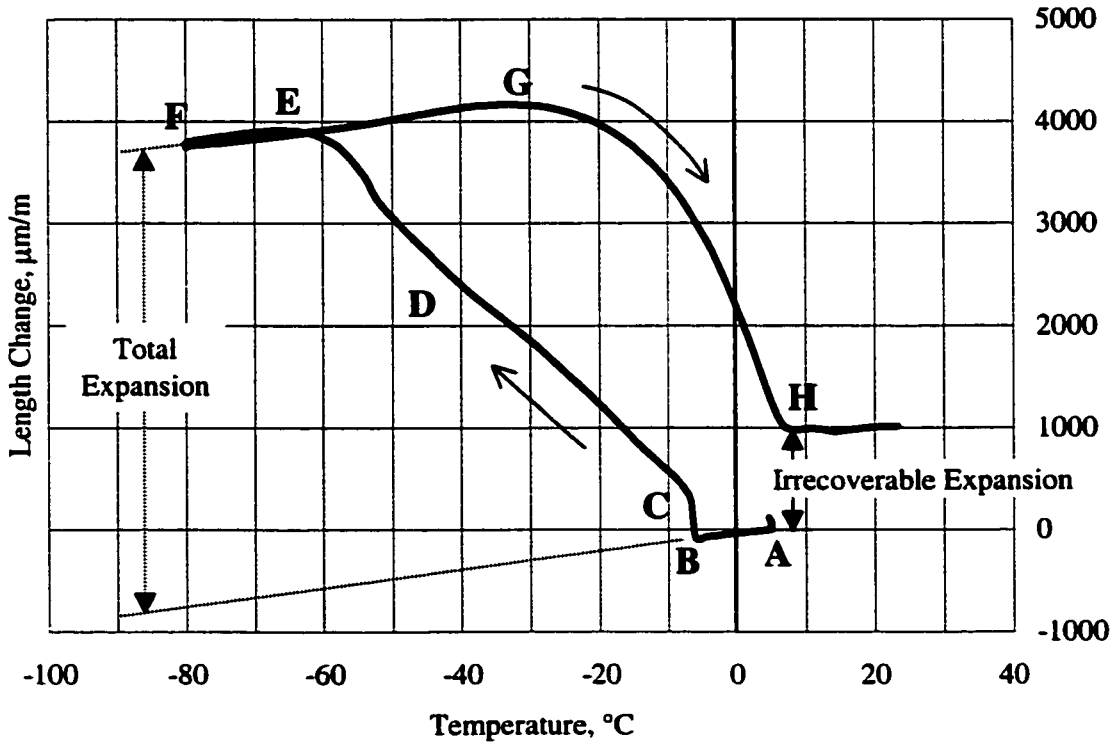

Fig. 4.1 *A typical plot of length change versus temperature obtained from the TMA measurement for a cement paste specimen of w/c ratio 0.50 at 7 days hydration subjected to a freezing and thawing cycle*

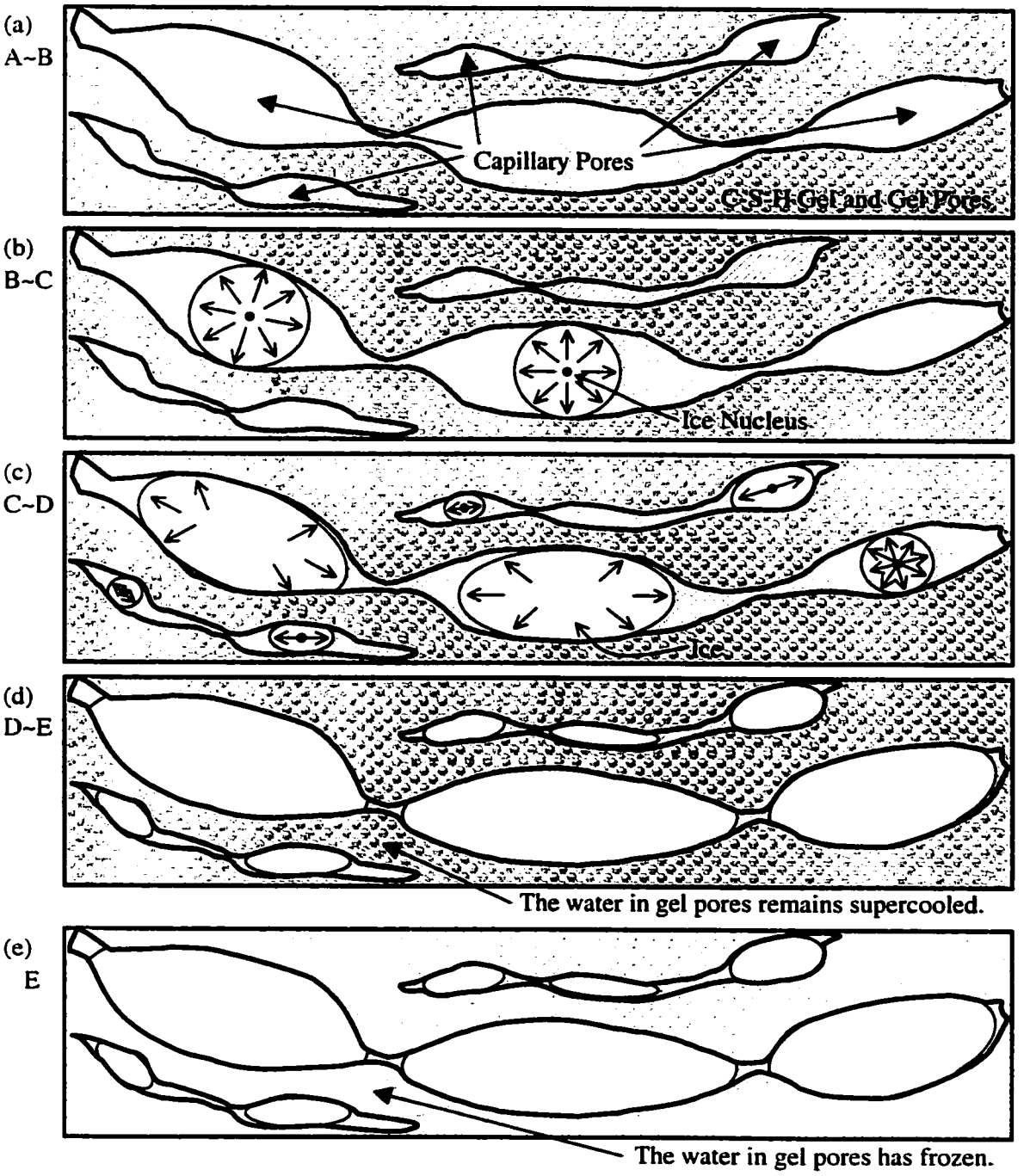

Fig. 4.2 *A schematic description of ice formation in a cement paste specimen corresponding to positions on the length change versus temperature curve, shown in Fig. 4.1*

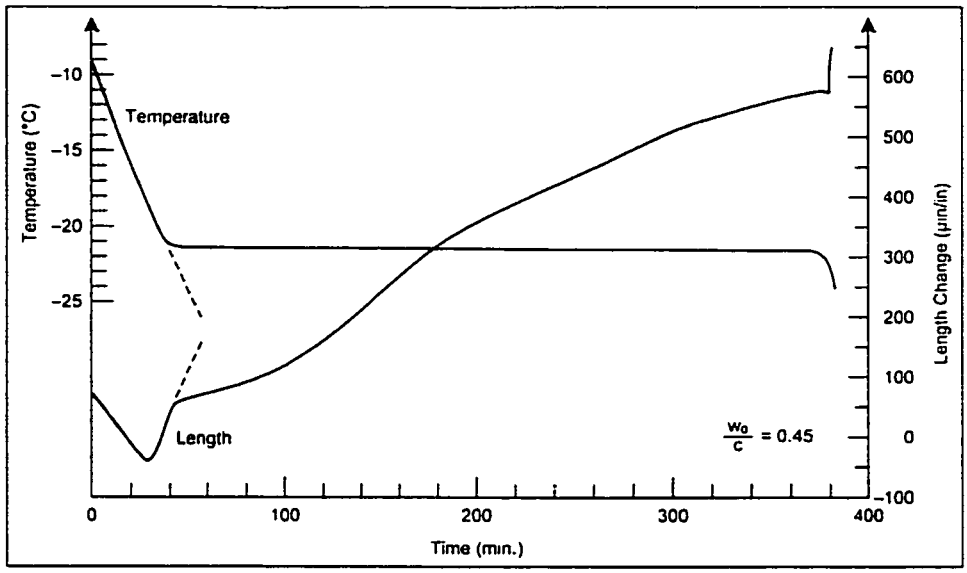

Fig. 4.3 Length change of cement paste at constant temperature

E ~ F: The specimen behaves as a homogeneous solid upon the completion of freezing. It therefore contracts as the temperature further decreases. The total expansion caused during the freezing can be defined by the length shown in Fig. 4.1, which is the vertical distance between F and the linear extension of A – B. The total expansion represents the total amount of water frozen, or freezable water, in the cement paste specimen.

Thawing section of Fig. 4.1:

F ~ G: An expansion of the specimen from F – G has occurred as a homogeneous solid as the temperature increases, indicating no thawing.

G ~ H: On thawing, similarly to freezing, the water in the pores does not melt at precisely 0°C owing to the depression of the melting temperature. The melting starts from point G at about –30°C, indicating that the melting is progressive and does not take place merely at 0°C. There is also a gap between the freezing and thawing temperature. In other words, the water in the pores does not melt at the temperature it freezes but melts at a higher temperature. Refer to the phase diagram in Fig. 2.11. The melting starts at the temperature at which the corresponding pressure becomes equivalent to the one on freezing, because the pressure generated on freezing remains constant until the melting occurs. The hysteresis caused after the freezing and thawing cycle can be defined as the irrecoverable expansion as shown in Fig. 4.1. The irrecoverable expansion indicates the extent of the damage the cement paste specimen has experienced after a single freezing and thawing

cycle, and reflects the durability of cement paste to freezing and thawing. Therefore a lower value of the irrecoverable expansion corresponds to a more durable cement paste.

The relation between the total and irrecoverable expansion, or the relation between the amount of freezable water and durability of cement paste will be discussed later.

4.2.2 ACIS

An investigation of the potential of an ACIS measurement to determine the durability of cement paste requires an understanding of the phenomena observed in the ACIS measurement. Two important characteristics to be focused on in the ACIS measurement are the high frequency arc and the depression angle parameter. The high frequency arc, shown in Fig. 4.4, yields two parameters. One is resistance R_1, which is the intercept on the real axis at the high frequency end. The other is resistance R_2, which is the diameter of the high frequency arc. The depression angle parameter can be obtained from the observed depression angle, ϕ_{dep}, which represents the extent to which the centre of the high frequency arc is depressed below the real axis. The significance of the high frequency arc and the depression angle parameter obtained from a typical ACIS measurement will be discussed in the following sections.

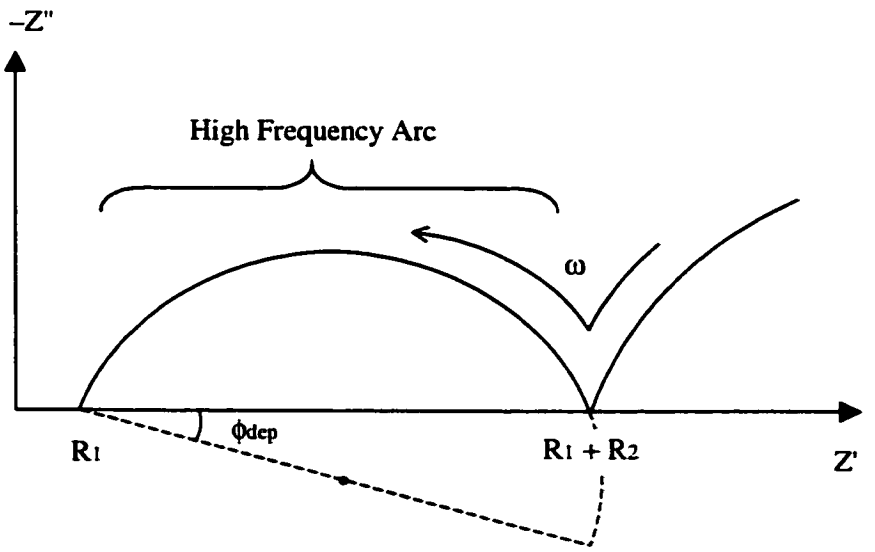

Fig. 4.4 The high frequency arc and depression angle of the ACIS measurement of a typical cement paste

4.2.2.1 The High Frequency Arc

The high frequency arc obtained from the ACIS measurement can be modelled by the equivalent circuit as shown in Fig. 2.31 (f). Recalling the mathematical expression of the equivalent circuit in Eq. (2.50);

$$Z = R_1 + \left(\frac{1}{\frac{1}{R_2} + j\omega C_d} \right) \tag{4.2}$$

At high frequencies, the capacitor, C_d conducts easily. The impedance, Z then becomes dependent on the resistance R_1. At low frequencies the capacitor C_d hardly conducts; the resistance R_2 becomes dominant. Xie et al. (1993) defined R_1 as the resistance of the pore water and R_2 and C_d are the resistance and capacitance of the C-S-H and pore water interface of cement paste at room temperature, respectively. Consider a cement paste subjected to a freezing process. The interpretation of these three parameters can be introduced as follows. Figure 4.5 (a) illustrates a pore in a cement paste before ice formation occurs. When an AC voltage is applied, R_1 represents the resistance of the pore water while R_2 and C_d represent the resistance and capacitance behaviour of the C-S-H and pore water interface, respectively. When the cement paste is subjected to freezing and the ice formation occurs, the C-S-H and pore water interface becomes the combination of the C-S-H and pore water interface and the C-S-H and ice interface as shown in Fig 4.5 (b). Because the values of R_2 and C_d of the C-S-H and ice interface are much greater than those of the C-S-H and pore water interface, the values of R_2 and C_d represent the resistance and capacitance of the C-S-H and ice interface. The value of R_1 represents the resistance of the unfrozen pore water. The value of R_1 is not affected by the C-S-H and pore water interface or the C-S-H and ice interface.

Figure 4.6 is a graph of resistance R_1 versus temperature for a cement paste specimen of w/c ratio 0.50 at 7 days hydration subjected to the freezing and thawing cycle. As the temperature decreases, the value of R_1 decreases as well. This is owing to the fact that the pore water of cement paste contains dissolved substances such as alkalis and chlorides which act as the electrolytes. The ice formed during a freezing process excludes these substances and results in a higher concentration of salts in the unfrozen pore water. Therefore, the charge can be carried more easily and results in a lower electrical resistance. At approximately –40°C, the value of R_1 stops decreasing and increases slightly as the temperature falls to –80°C. It should be noted that the value of R_1 represents the resistance of the unfrozen water either in the capillary pores or in the gel

pores. However, it was suggested that the freezing of the water in the capillary pores was completed at approximately –40°C. This implies that the value of R_1 below –40°C is an indicative of the resistance of the unfrozen water in the gel pores. The gel pores are sufficiently small that the migration of the water and the movement of the ions are limited, resulting in an increase of the electrical resistance. On thawing, the value of R_1 does not return to its value before freezing occurred, indicating that the dilation process of thawing of ice is affected. Microstructural changes of the cement paste specimen caused by the freezing might be a contributing factor.

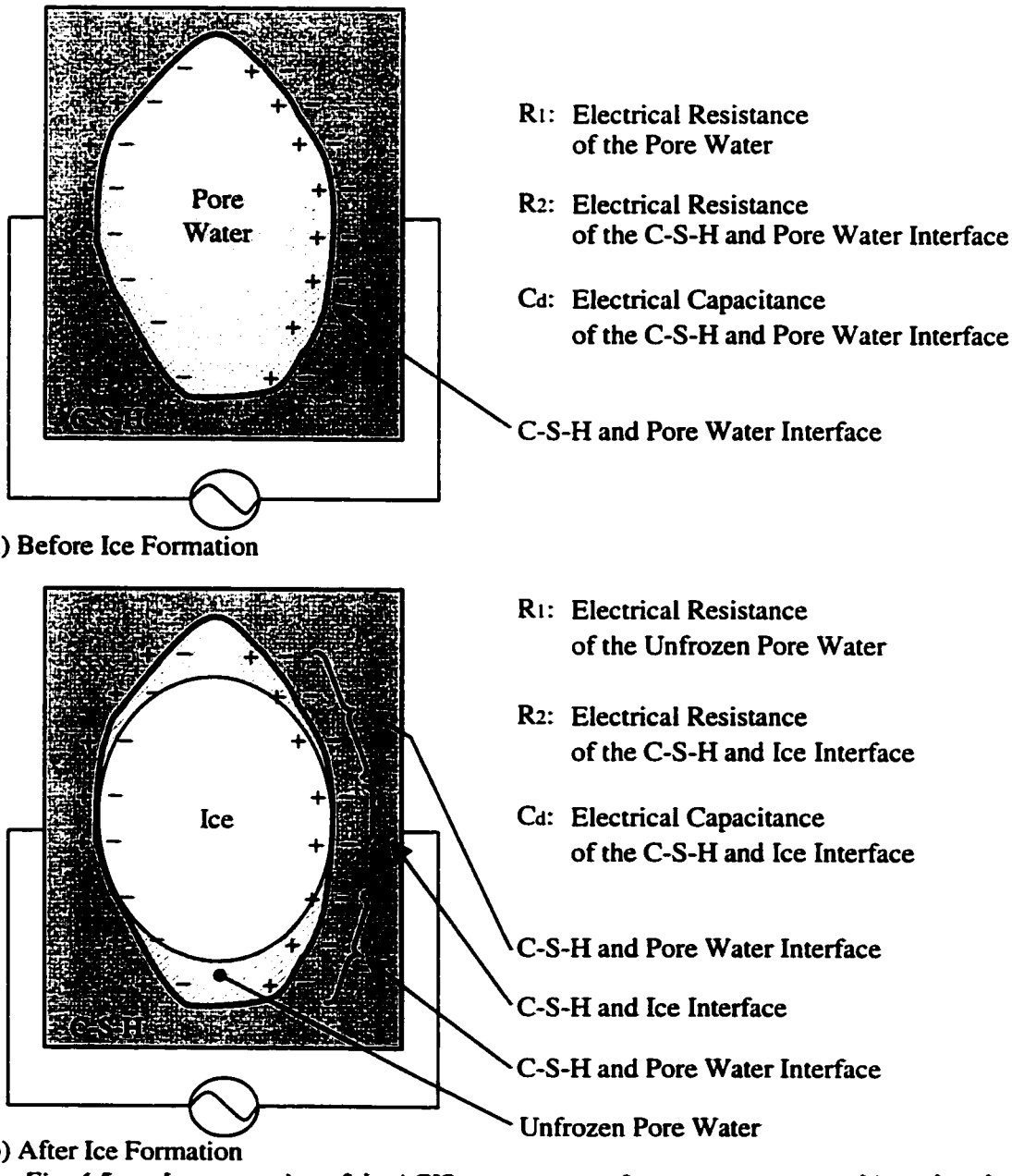

Fig. 4.5 Interpretation of the ACIS measurement for a cement paste subjected to the freezing and thawing cycle

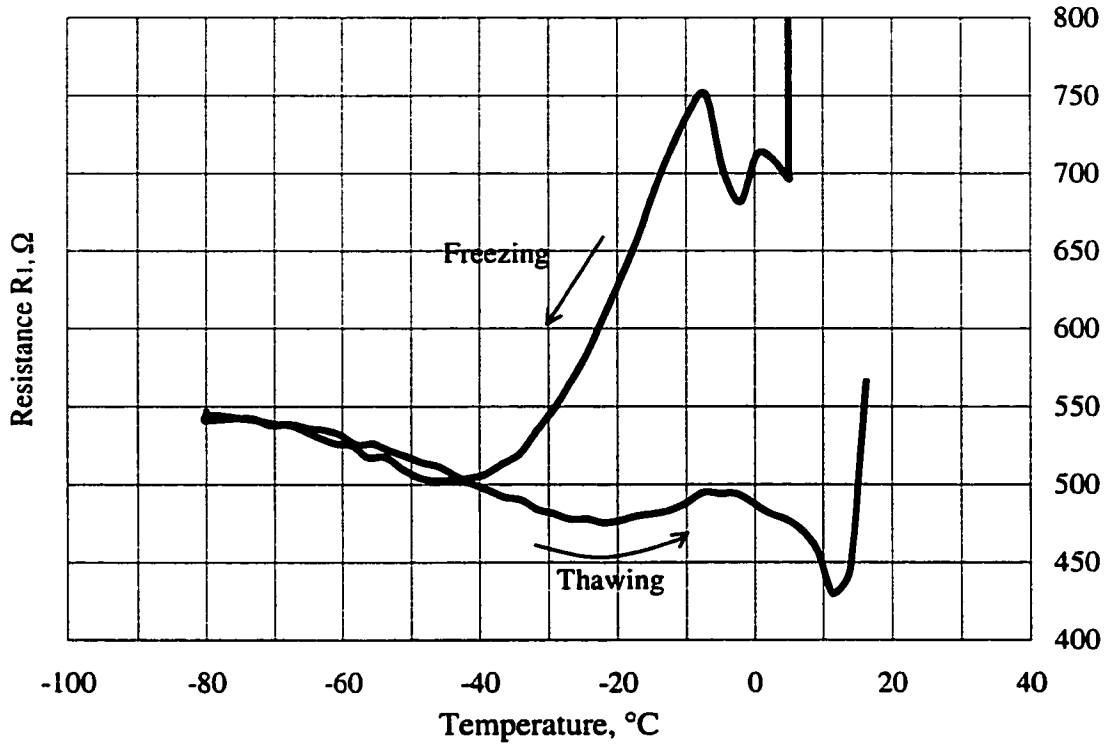

Fig. 4.6 Resistance R_1 versus temperature for a cement paste specimen of w/c ratio 0.50 at 7 days hydration subjected to the freezing and thawing cycle

The resistance R_2 is the resistance of the C-S-H and pore water interface of cement paste before ice formation and the resistance of the C-S-H and ice interface after ice formation. The value of R_2 can be best described on a logarithmic scale as shown in Fig. 4.7. Figure 4.7 is a plot of resistance R_2, on a logarithmic scale, versus temperature for a cement paste specimen of w/c ratio 0.50 at 7 days hydration subjected to the freezing and thawing cycle. Unlike the behaviour observed in the TMA measurement, the value of R_2 increases as soon as the temperature starts decreasing even before ice formation occurs. Its rate of change increases when ice formation is initiated approximately at –7°C. This indicates the beginning of the freezing of the water in the capillary pores. Then the value of R_2 continues to increase semi-logarithmically. As the interfacial area of the C-S-H and pore water changes to that of the C-S-H and ice, its resistance increases. The value of R_2 does not indicate differences between the freezing in the capillary pores and the freezing in the gel pores as apparently is the case for the TMA measurements or the value of R_1.

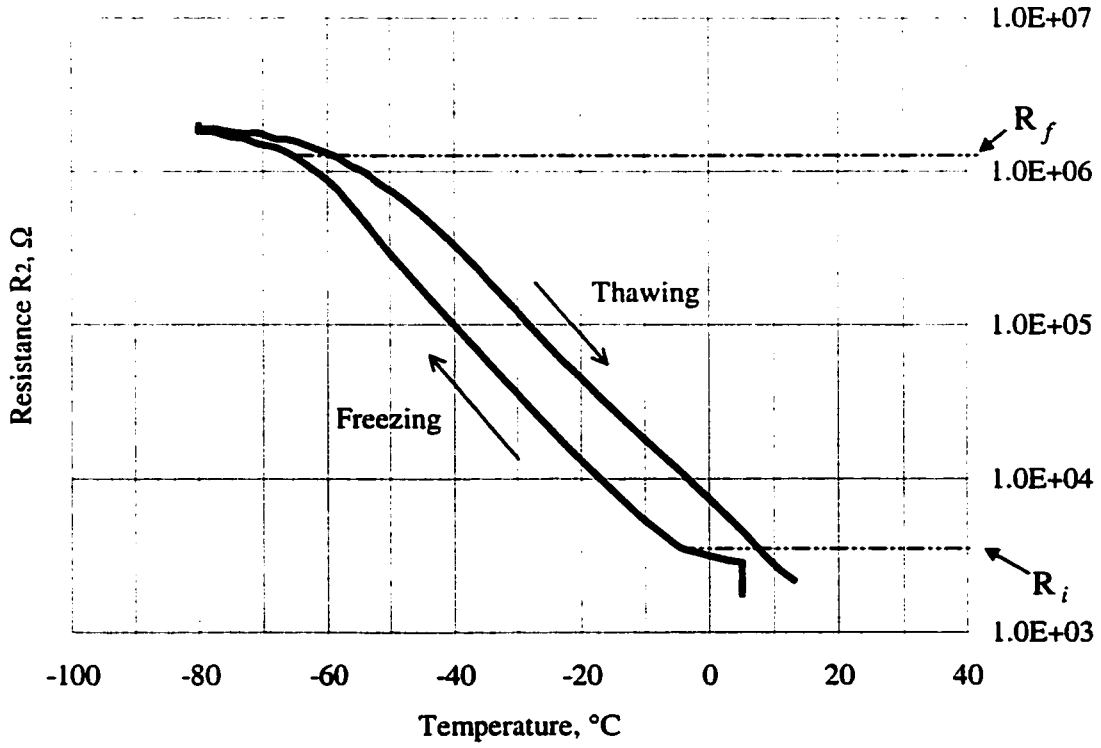

Fig. 4.7 *Resistance R2, on a logarithmic scale, versus temperature for a cement paste specimen of w/c ratio 0.50 at 7 days hydration subjected to the freezing and thawing cycle*

The slope of the graph in Fig. 4.7 between 5°C and –7°C and the one between –65°C and –80°C on freezing are approximately equal, indicating that the freezing of the water has completed at –65°C. This is equivalent to what was shown in the TMA measurement, Fig 4.1. An increase in the resistance R2 between –7°C and –65°C is caused by the freezing of the water. A resistance ratio, λ_R can then be introduced as follows;

$$\lambda_R = \frac{R_f}{R_i} \tag{4.3}$$

where λ_R = resistance ratio

R_f = resistance at completion of freezing of water, Ω

R_i = resistance at beginning of freezing of water, Ω

For all of the cement paste specimens, R_f and R_i can be defined as a value of resistance at –65°C and –7°C, respectively for the comparison purpose. For instance, the resistance ratio, λ_R taken from Fig. 4.7 is calculated as follows;

$$\lambda_R = \frac{R_f}{R_i} = \frac{1{,}297{,}535\,\Omega}{6{,}179\,\Omega} = 210.0 \tag{4.4}$$

The value of λ_R provides an index of the amount of resistance increase, and hence the amount of freezable water. The amount of freezable water obtained from the resistance R_2 can be related to the one obtained from the TMA measurement and is therefore related to the durability of cement paste. This relation will be discussed later.

Consider the following observation related to a thawing process. According to Fig. 4.1, the thawing does not occur until about –30°C. However, the value of R_2 begins to decrease as soon as the temperature starts to increase. This implies that there might be some melting occurring before point G in Fig. 4.1. The pores where the melting has occurred may have been so small that the contraction caused by melting between F and G was dominated by the expansion of the specimen itself.

4.2.2.2 The Depression Angle Parameter

The depression angle parameter is the other important parameter obtained from the ACIS measurement. It does not indicate the amount of freezable water or the durability of cement paste. However it provides valuable information for further understanding of the complex mechanism of frost action within a cement paste specimen during a freezing and thawing cycle. The depression angle parameter measures the extent that the semicircle is depressed below the real axis of the complex plot as shown in Fig. 4.4. It has a value of 1.00 when there is no depression (an ideal semicircle), and its value decreases as the depression angle, ϕ_{dep} increases because of their inverse relation shown in Eq. (2.51). As mentioned in Chapter 2, the depression angle parameter originates from the heterogeneity and roughness of an interface. As the interface becomes more heterogeneous and rough, the depression angle parameter decreases. Conversely, as the interface becomes less heterogeneous and rough, the depression angle parameter approaches 1.00. The heterogeneity and roughness of the interface interpreted from the depression angle parameter can

provide the explanation in detail for the behaviour of the cement paste specimen subjected to the freezing and thawing cycle.

Figure 4.8 is a plot of the depression angle parameter versus temperature for a cement paste specimen of w/c ratio 0.50 at 7 days hydration subjected to the freezing and thawing cycle. The depression angle parameter starts with a value of approximately 0.953 at 5°C and decreases to 0.945 as the temperature decreases to –25°C. It then increases to about 1.00 as the temperature decreases to –80°C. The changes of the depression angle parameter associated with the temperature variation can be explained by the heterogeneity of the interface. Recalling Figs. 4.5 (a) and (b), the C-S-H and pore water interface of a cement paste specimen before ice formation transforms into a more complex interface that consists of the combination of the C-S-H and pore water interface and the C-S-H and ice interface when ice formation occurs. Let us define the "C-S-H interface" as the C-S-H and pore water interface before ice formation or the combination of the C-S-H and pore water interface and the C-S-H and ice interface after ice formation. The "C-S-H interface" at 5°C, in Fig. 4.5 (a), is the C-S-H and pore water interface, because the "C-S-H interface" consists merely of the C-S-H and pore water interface. The "C-S-H interface" is therefore said to be homogeneous. As the temperature decreases, however, ice formation is initiated in the capillary pores and the "C-S-H interface" becomes the combination of the C-S-H and pore water interface and the C-S-H and ice interface. The "C-S-H interface" is therefore said to be heterogeneous. This is illustrated in Fig. 4.5 (b).

As shown in Fig. 4.8, the depression angle parameter decreases since the "C-S-H interface" becomes more heterogeneous as ice formation takes place. At a temperature of approximately –25°C, however, the depression angle parameter starts to increase. When the C-S-H and ice interface occupies about 0% to 50 % of the "C-S-H interface", the increase of the C-S-H and ice interface results in the more heterogeneous "C-S-H interface" and thus the decrease in the depression angle parameter. When the C-S-H and ice interface starts to occupy more than 50 % of the "C-S-H interface", the increase of the C-S-H and ice interface results in the more homogeneous "C-S-H interface", because the C-S-H and ice interface becomes more dominant than the C-S-H and pore water interface. It results in an increase of the depression angle parameter. This is what is happening at a temperature of approximately –25°C. The C-S-H and ice interface becomes more dominant than the C-S-H and pore water interface at –25°C. Then the "C-S-H interface" changes from more heterogeneous to more homogeneous. Therefore, the depression angle parameter stops decreasing and starts increasing at this temperature.

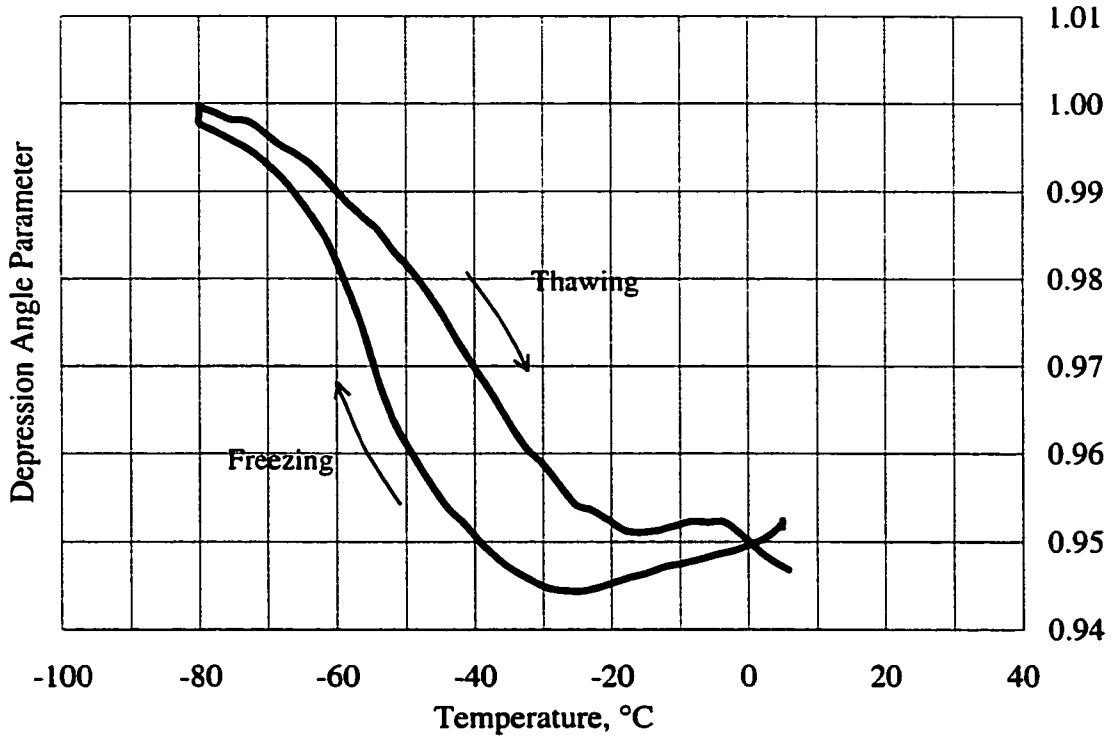

Fig. 4.8 The depression angle parameter versus temperature for a cement paste specimen of w/c ratio 0.50 at 7 days hydration subjected to the freezing and thawing cycle

The depression angle parameter continues to increase to approximately 1.00 as the C-S-H and ice interface occupies a greater proportion of the "C-S-H interface". However, there is a difference in the values between the depression angle parameter at 5°C and at –80°C. The depression angle parameter affected by the pores fully occupied by the C-S-H and pore water interface and fully occupied by the C-S-H and ice interface should be approximately equal in terms of heterogeneity of the interface. However, as shown in Fig. 4.8, the value of the depression angle parameter affected by the pores occupied by the C-S-H and pore water interface at 5°C is about 0.95, while the value for the C-S-H and ice interface at –80°C is close to 1.00. The reason could be related to the roughness of "C-S-H interface". Figure 4.9 is an illustration of the "C-S-H interface" of a capillary pore. Figure 4.9 (a) illustrates the C-S-H and pore water interface and Figure 4.9 (b) illustrates the C-S-H and ice interface, respectively. The C-S-H consists of small gel particles which may create a rough surface along the wall of the capillary pore as shown in Fig. 4.9 (a). When the water in the capillary pore freezes, shown in Fig. 4.9 (b), the "C-S-H interface" becomes less rough and thus the increase in the depression angle parameter. Furthermore, when the freezing takes place in the gel pores, it causes the surface of the C-S-H small particles less rough

and leads to the further increase in the depression angle parameter. Even between 5°C and –25°C, the "C-S-H interface" becomes less rough as soon as ice formation starts. However, the depression angle parameter decreases between 5°C and –25°C, because the effect of the heterogeneity of the "C-S-H interface" is more dominant than that of the roughness of the "C-S-H interface". When the temperature falls below –25°C, the "C-S-H interface" becomes less heterogeneous and rough, and results even in the higher depression angle parameter at –80°C than the one at 5°C.

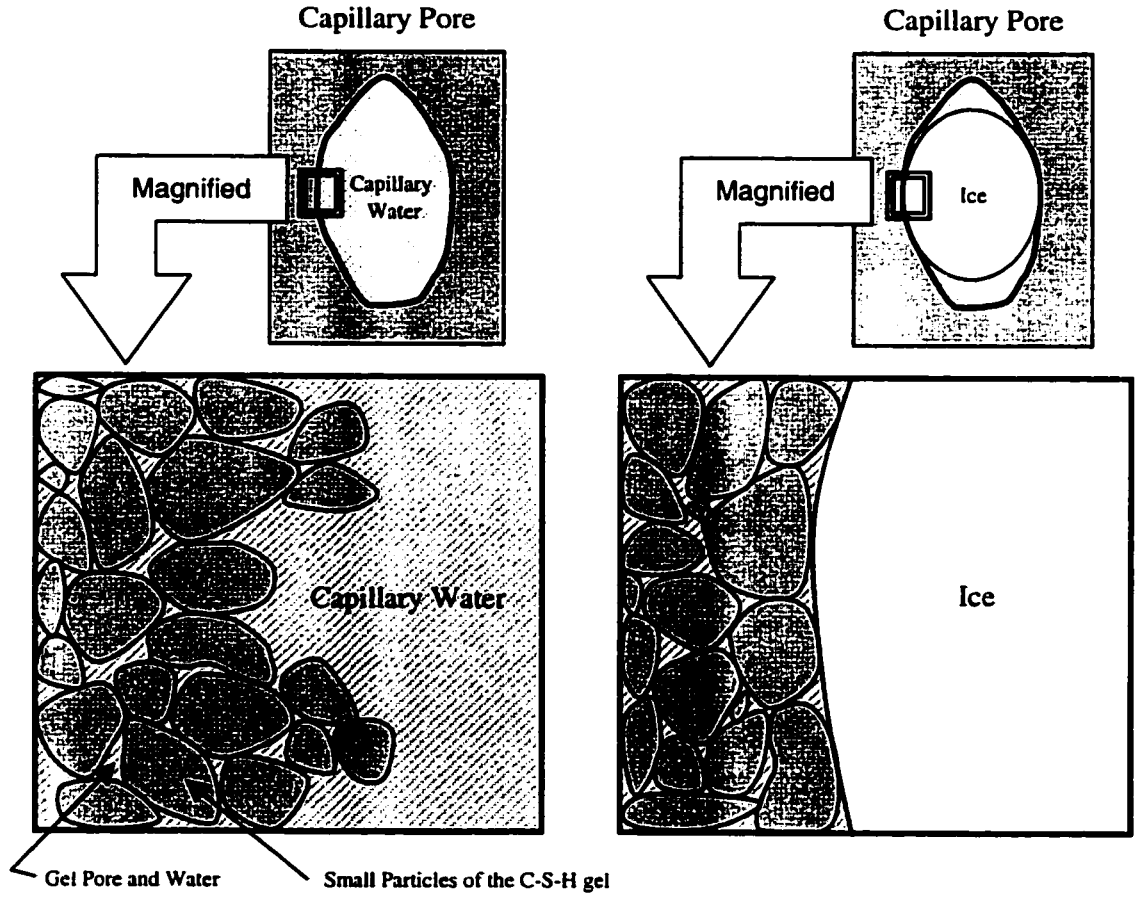

(a) C-S-H and pore water interface (b) C-S-H and ice interface

Fig. 4.9 Illustration of the "C-S-H interface" of capillary pore

The behaviour of the depression angle parameter associated with freezing is also described by Perron and Beaudoin (2002) as affected by the heterogeneity of a cement paste as a whole, that is, by the pore size distribution. First, Gu et al. (1994) observed that a pore system with a narrower pore size distribution resulted in a higher depression angle parameter, for example, porous glass with a pore size distribution narrower than that of cement paste exhibits this behaviour. The narrower pore size distribution indicates that the system has a more homogeneous pore size. Perron

and Beaudoin (2002) applied this observation to explain the increase of the depression angle parameter as ice formation takes place. A cement paste has a relatively broad pore size distribution. For instance, when ice formation is initiated in a large capillary pore and ice crystal fills the pore as shown in Fig. 4.5 (b), the unfrozen spaces of the pore can be considered as two smaller pores which would be uniform in size relative to other pores in which ice formation has not been initiated. Eventually, the unfrozen spaces of the cement paste at –80°C become very uniform, that is; the pore size distribution becomes narrower. The depression angle parameter, therefore, increases as the temperature decreases.

4.3 Effects of Water/Cement Ratio and Hydration Period

In the previous section, the mechanism of frost action of the selected cement paste specimen was interpreted from the coupled ACIS-TMA measurement. In this section, the coupled ACIS-TMA measurements will be compared for the cement paste specimens with respect to various w/c ratios and hydration periods. It is to establish the relationship between the ACIS and TMA measurements and to investigate the potential of the ACIS technique for determining the durability of cement paste on freezing and thawing. The cement paste specimens were prepared for w/c ratios of 0.35, 0.40, 0.50 and 0.60 and hydration periods of 1 day, 3 days, 7 days and 28 days.

4.3.1 TMA

The previous section explained the microstructural behaviour and mechanism of frost action within the selected cement paste specimen. In this section, the durability of the cement paste specimens to freezing and thawing will be discussed based on the total and irrecoverable expansion, defined previously in Section 4.2.1. The values of total and irrecoverable expansion for each cement paste specimen are shown in Appendix A. The TMA measurements of the cement paste specimens of w/c ratio 0.40 for 1 day, 3 days, 7 days and 28 days hydration periods are shown in Fig. 4.10. As described in the previous section, the cement paste specimens expand, at any stage of hydration, when they are subjected to the freezing process.

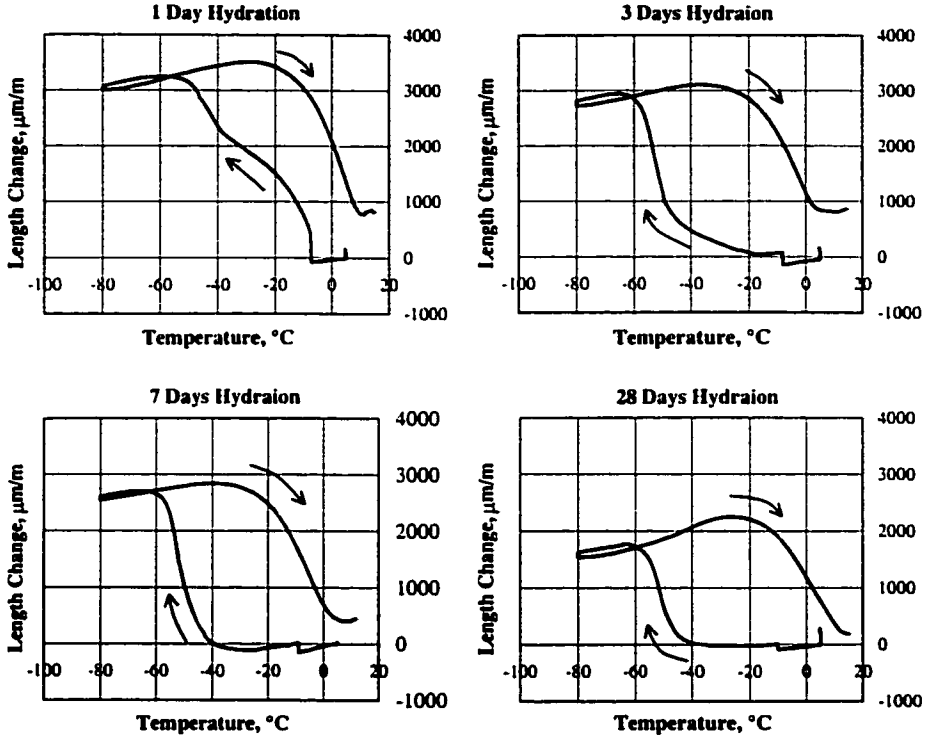

Fig. 4.10 Length change versus temperature for the cement paste specimens of w/c ratio 0.40 at 1 day, 3 days, 7 days and 28 days hydration

Figure 4.10 shows that as the degree of hydration increases, the total expansion decreases. In older cement paste specimens, there is less water which has not reacted with cement (capillary water); thus less freezable water to cause the total expansion. This is consistent not only for the specimens of w/c ratio 0.40, but also for the specimens of w/c ratio 0.35, 0.50 and 0.60. This can be observed in Fig. 4.11, which is the graph of the total expansion versus hydration period of w/c ratio 0.35, 0.40, 0.50 and 0.60. The total expansion decreases with the higher degree of hydration. However, the specimens of w/c ratio 0.60 had a unique behaviour. The total expansion of the specimens of w/c ratio 0.60 increases between 1 day and 7 days hydration. The total expansion at 28 days hydration, however, decreases as expected. There may have been some inhomogeneity in the specimens of w/c ratio 0.60 resulting from preparation of very high w/c ratio specimens. Figure 4.11 also indicates that, at each hydration period, the higher the w/c ratio, the greater is the total expansion. This is because the specimens with the higher w/c ratio have more freezable water, and thus greater total expansion. The irrecoverable expansion observed at the end of a freezing and thawing cycle is also dependent on the degree of hydration.

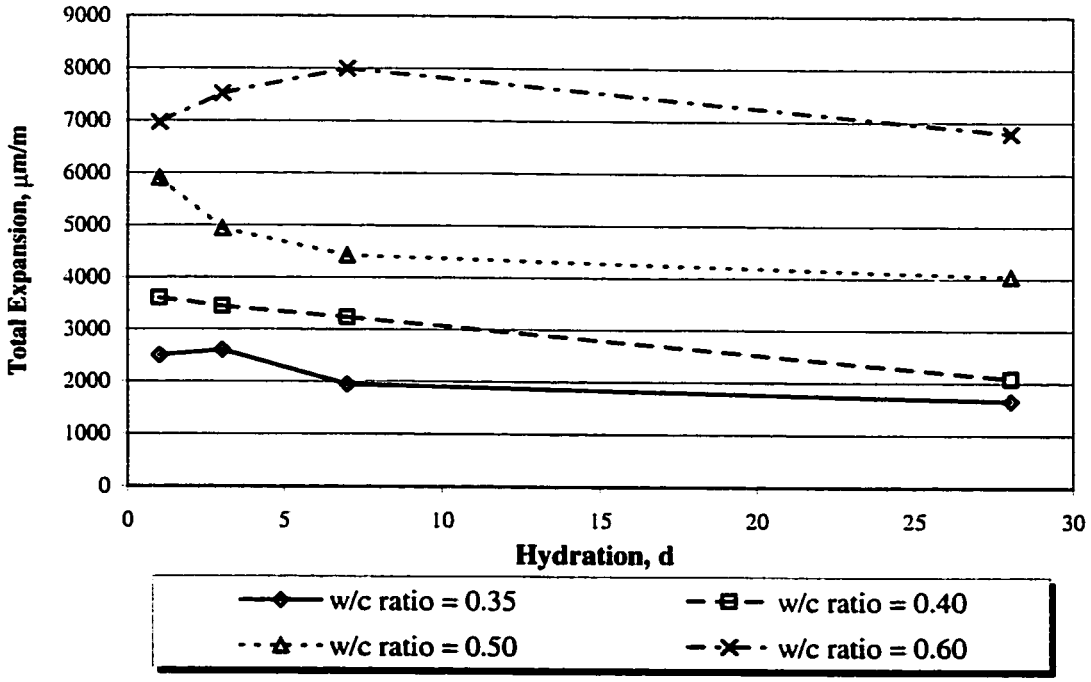

Fig. 4.11 Total expansion versus hydration period for various w/c ratios

Figure 4.12 is the graph of the irrecoverable expansion versus hydration period of w/c ratio 0.35, 0.40, 0.50 and 0.60. The cement paste specimens at the higher degree of hydration have less irrecoverable expansion and are more durable. Considering Figs. 4.11 and 4.12, it is clear that the amount of freezable water in a cement paste specimen obtained from the total expansion is the primary factor which determines its irrecoverable expansion, and hence durability.

It should be recalled that the amount of capillary water decreases and the amount of gel water increases as the hydration continues. These phenomena can be observed from Fig. 4.10 as well. The sudden expansion at approximately –8°C for each hydration period is caused by the freezing in the large capillary pores. At 1 day hydration, the sudden expansion is about 400 μm/m; it decreases to about 100 μm/m at 28 days hydration, indicating the presence of more capillary water in younger cement pastes. More expansion tends to occur below –40°C, as hydration takes place. This is because that the amount of capillary water, which freezes above –40°C, decreases with hydration and the amount of gel water, which freezes below –40°C, increases with hydration.

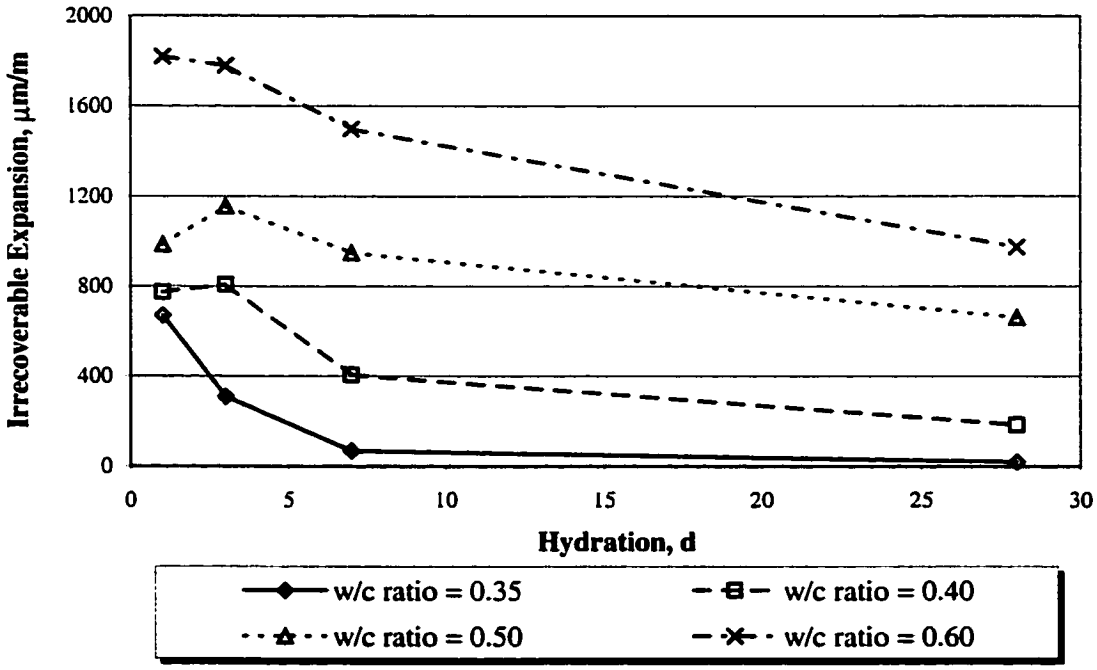

Fig. 4.12 Irrecoverable expansion versus hydration period for various w/c ratios

Figure 4.13 shows the length change versus temperature of the cement paste specimens of w/c ratio 0.35, 0.40, 0.50 and 0.60, at 28 days hydration. It is obvious that the cement paste specimens with the higher w/c ratio have the greater total and irrecoverable expansion. Most of the expansion that occurred for the cement paste specimens of w/c ratio 0.35 and 0.40 is caused by the freezing of gel water, since the most of the expansion occurred below –40°C, however, a relatively large expansion occurred above –40°C for the cement paste specimens of w/c ratio 0.50 and 0.60, indicating that there is still a large amount of capillary water in specimens of w/c ratio 0.50 and 0.60 even at 28 days hydration.

4.3.2 ACIS

4.3.2.1 Resistance R_2

The resistance R_2, obtained from the ACIS measurement provides useful information on the microstructural behaviour of the cement paste specimen during the freezing and thawing cycle. The amount of freezable water can be represented by the resistance ratio, λ_R defined earlier. This ratio is also related to the amount of freezable water obtained from the TMA measurement, and thus to

the durability of cement paste. In terms of investigation of durability, the value of R_2 is a more informative parameter than that of R_1. The value of R_2, therefore, is the focus of the discussion in the following section.

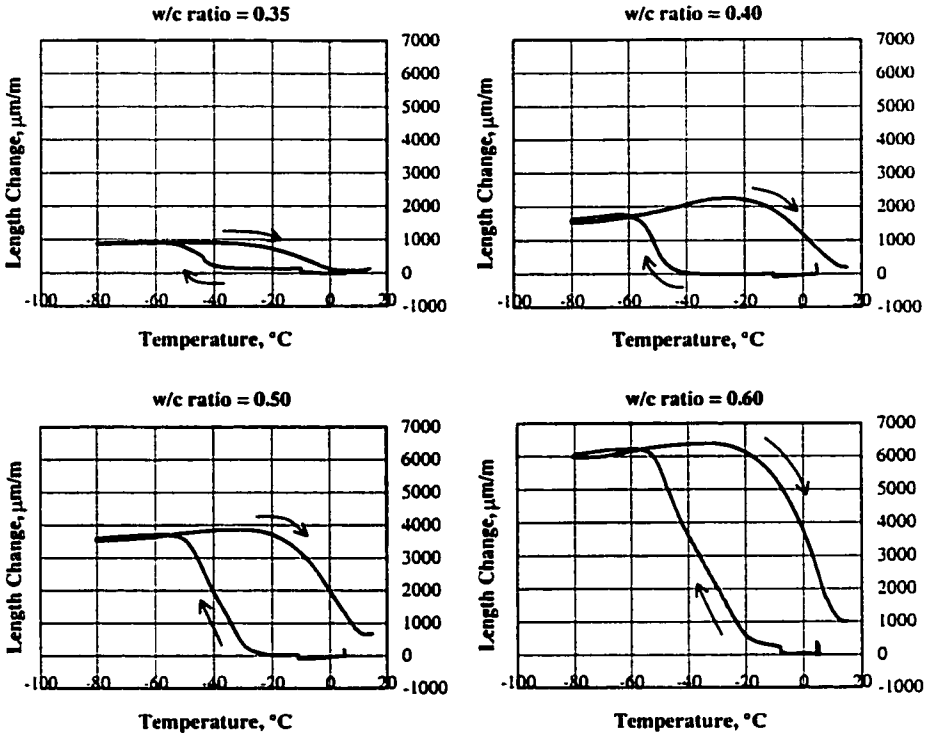

Fig. 4.13 Length change versus temperature for the cement paste specimens of w/c ratio 0.35, 0.40, 0.50 and 0.60 at 28 days hydration

Graphs shown in Fig. 4.14 are the plots of the resistance R_2, versus temperature for the cement paste specimens of w/c ratio 0.40 at 1 day, 3 days, 7 days and 28 days hydration. The value of R_2 is plotted on the logarithmic scale. The value of R_2, at 5°C, indicates the extent of hydration of the cement paste specimens. The value of R_2 at 5°C of the specimen at 1 day hydration is approximately 5,000 Ω whereas the one at 28 days hydration is 50,000 Ω.

This is simply owing to the fact that the cement paste specimen at 1 day hydration contains more capillary water and conducts more electricity than the one at 28 days hydration. The R_2 curve of the specimen at 1 day hydration increases almost constantly as the temperature decreases, whereas the R_2 curves of the other specimens have variations in their slopes. Since the cement paste specimen is very porous and not well developed at 1 day hydration, ice formation can take

place without much restriction by the C-S-H gel. Ice formation in older specimens occurs with less freezable water and a very different microstructure.

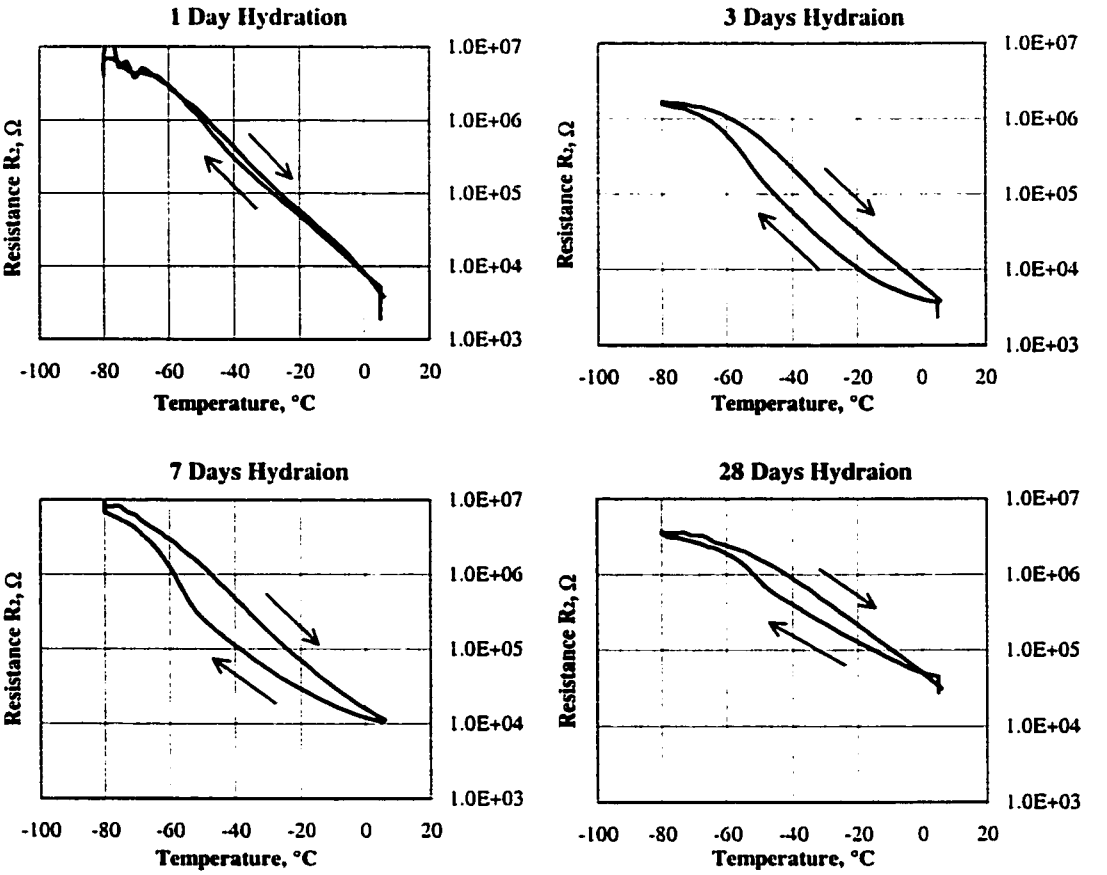

Fig. 4.14 Resistance R2 versus temperature for the cement paste specimens of w/c ratio 0.40 at 1 day, 3 days, 7 days and 28 days hydration

The resistance ratio, λ_R obtained from the resistance R2 corresponds to the amount of freezable water. The values of resistance ratio for each cement paste specimen were calculated and are shown in Appendix A. The resistance ratio, λ_R was calculated and plotted against the hydration period in Fig. 4.15 for the specimens of w/c ratio 0.35, 0.40, 0.50 and 0.60. It is clear that the value of λ_R decreases as hydration takes place, since the greater the hydration period, the lower is the amount of freezable water. The behaviour observed in Fig. 4.15 is similar to the total expansion observed in Fig. 4.11, because the total expansion obtained from the TMA measurement and the resistance ratio, λ_R from the ACIS measurement both represent the amount of freezable water in the cement paste specimen. In other words, since the total expansion corresponds to the

irrecoverable expansion representative of the durability of cement paste, the value of λ_R can also be considered as a meaningful parameter to investigate the durability of cement paste.

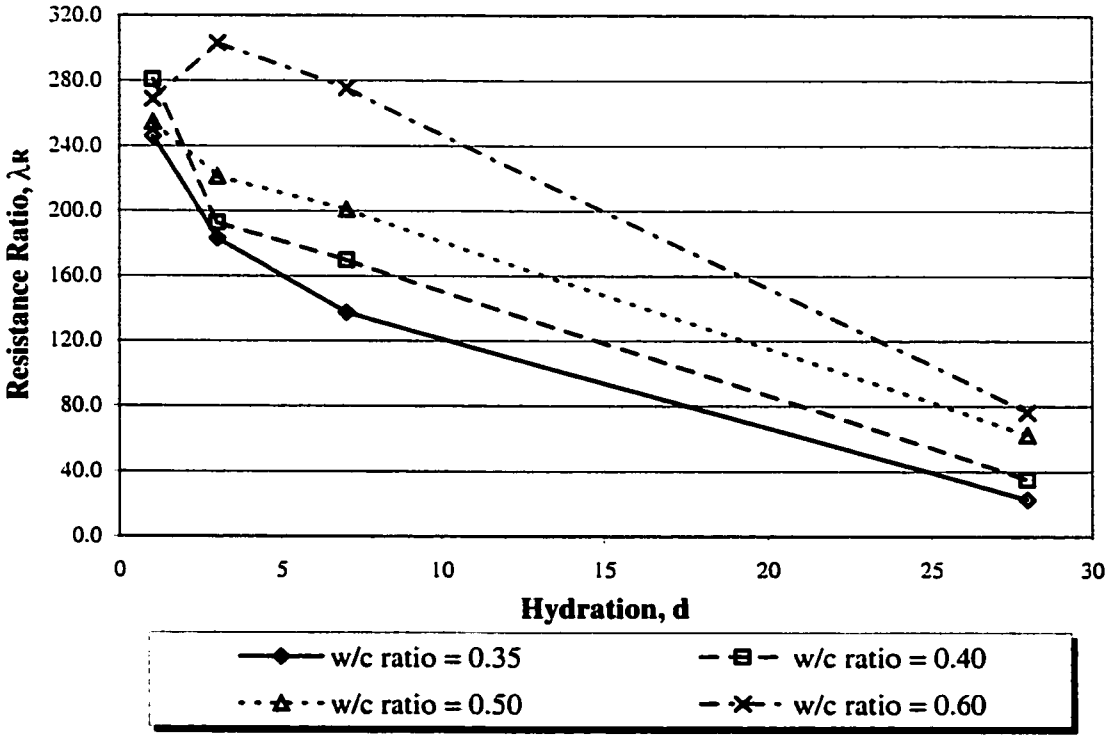

Fig. 4.15 Resistance ratio, λ_R versus hydration period for various w/c ratios

Figure 4.15 also indicates that the cement paste specimens contain a greater amount of freezable water as w/c ratio becomes higher. The cement paste specimens with a relatively lower w/c ratio have a significantly reduced amount of freezable water in the first 7 days. The specimens of a relatively higher w/c ratio have a gradually reduced amount of freezable water. At 1 day hydration, the value of λ_R is not necessarily in order in terms of the w/c ratios. The value of λ_R of the specimen with higher w/c ratio was expected to be higher. This might be due to the effect of unhydrated cement and a greater degree of hydration at 1 day for the higher w/c ratio preparation.

Figure 4.16 shows the plots of the resistance R_2 versus temperature for the cement paste specimens of w/c ratio 0.35, 0.40, 0.50 and 0.60 at 28 days hydration. As w/c ratio increases, the value of R_2 at 5°C decreases. The value of R_2 at 5°C, w/c ratio 0.35, is approximately 66,500 Ω whereas the specimen of w/c ratio 0.60 is 20,700 Ω, indicating that the cement paste specimen of w/c ratio 0.60 has more capillary water than that of w/c ratio 0.35 even after 28 days of hydration. Also, as w/c ratio increases, the specimens experience greater hysteresis.

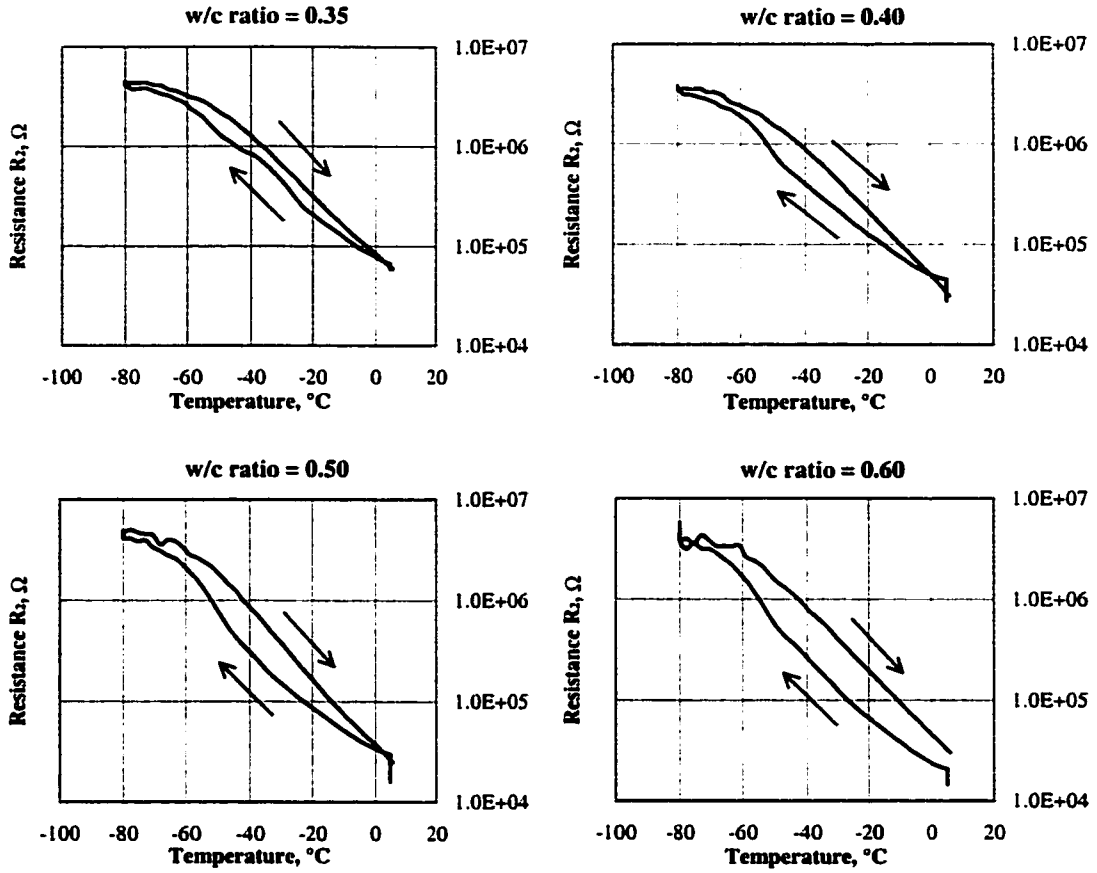

Fig. 4.16 Resistance R2 versus temperature for the cement paste specimens of w/c ratio 0.35, 0.40, 0.50 and 0.60 at 28 days hydration

4.3.2.2 The Depression Angle Parameter

The depression angle parameter obtained from the ACIS measurement reflects heterogeneity and roughness of the "C-S-H interface" as previously defined. Graphs plotted in Fig. 4.17 are the depression angle parameter versus temperature for the cement paste specimens of w/c ratio 0.40 at 1 day, 3 days, 7 days and 28 days hydration. Specimens at 3 days and 7 days hydration show a similar behaviour to that described previously. The depression angle parameter decreases as the temperature decreases to about –25°C as the "C-S-H interface" becomes more heterogeneous. Then, the parameter starts increasing at –25°C as the C-S-H and ice interface occupies more than 50% of the "C-S-H interface". The roughness of the "C-S-H interface" increases the value of the depression angle parameter as the temperature approaches –80°C.

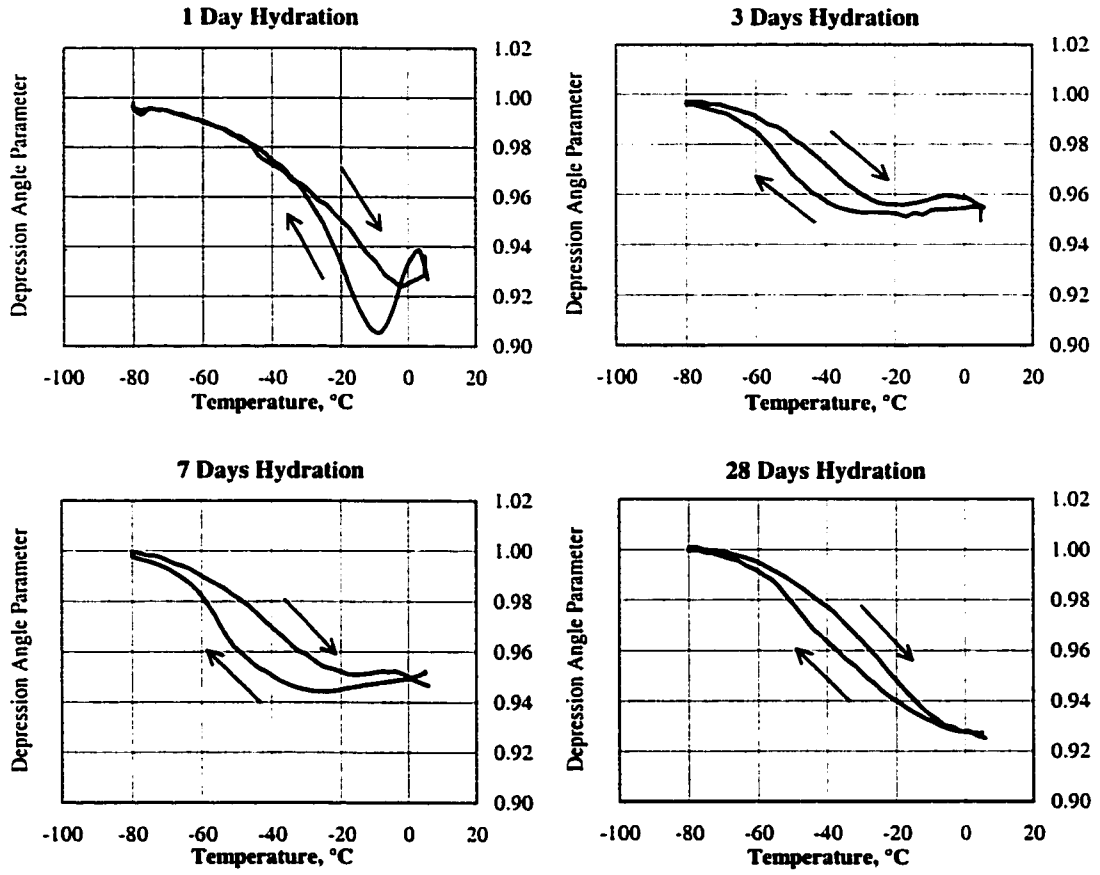

Fig. 4.17 Depression angle parameter versus temperature for the cement paste specimens of w/c ratio 0.40 at 1 day, 3 days, 7 days and 28 days hydration

Unlike the specimens at 3 days and 7 days hydration, the specimen at 28 days hydration has a different behaviour for the depression angle parameter. The depression angle parameter does not decrease between 5°C and –25°C, but increases as the temperature starts decreasing from 5°C. Furthermore, the value of the depression angle parameter at 5°C for the 28 days hydration specimen is lower than those values for the 3 days and 7 days hydration specimens. It is recalled that the hydration of cement paste is a process involving growth of the C-S-H particles into the capillary pores; this causes the "C-S-H interface" to be rougher. The depression angle parameter can, therefore, be expected to be lower as the hydration takes place. A possible explanation for the behaviour that the depression angle parameter increases as the temperature decreases from 5°C is that the amount of capillary pores is lower at a higher degree of hydration. Therefore, even though there is an effect of heterogeneity of the "C-S-H interface", it is not as dominant as it is

for younger specimens. The effect of roughness of the "C-S-H interface" becomes more significant and the depression angle parameter continues to increase as the temperature falls to –80°C. The specimen at 1 day hydration also has a different behaviour. The depression angle parameter decreases its value to the minimum where ice formation is initiated. Then the parameter starts increasing and approaches about 1.00 at –80°C. The ice crystals grow and fill up the capillary pores rapidly without any physical restriction by the C-S-H gel, since the C-S-H gel itself has not been well developed at 1 day hydration. The heterogeneity of the "C-S-H interface", therefore, does not play a significant role, but the roughness of the "C-S-H interface" does.

4.4 Effect of Wollastonite Micro-Fibre Reinforcement

The potential of the ACIS measurement as one of the practical methods for investigating the durability of cement paste was discussed in the previous section. In this section, the durability of the wollastonite micro-fibre reinforced cement paste will be examined by the coupled ACIS-TMA measurements. The variation of wollastonite content was 0%, 5.1%, 8.1 % and 10.2% by volume. The cement paste specimens at each wollastonite content were prepared for w/c ratio 0.35, 0.40, 0.50 and 0.60. The hydration periods of 1 day, 3 days, 7 days and 28 days were used. The test matrix is given in Table 3.1. Although the hydration period varies from 1 day to 28 days, emphasis will be given to the properties of the cement paste specimens at 28 days hydration with various wollastonite contents.

4.4.1 TMA

As mentioned previously, the TMA measurement provides both the total and irrecoverable expansion. The magnitude of each deformation represents the amount of freezable water and durability of cement paste, respectively. Figure 4.18 is a plot of the irrecoverable expansion versus wollastonite micro-fibre content for the cement paste specimens at 28 days hydration after a single freezing and thawing cycle for various w/c ratios. As the graph indicates, the values of the irrecoverable expansion of the cement paste specimens after the single freezing and thawing cycle increase as the wollastonite content increases from 0% to 8.1%; however, they decrease as the

wollastonite content increases to 10.2%. Comparing values of the irrecoverable expansion of the cement paste specimens containing 0% and 10.2% wollastonite content indicates that the addition of the wollastonite micro-fibres does not significantly improve the durability of the specimen of w/c ratio 0.35. However, the durability for each specimen of w/c ratio 0.40, 0.50 and 0.60 is significantly improved. The value of the percentage improvement of durability between 0% and 10.2% wollastonite content for each w/c ratio is presented in the graph. Mixing the cement paste matrix with wollastonite micro-fibres at w/c ratio as low as 0.35 was done with some difficulties in terms of workability. Some variation in homogeneity may have occurred. However, it is unrealistic to expect large improvement when the durability is already excellent without the wollastonite micro-fibres.

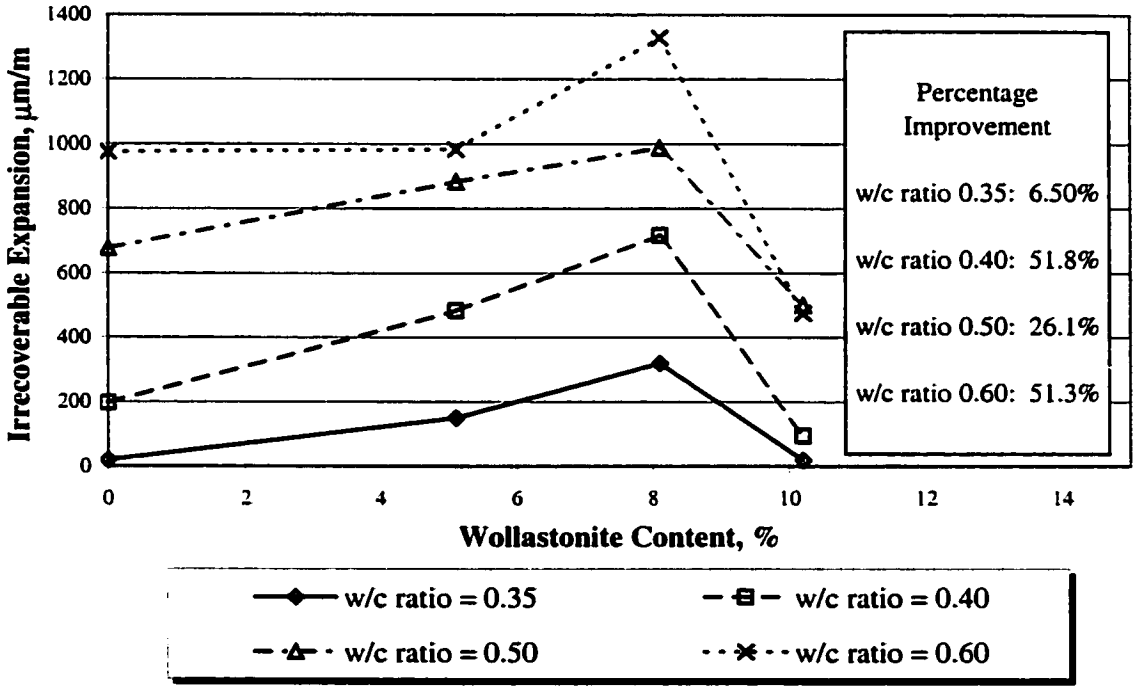

Fig. 4.18 Irrecoverable expansion versus wollastonite content for the cement paste specimens at 28 days hydration for various w/c ratios

The graph shown in Fig. 4.19 is a plot of the total expansion versus the wollastonite content for the cement paste specimens at 28 days hydration after a single freezing and thawing cycle for various w/c ratios. The values of the total expansion for cement paste specimens of w/c ratio 0.35, 0.40 and 0.50 increase as the wollastonite content increases from 0% to 5.1%. Then the values of the total expansion for cement paste specimens of w/c ratio 0.35 and 0.40 decrease as the wollastonite content increases to 10.2%. On the other hand, the value of the total expansion for cement

paste specimens of w/c ratio 0.50 increases as the wollastonite content increases to 8.1% and it decreases as the wollastonite content increases to 10.2%. For the cement paste specimens of w/c ratio 0.60, the value of the total expansion is constant as the wollastonite content increases to 8.1% and it decreases as the wollastonite content increases to 10.2%. Comparing values of the total expansion of the cement paste specimens containing 0% and 10.2% wollastonite content indicates that the durability for each specimen of w/c ratio 0.40, 0.50 and 0.60 is significantly improved. This is similar to the observations for the irrecoverable expansion in Fig. 4.18. The values of the total expansion for the specimens containing 10.2% wollastonite content are lower than those without the wollastonite content. This implies that the total expansion of the cement paste specimen is the primary factor that determines its irrecoverable expansion, hence durability.

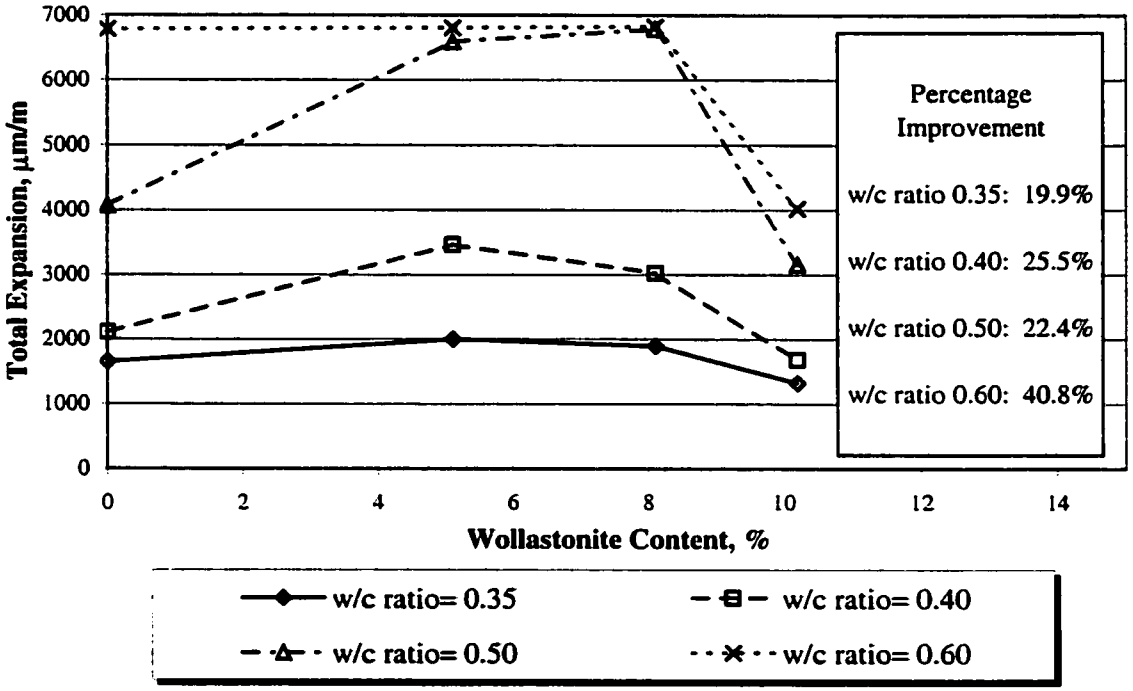

Fig. 4.19 Total expansion versus wollastonite content for the cement paste specimens at 28 days hydration for various w/c ratios

4.4.2 *ACIS*

4.4.2.1 Resistance R_2

The resistance ratio, λ_R obtained from the resistance R_2 corresponds to the amount of freezable water. The resistance ratio, λ_R of the cement paste specimens at 28 days hydration were plotted

against the wollastonite content for various w/c ratios and shown in Fig. 4.20. The value of λ_R for each w/c ratio increases as the wollastonite content increases from 0% to 5.1%. The cement paste specimens decrease their values of λ_R as the wollastonite content increases to 8.1%, except that the cement paste specimen of w/c ratio 0.60 increases its value of λ_R. Then, including the specimen of w/c ratio 0.60, the values of λ_R decrease as the wollastonite content increases to 10.2%. A comparison of the values of λ_R for the cement paste specimens with the 0% and 10.2% wollastonite content indicates that it does not significantly improve the specimen of w/c ratio 0.35. However, the value of λ_R for each specimen prepared for w/c ratio 0.40, 0.50 and 0.60 is significantly improved. This is a similar trend to that observed for the TMA measurement, and also indicates that the ACIS measurement has a potential as a reliable tool to examine the durability of cement paste.

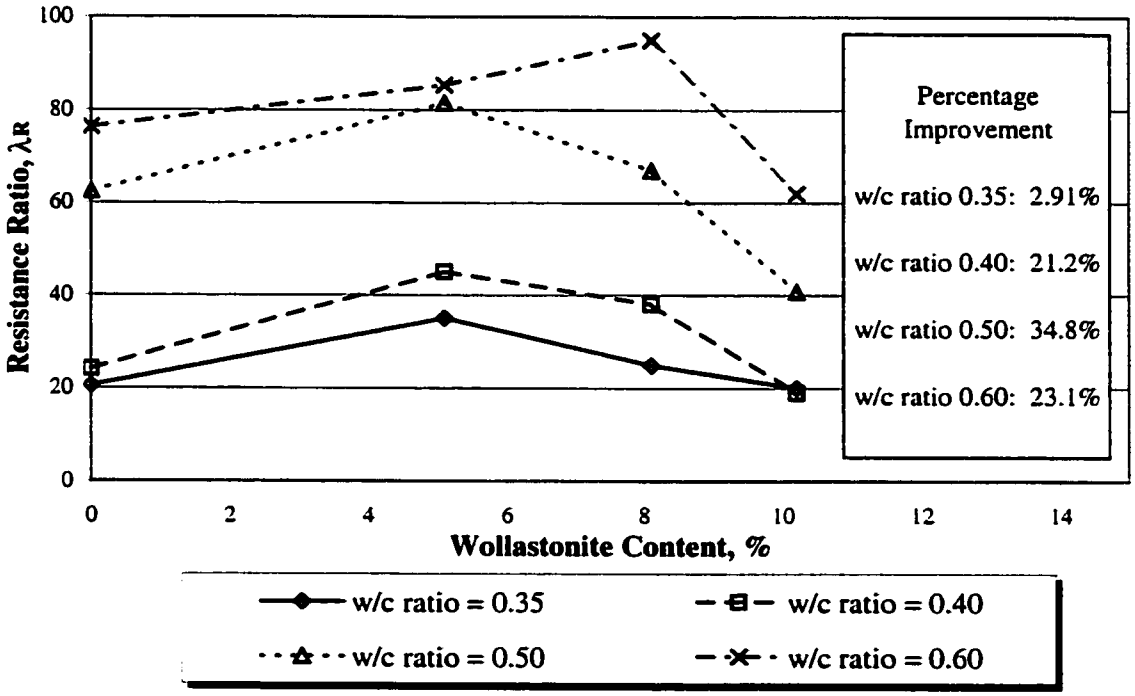

Fig. 4.20 Resistance ratio, λ_R versus wollastonite content for the cement paste specimens at 28 days hydration for various w/c ratios

Figure 4.21 is the resistance ratio, λ_R versus hydration period for the cement paste specimens containing 10.2% wollastonite micro-fibres for various w/c ratios. The values of λ_R decrease as the hydration takes place. This behaviour is similar to Fig. 4.15, which is the value of λ_R of the cement paste specimens without the wollastonite micro-fibres. The effect of the wollastonite mi-

cro-fibre reinforcement is to increase the resistance ratio, λ_R at 1 day and 3 days hydration relative to the specimens without wollastonite micro-fibres. The effect for the two low w/c ratio specimens is similar at 7 days hydration. Differences are not significant for all specimens at 28 days hydration.

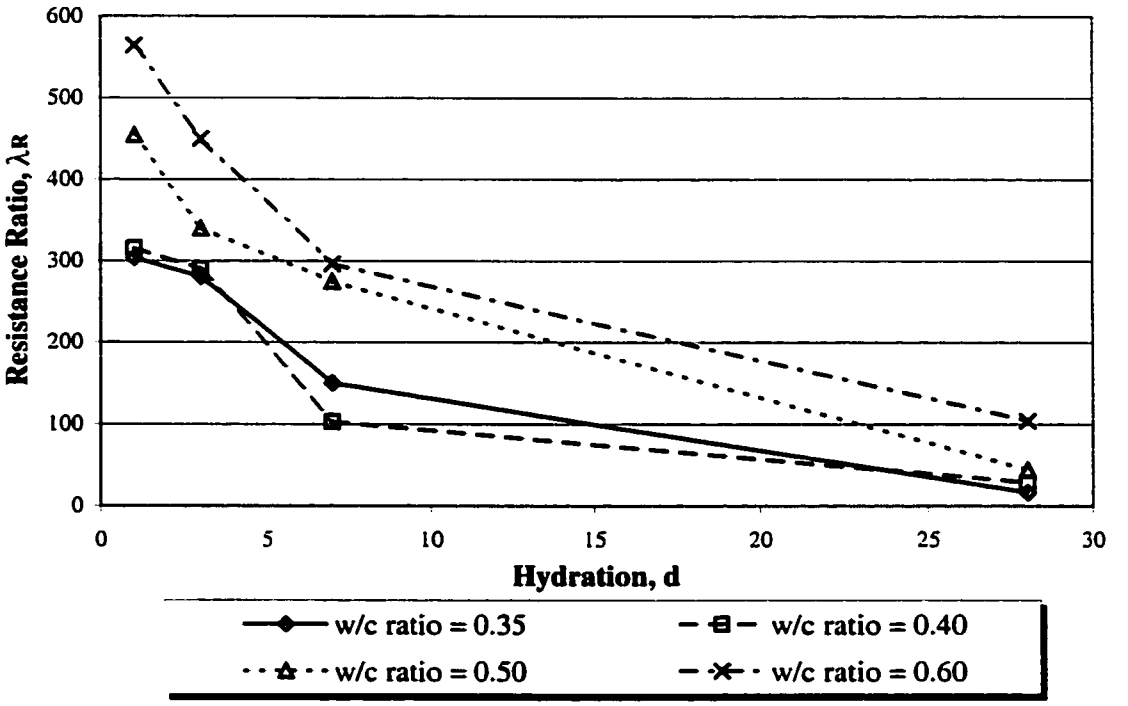

Fig. 4.21 Resistance ratio, λ_R versus hydration period for the cement paste specimens containing 10.2% wollastonite micro-fibres for various w/c ratios

4.4.2.2 The Depression Angle Parameter

The effect of the wollastonite micro-fibre reinforcement on the cement paste specimens observed from the depression angle parameter was investigated. Figure 4.22 shows the plots of the depression angle parameter, versus temperature, for the cement paste specimens of w/c ratio 0.40 at 28 days hydration for the wollastonite content of 0%, 5.1%, 8.1% and 10.2%. As shown previously in Fig. 4.17, the depression angle parameter for the plain cement paste specimen at 28 days hydration starts to increase as soon as the temperature starts to decrease from 5°C. The roughness of the "C-S-H interface" becomes more significant at a higher degree of hydration, whereas the values of the depression angle parameter of the cement paste specimens at 3 days and 7 days hydration decrease as the temperature falls to –25°C because of the heterogeneous "C-S-H interface". Then the parameter approaches 1.00 as the ice crystals fill the pores and the "C-S-H interface" becomes more homogeneous.

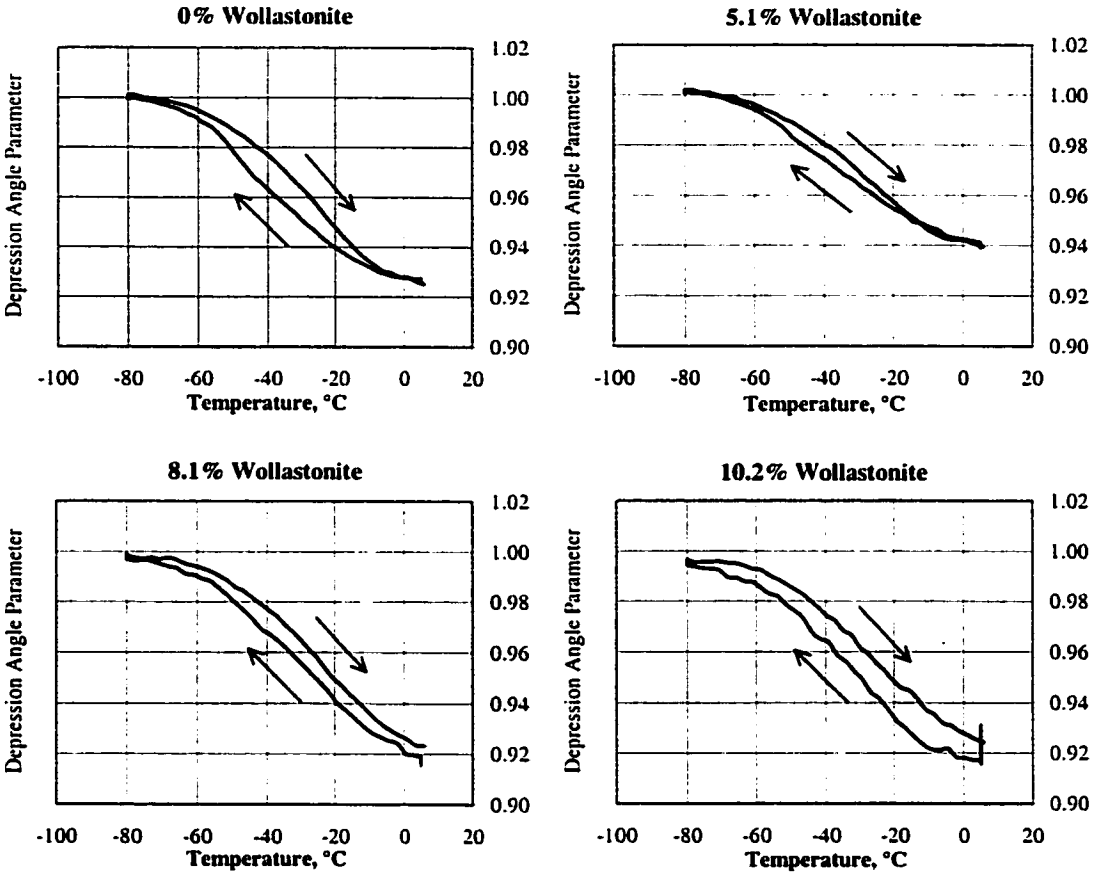

Fig. 4.22 Depression angle parameter versus temperature for the cement paste specimens of the w/c ratio 0.40 at 28 days hydration containing wollastonite content of 0%, 5.1%, 8.1% and 10.2%

The depression angle parameter for each wollastonite content shown in Fig. 4.22 starts increasing as the temperature starts decreasing from 5°C regardless of the wollastonite content. This indicates that the roughness of the "C-S-H interface" is more dominant than the heterogeneity of the "C-S-H interface" regardless of the wollastonite content. The fact that the wollastonite micro-fibres reinforcement produces even rougher "C-S-H interface" can be observed from the behaviour of specimens containing 8.1% and 10.2% wollastonite. The graphs of the depression angle parameter of these specimens have a large hysteresis while the graphs of the depression angle parameter of the specimens containing 0% and 5.1% wollastonite micro-fibres have no hysteresis. This indicates that the values of the depression angle parameter of the specimens containing 8.1% and 10.2% wollastonite started with lower values at 5°C because the 8.1% and 10.2% wollastonite micro-fibre reinforcement caused rougher "C-S-H interface".

The effect of the wollastonite micro-fibre reinforcement at various hydration periods is illustrated in Fig. 4.23. The four graphs shown in Fig. 4.23 are the plots of the depression angle parameter versus temperature for the cement paste specimens of w/c ratio 0.40 and the wollastonite content of 10.2% at 1 day, 3 days, 7 days and 28 days hydration. A comparison with Fig. 4.17, which shows the graphs of the depression angle parameter for plain cement paste specimens, is instructive. The values of depression angle parameter have similar behaviour regardless of the wollastonite content. As discussed previously, the wollastonite micro-fibre reinforcement could produce rougher "C-S-H interface" and thus more domination of the roughness of the "C-S-H interface" than its heterogeneity. However, Fig. 4.23 does not show any significant effect of the wollastonite micro-fibre reinforcement on the depression angle parameter.

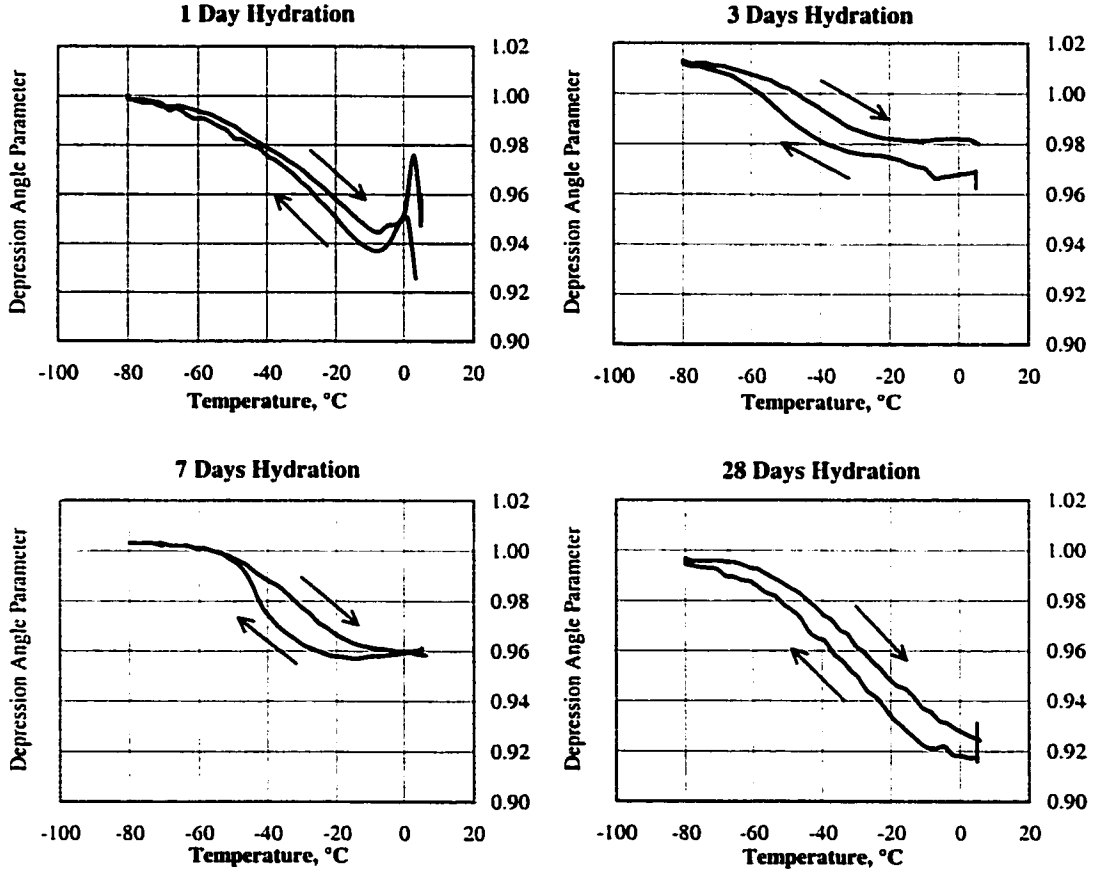

Fig. 4.23 Depression angle parameter, versus temperature for the cement paste specimens of w/c ratio 0.40 containing 10.2% wollastonite content at 1 day, 3 days, 7 days and 28 days hydration

CHAPTER 5

RESULTS AND DISCUSSION:

The DSC Experiment

5.1 Introduction

The main objective of the Differential Scanning Calorimetry (DSC) experiment is to support the interpretation of phenomena observed in the coupled ACIS-TMA measurement. By measuring the heat flow of a cement paste specimen subjected to a freezing and thawing cycle, phenomena occurring within the cement paste specimen can be explained. Mixes of cement paste specimens prepared for the DSC experiment were identical to those prepared for the coupled ACIS-TMA experiment and listed in Table 3.1.

This chapter will discuss the results in three stages. First, a typical DSC measurement of one of the cement paste specimens will be chosen and its microstructural behaviour and mechanism of frost action occurring within the specimen will be interpreted in detail. Then, the DSC measurements of the cement paste specimens with no wollastonite micro-fibre reinforcement will be compared on the basis of w/c ratio and hydration period. Finally, the effect of the wollastonite micro-fibre reinforcement on freezing and thawing behaviour of cement paste will be discussed with respect to the DSC measurements.

5.2 Microstructural Behaviour and Mechanism of Frost Action of Cement Paste Subjected to a Freezing and Thawing Cycle

The DSC measures the heat flow into or out of a substance associated with phase transitions. Phase transitions can then be detected as peaks in a plot of the apparent specific heat capacity versus temperature. An area under each peak with a linear baseline is the amount of heat per unit mass of the substance. The actual amount of water that freezes or melts during the phase transition per unit mass of the substance can therefore be calculated using Eq. (2.58). Figure 5.1 (a) is a typical plot of the apparent specific heat capacity versus temperature obtained from the DSC measurement for a cement paste specimen of w/c ratio 0.40 at 7 days hydration. Figures 5.1 (b) and (c) are the magnified plots of the freezing and thawing sections shown in Fig. 5.1 (a), respectively. As shown in Fig. 5.1 (b), the beginning of freezing can be observed as a peak at about –8°C, indicating that a large amount of capillary water has rapidly frozen. The water in the smaller capillary pores freezes as the temperature decreases further. Another peak can be observed at about –40°C, indicating that the gel water starts freezing at this temperature. On thawing shown in Fig. 5.1 (c), the value of the apparent specific heat capacity decreases gradually, then has a peak at a temperature close to 0°C.

The actual amount of water frozen or melted per unit mass of a cement paste specimen can be calculated by obtaining the area under the curve. On freezing, the area under the curve is divided above and below the temperature –40°C as shown in Fig. 5.1 (b). The actual amounts of water per unit mass calculated from the area under the curve above and below –40°C are denoted as w_{f+40} and w_{f-40}. Also w_t is the actual amount of ice melted per unit mass on thawing. The area under each curve was calculated by the software, Universal Analysis of TA Instruments. For instance, if the values of the area under the curve above and below –40°C were obtained as 12.07 J/g and 13.75 J/g respectively, then the values of w_{f+40} and w_{f-40} can be calculated by using Eq. (2.58) as follows. For the sake of clarity, the unit mass of substance and water are denoted as $g_{substance}$ and g_{water} respectively.

$$w_{f+40} = \frac{q_P}{\Delta H_f} \tag{5.1}$$

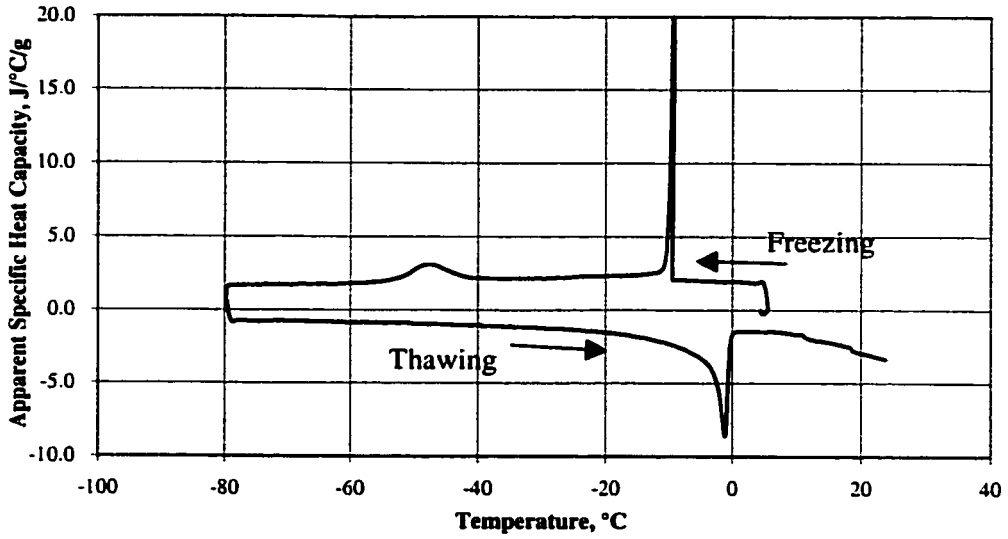

(a)

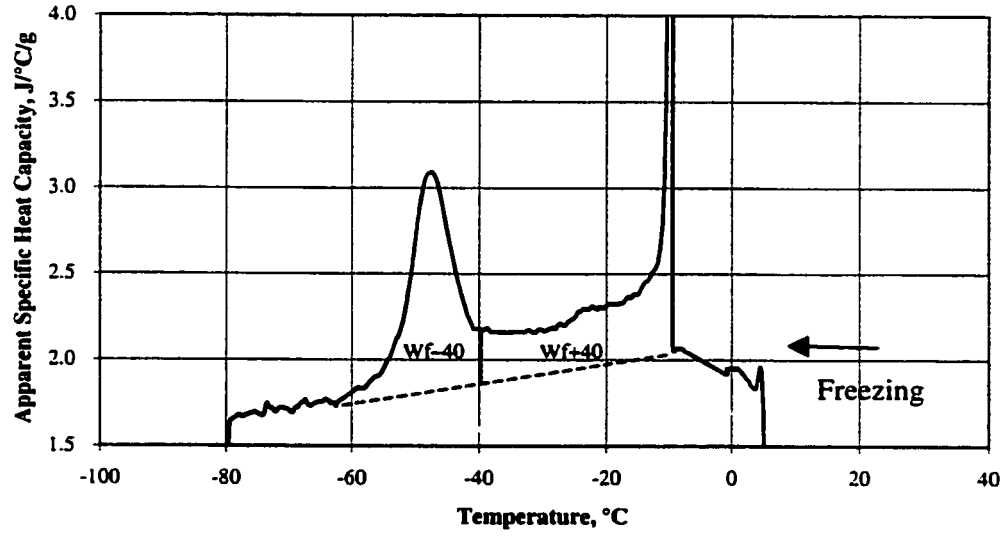

(b)

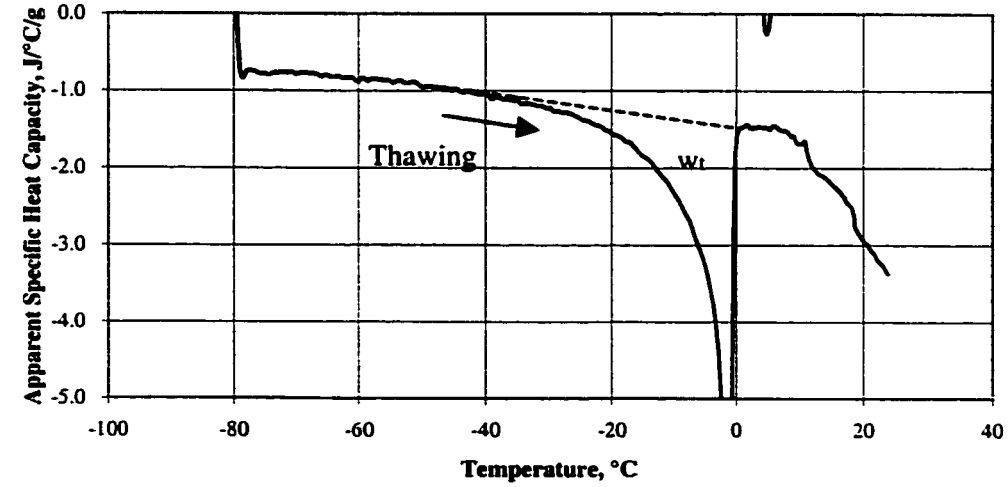

(c)

Fig. 5.1 *A typical plot of the apparent specific heat capacity versus temperature obtained from the DSC measurement for a cement paste specimen of w/c ratio 0.40 at 7 days hydration*

$$= \frac{(12.07\ J/g_{substance})}{(334.73\ J/g_{water})} \quad (5.2)$$

$$= 0.036\ g_{water}/g_{substance} \quad (5.3)$$

where w_{f+40} = the actual amount of water frozen above the temperature –40°C per unit mass of cement paste specimen, $g_{water}/g_{substance}$

$$w_{f-40} = \frac{q_P}{\Delta H_f} \quad (5.4)$$

$$= \frac{(13.75\ J/g_{substance})}{(334.73\ J/g_{water})} \quad (5.5)$$

$$= 0.041\ g_{water}/g_{substance} \quad (5.6)$$

where w_{f-40} = the actual amount of water frozen below the temperature –40°C per unit mass of cement paste specimen, $g_{water}/g_{substance}$

In this example, the amount of water frozen above –40°C and the amount of water frozen below –40°C per unit mass of the cement paste specimen were 0.036 $g_{water}/g_{substance}$ and 0.041 $g_{water}/g_{substance}$ respectively.

5.3 Effects of Water/Cement Ratio and Hydration Period

The values of w_{f+40}, w_{f-40} and w_t were calculated for the cement paste specimens of w/c ratio 0.35, 0.40, 0.50 and 0.60 for the hydration periods of 1 day, 3 days, 7 days and 28 days without the wollastonite micro-fibre reinforcement. The results of calculation are presented in Appendix B. The values of the w_{f+40} and w_{f-40} were plotted against hydration period for various w/c ratios and are shown in Fig. 5.2.

It clearly shows that the value of w_{f+40} decreases and the value of w_{f-40} increases with hydration. In other words, the amount of water which has frozen above the temperature –40°C decreases and

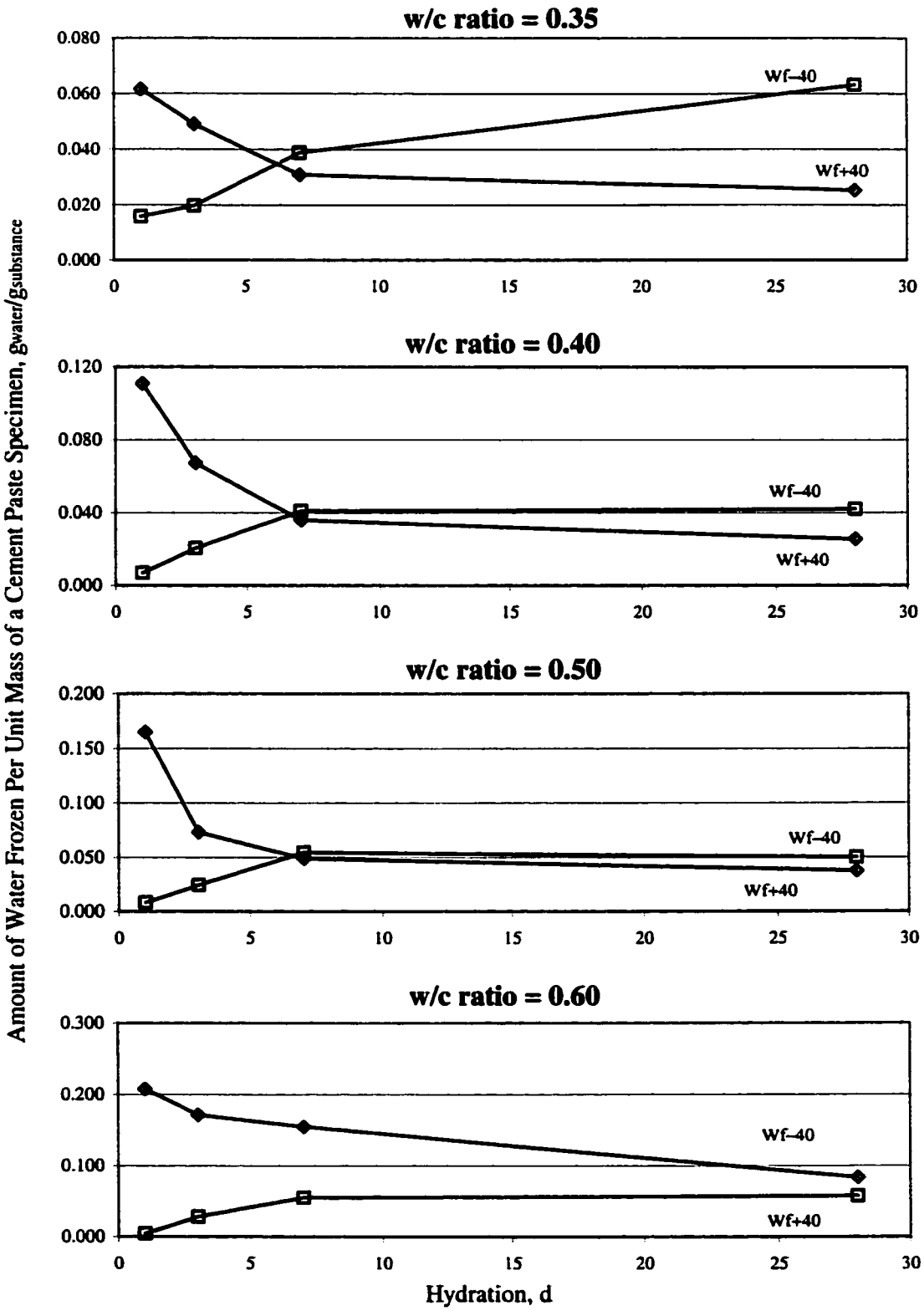

Fig. 5.2 The amount of water frozen above –40°C, w_{f+40} and the amount of water frozen below –40°C, w_{f-40} versus hydration period for various w/c ratios

the amount of water which has frozen below the temperature –40°C increases as hydration takes place. Recalling that the amount of capillary water decreases and the amount of gel water increases with hydration, it is apparent that the values of w_{f+40} and w_{f-40} represent the amount of capillary water and the amount of gel water in a cement paste specimen, respectively. This agrees with the observation in the coupled ACIS-TMA measurement. The TMA measurement indicated that the freezing started in the large capillary pores (50 – 100 nm) at approximately –7°C and the water in smaller capillary pores started freezing as the temperature decreased. The capillary water completed freezing at about –40°C. Then the supercooled water in gel pores started freezing at –40°C. Those phenomena correspond to the observation in the DSC measurement.

Figures 5.3 (a) and (b) show the plots of w_{f+40} and w_{f-40} versus w/c ratio for various hydration periods. As shown in Fig. 5.3 (a), the value of w_{f+40} for each hydration period increases as w/c ratio increases, whereas the value of w_{f-40}, shown in Fig. 5.3 (b), does not significantly change regardless of w/c ratio. This is owing to the fact that the amount of gel water is determined by the C-S-H gel, which is the hydration product. The amount of the C-S-H gel is mainly dependent on the hydration period at a given w/c ratio, but independent of w/c ratio at a given hydration period especially at the early stage of hydration. This explains the results obtained in Fig. 5.3 (b). Figure 5.3 (a) also illustrates that the higher the degree of hydration, the lower is the amount of capillary water. Figure 5.3 (b) shows that the higher the degree of hydration, the greater is the amount of gel water.

The amount of water thawed, w_t is plotted in Fig 5.4 against hydration period for various w/c ratios. The amount of water thawed should be equal to or slightly less than the summation of w_{f+40} and w_{f-40} taking the loss of moisture during the experiment into consideration. In other words, the amount of water thawed is the amount of freezable water in a cement paste specimen and therefore should be similar to the observation in Figs. 4.11 and 4.15 which are the amount of freezable water obtained from the TMA and ACIS measurements respectively.

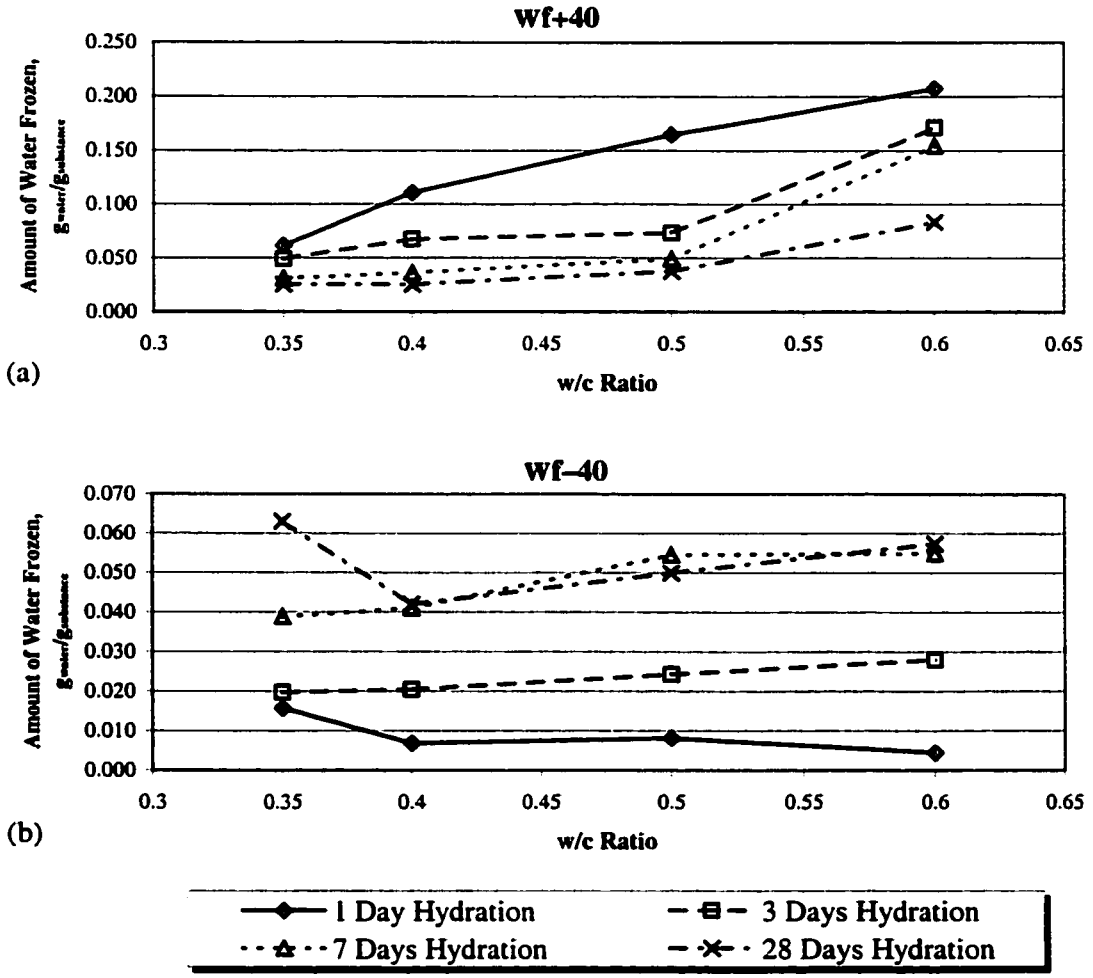

Fig. 5.3 *(a) The amount of water frozen above –40°C, w_{f+40} and (b) the amount of water frozen below –40°C, w_{f-40} versus w/c ratio for various hydration periods*

5.4 Effect of Wollastonite Micro-Fibre Reinforcement

The amount of water frozen above and below –40°C and the amount of water thawed were calculated for the cement paste specimens containing the wollastonite content of 0%, 5.1%, 8.1% and 10.2% and are presented in Appendix B. At a given wollastonite micro-fibre content, the effects of w/c ratio and hydration period are similar to those without wollastonite micro-fibres. For example, Figs 5.5 (a) and (b) illustrate each of the values w_{f+40} and w_{f-40} versus w/c ratio for the

cement paste specimens containing 10.2 % wollastonite content for various hydration periods. Figure 5.5 (a) shows that the value of w_{f+40} for each hydration period increases as w/c ratio increases and also that the higher the degree of hydration, the lower is the amount of capillary water. Figure 5.5 (b) illustrates that the value of w_{f-40} does not significantly change regardless of w/c ratio, as observed in Fig. 5.3 (b). It also indicates that the higher the degree of hydration, the greater is the amount of gel water.

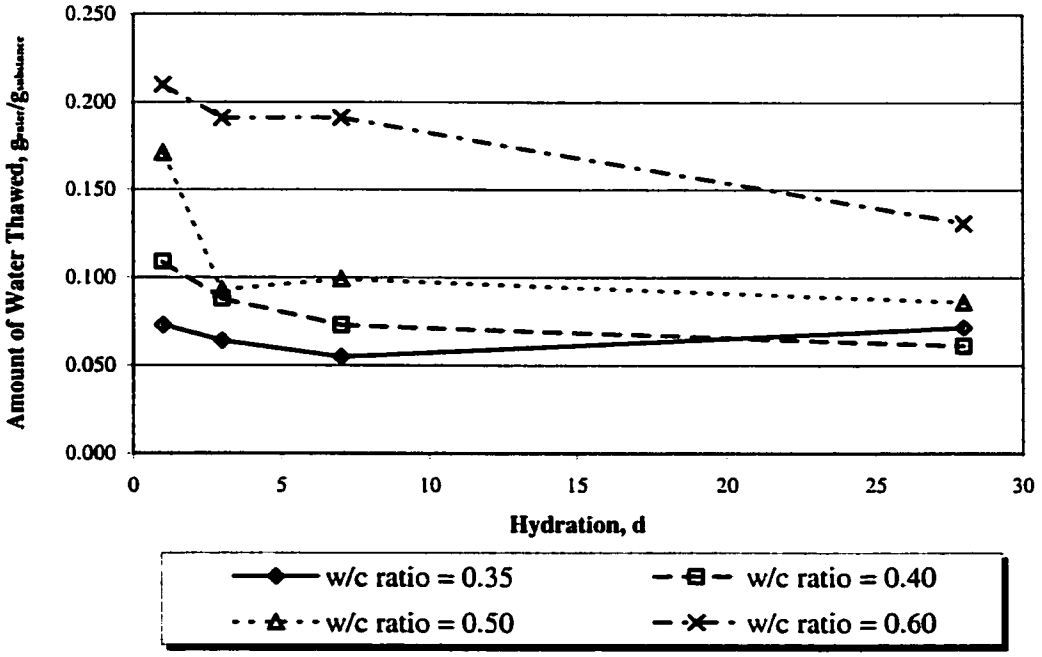

Fig. 5.4 The amount of water thawed, w_t versus hydration period for various w/c ratios

Figures 5.6 (a) and (b) are the plots of the values of w_{f+40} and w_{f-40} versus wollastonite content for the cement paste specimens at 28 days hydration for various w/c ratios. The values of w_{f+40} of the cement paste specimens of w/c ratio 0.35, 0.40 and 0.50, shown in Fig 5.6 (a), are similar in character. The values of w_{f+40} decrease as the wollastonite content increases to 5.1%, then they increase as the wollastonite content increases to 8.1%, and slightly decrease as it increases to 10.2%. The value of w_{f+40} of the cement paste specimen of w/c ratio 0.60, however, decreases as the wollastonite content increases. The cement paste specimens of w/c ratio 0.35, 0.50 and 0.60 in Fig. 5.6 (b), have similar behaviour to the cement paste specimens of w/c ratio 0.35, 0.40 and 0.50, shown in Figure 5.6 (a). The cement paste specimen of w/c ratio 0.40, however, has a unique behaviour.

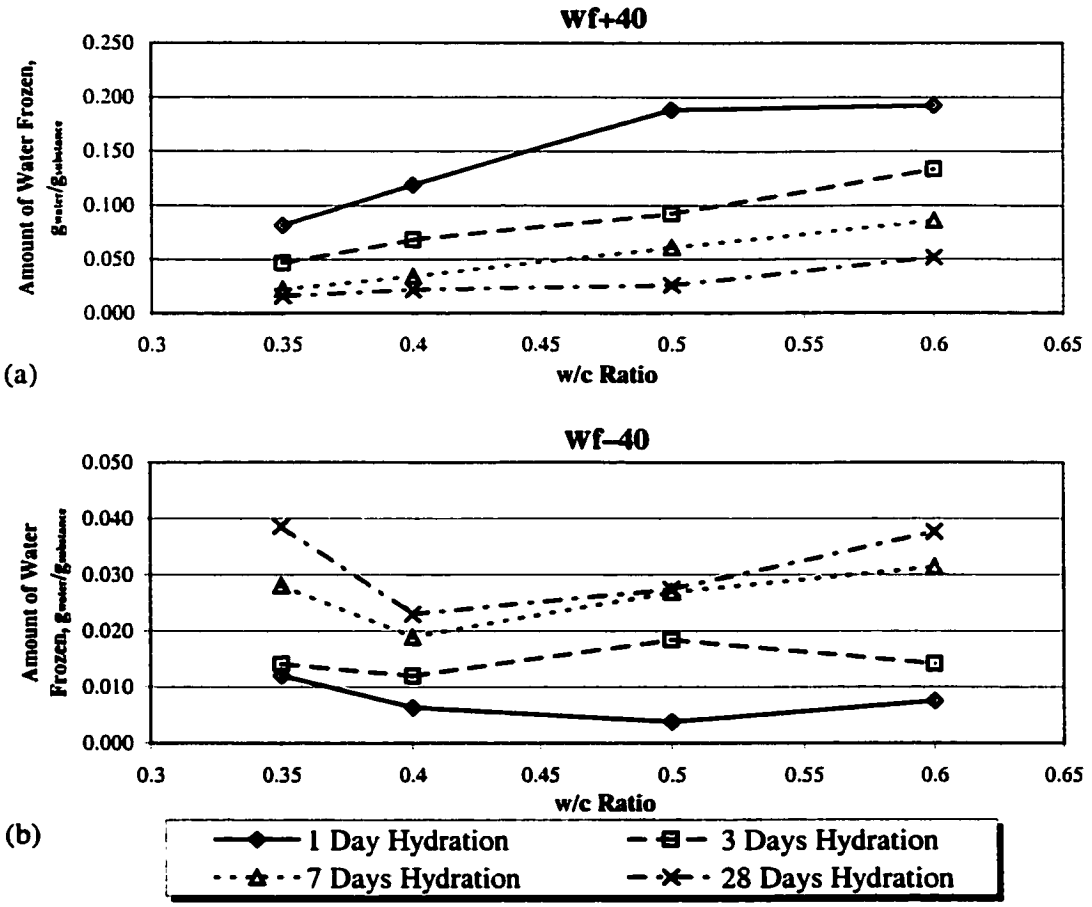

Fig. 5.5 *(a) The amount of water frozen above –40°C, w_{f+40}, and (b) the amount of the water frozen below –40°C, w_{f-40} versus w/c ratio for the cement paste specimens containing 10.2% wollastonite content for various hydration periods*

Figure 5.7 shows a plot of the amount of water thawed, w_t, versus wollastonite content for various w/c ratios. The values of w_t in Fig. 5.7 should be similar to the values plotted in Figs. 4.19 and 4.20, i.e. the amount of freezable water obtained from the TMA and ACIS measurements respectively, since the amount of water thawed should be equal to the amount of freezable water. The values of w_t in Fig. 5.7 decrease when the wollastonite content increases to 5.1%. However, the cement paste specimens containing 10.2% wollastonite content have a lower amount of water thawed, or frozen, than those without the wollastonite micro-fibres. This was also observed from the ACIS-TMA measurements as well. It can be explained by the dilation effect as wollastonite micro-fibres replace the cement paste volume which would contain water.

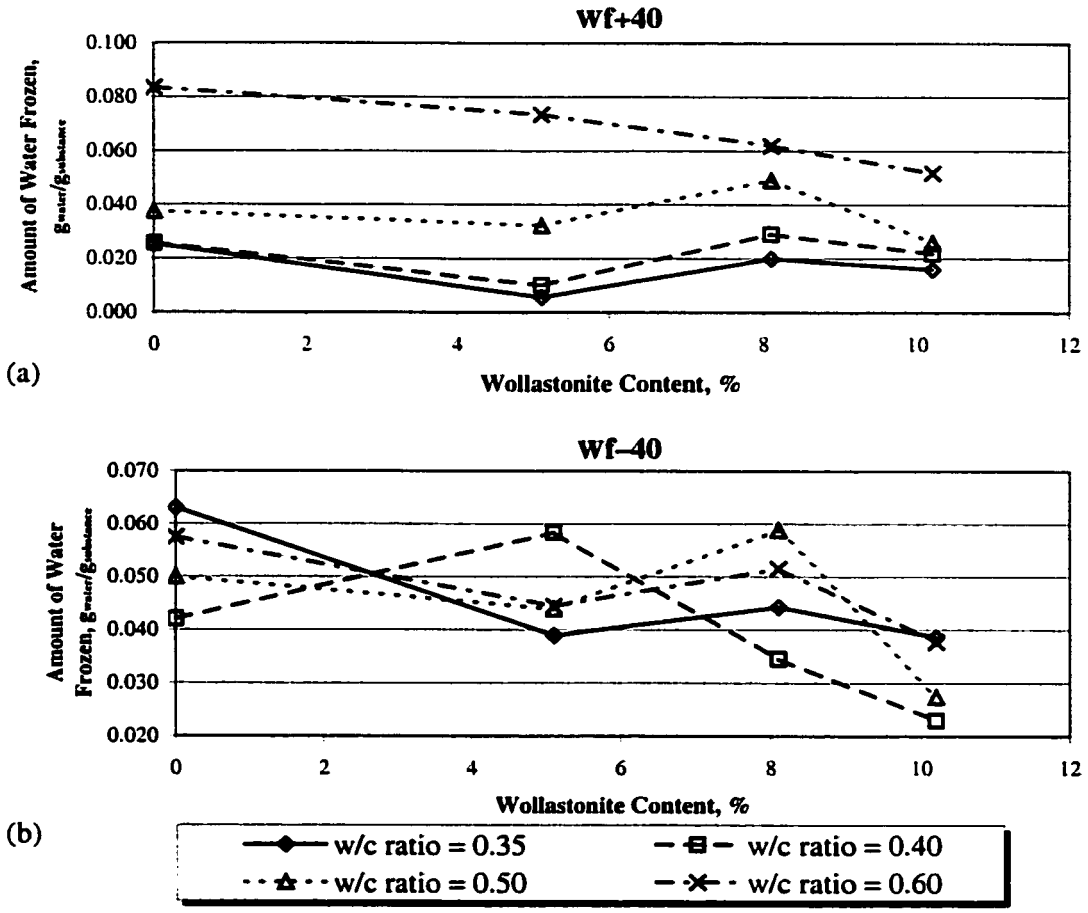

Fig. 5.6 *(a) The amount of water frozen above –40°C, w_{f+40}, and (b) the amount of the water frozen below –40°C, w_{f-40} versus wollastonite content for the cement paste specimens at 28 days hydration for various w/c ratios*

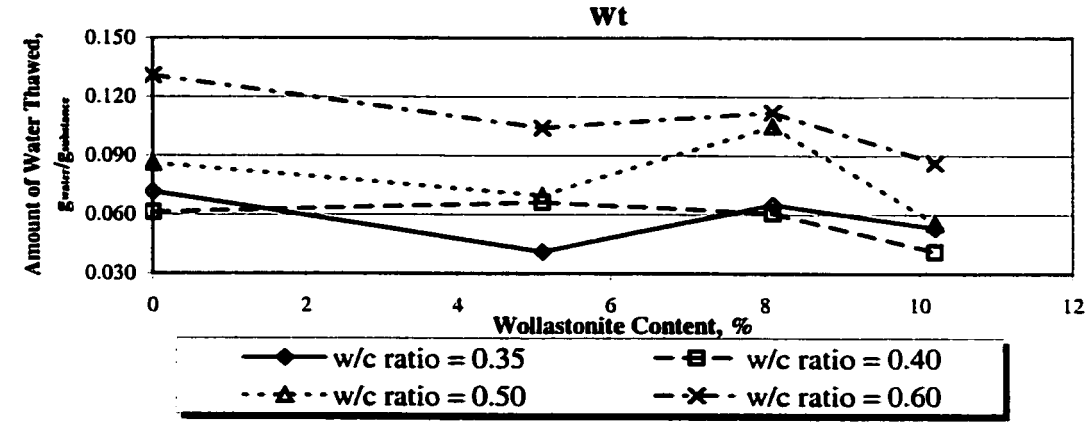

Fig. 5.7 *The amount of water thawed, w_t versus wollastonite content for the cement paste specimens at 28 days hydration for various w/c ratios*

CHAPTER 6

CONCLUSIONS AND RECOMMENDATIONS FOR FUTURE RESEARCH

6.1 Introduction

This study had three primary objectives: to further the understanding of the mechanism of frost action within cement paste subjected to freezing and thawing; to investigate the potential of the ACIS as a possible technique to determine the durability of cement paste with respect to freezing and thawing; to investigate the durability of the wollastonite micro-fibre reinforced cement paste to freezing and thawing. In order to accomplish these three objectives, two main experiments were conducted: the coupled ACIS-TMA experiment and the DSC experiment. The coupled ACIS-TMA experiment was designed to further the understanding of the complex mechanism of frost action within cement paste and to investigate the potential of the ACIS technique for determining the durability of cement paste. The durability of the wollastonite micro-fibre reinforced cement paste to freezing and thawing was then investigated applying the coupled ACIS-TMA experiment. The DSC experiment was designed to support the interpretation of phenomena observed in the coupled ACIS-TMA experiment.

This chapter will present the conclusions in three stages. First, the specific findings in each experiment will be presented. Then the overall conclusions of the study will be given. Finally, the recommendations for future research will be provided.

6.2 Specific Findings in the Coupled ACIS-TMA Experiment

6.2.1 Microstructural Behaviour and Mechanism of Frost Action of Cement Paste Subjected to a Freezing and Thawing Cycle

6.2.1.1 TMA

1. The nucleation of ice was initiated in the capillary pores approximately at –7°C. The water was pushed out of capillary pores generating a hydraulic pressure; ice formation resulted in a 9% increase in volume.
2. The greater the degree of supercooling, the more rapid is the ice crystal growth. Therefore, the ice crystal growth depends mainly on the pore size; the water in the smaller pores experiences a greater degree of supercooling.
3. The expansion is caused not only by the hydraulic pressure, but also by the migration of the pore water itself. When the temperature was held constant at –21.3°C, the supercooled water in the gel pores migrated into the capillary pores and caused the expansion.
4. The freezing of the water in most of the capillary pores was completed at a temperature of approximately –40°C. Then, the freezing of the water in the gel pores was initiated. It was completed at a temperature of approximately –65°C.
5. The total expansion was related to the total amount of water frozen in a cement paste specimen during a single freezing and thawing cycle.
6. The pore water did not melt at precisely 0°C owing to the depression of the melting temperature. The melting temperature of the water for a given pore size was higher than the freezing temperature of the water for the same pore size.
7. The irrecoverable expansion was defined as the residual deformation after the single freezing and thawing cycle; this is often referred to as a durability indicator.

6.2.1.2 ACIS

1. The value of R_1 represents the electrical resistance of the pore water before ice formation occurs while the values of R_2 and C_d represent the resistance and capacitance behaviour of the C-S-H and pore water interface, respectively. The value of R_1 after ice formation, represents the electrical resistance of the unfrozen pore water while the values of R_2 and C_d

represent the resistance and capacitance behaviour of the C-S-H and ice interface, respectively.

2. The value of R_1, electrical resistance of the unfrozen pore water, decreased as the temperature decreased. The pore water of cement paste contained dissolved substances which acted as the electrolytes. The ice formed during a freezing process excluded these substances and resulted in a higher concentration of salts in the unfrozen pore water. Therefore, the charge was carried more easily and resulted in a lower electrical resistance.
3. The value of R_2, electrical resistance of the C-S-H and ice interface, indicated that the ice formation was initiated approximately at –7°C and the freezing of water was completed approximately at –65°C.
4. A resistance ratio, λ_R was defined as the ratio of the value of R_2 at –65°C to the one at –7°C and corresponded to the amount of water frozen in a cement paste specimen during a single freezing and thawing cycle.
5. The value of R_2 indicated that the melting of a very small amount of water occurred below –30°C on thawing.
6. The depression angle parameter represents the heterogeneity of the C-S-H and pore water interface before ice formation. It becomes representative of the heterogeneity of an interface that consists of the combination of the C-S-H and pore water interface and the C-S-H and ice interface after ice formation occurs. The term "C-S-H interface" was defined as the C-S-H and pore water interface before ice formation or the combination of the C-S-H and pore water interface and the C-S-H and ice interface after ice formation.
7. The depression angle parameter indicated that about 50% of the "C-S-H interface" was occupied by the C-S-H and ice interface at a temperature of approximately –25°C.
8. The depression angle parameter also represents the roughness of the "C-S-H interface". The roughness of the "C-S-H interface" before ice formation is greater than that after ice formation.

6.2.2 Effects of Water/Cement Ratio and Hydration Period

6.2.2.1 TMA

1. The total expansion increased as the w/c ratio increased. The higher the w/c ratio, the higher is the amount of freezable water to cause the total expansion.

2. The total expansion decreased as the hydration period increased. The higher the degree of hydration, the lower is the amount of water which has not reacted with cement; thus the lower is the amount of freezable water to cause the expansion.
3. The irrecoverable expansion increased as the w/c ratio increased. The higher the w/c ratio, the less durable is a cement paste specimen.
4. The irrecoverable expansion decreased as the hydration period increased. The higher the degree of hydration, the more durable is the cement paste specimen.
5. The amount of freezable water in a cement paste obtained from the total expansion is the primary factor which determines its irrecoverable expansion, and hence durability.
6. The amount of capillary water, which froze above –40°C decreased and the amount of gel water, which froze below –40°C increased with hydration period.

6.2.2.2 ACIS

1. The resistance ratio, λ_R obtained from the resistance R_2, increased as the w/c ratio increased. The higher the w/c ratio, the higher is the amount of freezable water.
2. The resistance ratio, λ_R decreased as the hydration period increased. The higher the degree of hydration, the lower is the amount of freezable water.
3. Both of the resistance ratio, λ_R obtained from the ACIS measurement and the total expansion obtained from the TMA measurement represent the amount of freezable water in a cement paste specimen. Therefore, the resistance ratio can be considered as a primary index which indicates the durability of cement paste, since the amount of freezable water is the primary factor which determines its durability.
4. At a room temperature, the lower the w/c ratio and the higher the degree of hydration, the higher was the resistance R_2. A cement paste specimen with the lower w/c ratio at the higher degree of hydration contains a lower amount of capillary water and conducts less electricity.
5. As hydration takes place, the influence of the roughness of the "C-S-H interface" on the depression angle parameter above the temperature of –25°C becomes more dominant than the influence by the heterogeneity of the "C-S-H interface". The "C-S-H interface" becomes rougher with hydration period, as the hydration of cement paste is a process involving growth of the C-S-H particles into the capillary pores.

6.2.3 Effect of Wollastonite Micro-Fibre Reinforcement

6.2.3.1 TMA

1. The irrecoverable expansion for the cement paste specimens of w/c ratio 0.35, 0.40, 0.50 and 0.60 at 28 days hydration increased as the wollastonite content increased from 0% to 8.1%; however, it decreased as the wollastonite content increased to 10.2%.
2. Comparing the irrecoverable expansion of the cement paste specimens containing the 0% and 10.2% wollastonite content at 28 days hydration indicated that the wollastonite micro-fibre reinforcement did not significantly improve the durability for the specimen of w/c ratio 0.35, but did improve the durability for the specimens of w/c ratio 0.40, 0.50 and 0.60.
3. The total expansion had a similar behaviour to the irrecoverable expansion. The values of the total expansion for the cement paste specimens containing 10.2% wollastonite content with w/c ratio 0.40, 0.50 and 0.60 were lower than those for the cement paste specimens with no wollastonite content.

6.2.3.2 ACIS

1. The resistance ratio, λ_R of the cement paste specimens of w/c ratio 0.35, 0.40, 0.50 and 0.60 at 28 days hydration increased as the wollastonite content increased from 0% to 5.1%. The specimens decreased the values of λ_R as the wollastonite content increased to 8.1%, except the specimen of w/c ratio 0.60 increased its value of λ_R.
2. A comparison of the resistance ratio, λ_R with the 0% and 10.2% wollastonite content at 28 days hydration indicated that the wollastonite micro-fibre reinforcement did not significantly improve the durability for the specimen of w/c ratio 0.35, but did improve the durability for the specimens of w/c ratio 0.40, 0.50 and 0.60.
3. The observation regarding the effect of the wollastonite micro-fibre reinforcement obtained from the value of λ_R was very similar to the one obtained from the TMA measurement. This indicates that the ACIS measurement has a potential as a reliable technique to determine the durability of cement paste.
4. At 28 days hydration, the influence of the roughness of the "C-S-H interface" on the depression angle parameter was more dominant, regardless of wollastonite content, than the influence of the heterogeneity of the "C-S-H interface".
5. The values of the depression angle parameter of the specimens containing 8.1% and 10.2% had a large hysteresis after a single freezing and thawing cycle, while the ones containing

0% and 5.1% wollastonite micro-fibres had no hysteresis. This indicates that the 8.1% and 10.2% wollastonite micro-fibre reinforcement caused rougher "C-S-H interface".

6.3 Specific Findings in the DSC Experiment

6.3.1 Microstructural Behaviour and Mechanism of Frost Action of Cement Paste Subjected to a Freezing and Thawing Cycle

1. The DSC measurement showed two peaks at –8°C and –40°C, which indicated two major phase transitions of the pore water in a cement paste specimen.
2. The terms, w_{f+40} and w_{f-40} were defined as the actual amounts of water frozen above and below –40°C per unit mass of cement paste, respectively. The term, w_t was defined as the actual amount of ice melted on thawing per unit mass of cement paste.

6.3.2 Effects of Water/Cement Ratio and Hydration Period

1. The amount of water which had frozen above the temperature –40°C, w_{f+40}, decreased and the amount of water which had frozen below the temperature –40°C, w_{f-40}, increased as hydration took place. It indicates that the values of w_{f+40} and w_{f-40} represent the amount of capillary water and the amount of gel water, respectively. This observation agrees with the one in the coupled ACIS-TMA measurement.
2. The value of w_{f+40} increased as the w/c ratio increased. The value of w_{f-40} did not significantly change regardless of w/c ratio. The amount of gel water is mainly dependent on the hydration period at a given w/c ratio, but independent of the w/c ratio at a given hydration period, especially at the early stage of hydration.
3. The value of w_t showed the similar behaviour to the amount of freezable water observed in the coupled ACIS-TMA measurement.

6.3.3 Effect of Wollastonite Micro-Fibre Reinforcement

1. The cement paste specimens containing 10.2% wollastonite content had a similar behaviour to the ones without the wollastonite content.
2. The value of w_{f+40} of the specimens containing 10.2% wollastonite content increased as the w/c ratio increased. The value of w_{f-40} of the specimens containing 10.2% wollastonite content did not significantly change regardless of w/c ratio.

6.4 Overall Conclusions

Summarizing the specific findings previously presented, the overall conclusions can be given as follows;

1. The microstructural behaviour and mechanism of frost action within cement paste was elucidated in detail based on interpretation of phenomena observed in the coupled ACIS-TMA measurement and the DSC measurement. An approach of the coupled ACIS-TMA measurement is original and has been developed at the University of Ottawa and the National Research Council Canada.
2. The investigation of the potential of the ACIS as one of the techniques for determining the durability of cement paste with respect to freezing and thawing was accomplished. The hypothesis of the useful ACIS application was confirmed.
3. The improvement of the durability of the wollastonite micro-fibre reinforced cement paste to freezing and thawing was acknowledged in some conditions. The addition of the wollastonite micro-fibres is recommended, particularly for cement pastes with a high w/c ratio, when exposure condition is expected to be severe.

6.5 Recommendations for Future Research

The overall objectives in this study were accomplished; however, future research will be required to improve the current study and to lead to the practical application of the ACIS technique in the field. It is suggested that future research includes:

1. Additional coupled ACIS-TMA experiments with different temperature variations, freezing rates and multiple freezing and thawing cycles
2. Experiments using the ACIS to determine the effects of different pore size distributions on the depression angle parameter for cement paste
3. The coupled ACIS-TMA experiments for cement paste saturated with various non-acqueous solutions with different properties from water, such as a freezing temperature and resistivity
4. The coupled ACIS-TMA experiments for cement paste with air entrainment and also for mortar and concrete
5. A development of the procedure and experimental methods for the practical application of the ACIS technique in the field
6. A standardization of the ACIS technique for the freezing and thawing durability of cement paste for submission to appropriate CSA committees

APPENDIX A

A.1 Values of Total Expansion, Irrecoverable Expansion and Resistance Ratio

Wollastonite Content [%]	w/c Ratio	Hydration Period [d]	Total Expansion μm/m	Irrecoverable Expansion μm/m	Resistance Ratio λ_R
0	0.35	1	2500	672	246.0
		3	2600	309	183.1
		7	1946	69	137.4
		28	1658	20	22.9
	0.40	1	3600	775	280.8
		3	3448	809	192.8
		7	3237	405	169.9
		28	2086	184	35.0
	0.50	1	5905	988	254.6
		3	4938	1156	221.4
		7	4427	950	210.0
		28	4042	662	62.4
	0.60	1	6967	1819	268.9
		3	7523	1779	303.2
		7	8002	1500	275.6
		28	6787	975	76.3
5.1	0.35	1	3346	890	296.1
		3	2976	316	264.1
		7	2641	223	164.5
		28	2000	150	35.0
	0.40	1	3612	1032	334.6
		3	3698	1109	250.0
		7	3513	860	198.3
		28	3463	483	45.0
	0.50	1	7645	1416	369.1
		3	6897	1291	346.5
		7	7135	1320	331.0
		28	6591	883	81.4
	0.60	1	7644	1995	325.4
		3	7439	1986	335.6
		7	8103	1698	274.5
		28	6805	983	85.3

(continued on the next page)

(continued from the previous page)

Wollastonite Content [%]	w/c Ratio	Hydration Period [d]	Total Expansion μm/m	Irrecoverable Expansion μm/m	Resistance Ratio λ_R
8.1	0.35	1	3597	1121	379.5
		3	3267	669	366.5
		7	2946	503	299.1
		28	1897	319	24.9
	0.40	1	3519	1269	321.4
		3	3753	1323	243.1
		7	3764	853	265.1
		28	3024	717	38.0
	0.50	1	7794	1794	451.6
		3	6679	1590	389.4
		7	7946	1643	359.1
		28	6786	988	67.0
	0.60	1	7689	2046	369.1
		3	7986	1911	347.1
		7	8635	1756	296.3
		28	6824	1329	95.1
10.2	0.35	1	2946	533	201.2
		3	2556	312	164.3
		7	2223	56	112.6
		28	1322	19	20.0
	0.40	1	3586	503	264.1
		3	3316	467	167.4
		7	2923	326	153.2
		28	1680	94	19.0
	0.50	1	5102	1097	256.7
		3	4768	1132	200.3
		7	3864	798	194.8
		28	3156	500	40.7
	0.60	1	7568	1659	302.8
		3	7412	1533	286.7
		7	7132	1367	212.2
		28	4019	475	62.0

APPENDIX B

B.1 Values of w_{f+40}, w_{f-40} and w_t

Wollastonite Content [%]	w/c Ratio	Hydration Period [d]	w_{f+40} gwater/gsubstance	w_{f-40} gwater/gsubstance	w_t gwater/gsubstance
0	0.35	1	0.062	0.016	0.073
		3	0.049	0.020	0.064
		7	0.031	0.039	0.055
		28	0.025	0.063	0.072
	0.40	1	0.111	0.007	0.109
		3	0.067	0.021	0.088
		7	0.036	0.041	0.073
		28	0.026	0.042	0.061
	0.50	1	0.165	0.008	0.171
		3	0.073	0.024	0.093
		7	0.049	0.055	0.099
		28	0.037	0.050	0.086
	0.60	1	0.208	0.004	0.210
		3	0.172	0.028	0.191
		7	0.155	0.055	0.191
		28	0.084	0.057	0.131
5.1	0.35	1	0.056	0.020	0.071
		3	0.062	0.019	0.076
		7	0.036	0.032	0.067
		28	0.006	0.039	0.041
	0.40	1	0.069	0.016	0.084
		3	0.066	0.014	0.074
		7	0.043	0.028	0.069
		28	0.010	0.058	0.066
	0.50	1	0.101	0.010	0.109
		3	0.077	0.018	0.100
		7	0.075	0.028	0.102
		28	0.032	0.044	0.070
	0.60	1	0.251	0.006	0.232
		3	0.156	0.015	0.161
		7	0.146	0.027	0.164
		28	0.074	0.044	0.104

(continued on the next page)

(continued from the previous page)

Wollastonite Content [%]	w/c Ratio	Hydration Period [d]	w_{f+40} gwater/gsubstance	w_{f-40} gwater/gsubstance	w_t gwater/gsubstance
8.1	0.35	1	0.150	0.012	0.153
		3	0.080	0.014	0.092
		7	0.035	0.026	0.058
		28	0.020	0.044	0.065
	0.40	1	0.154	0.004	0.156
		3	0.061	0.018	0.076
		7	0.035	0.025	0.056
		28	0.029	0.035	0.061
	0.50	1	0.158	0.006	0.163
		3	0.084	0.019	0.109
		7	0.065	0.030	0.094
		28	0.049	0.059	0.105
	0.60	1	0.238	0.007	0.239
		3	0.150	0.015	0.162
		7	0.083	0.029	0.110
		28	0.062	0.052	0.112
10.2	0.35	1	0.082	0.012	0.091
		3	0.047	0.014	0.060
		7	0.022	0.028	0.047
		28	0.016	0.039	0.053
	0.40	1	0.119	0.006	0.122
		3	0.069	0.012	0.076
		7	0.034	0.019	0.049
		28	0.022	0.023	0.041
	0.50	1	0.189	0.004	0.188
		3	0.092	0.018	0.112
		7	0.061	0.027	0.084
		28	0.026	0.027	0.056
	0.60	1	0.192	0.008	0.198
		3	0.134	0.014	0.144
		7	0.086	0.031	0.113
		28	0.052	0.038	0.086

REFERENCES

Andrews, R.W. (1970), *Wollastonite*, Her Majesty's Stationary Office, London.

ASTM (1992) "C150: Standard Specification for Portland Cement," *Annual Book of ASTM Standards*, Vol. 4, No. 1, Cement; Lime; Gypsum, pp.132-136.

ASTM (1992) "C666: Standard Test Method for Resistance of Concrete to Rapid Freezing and Thawing," *Annual Book of ASTM Standards*, Vol. 4, No. 2, Concrete and Aggregate, pp.310-315.

ASTM (1992) "C671: Standard Test Method for Critical Dilation of Concrete Specimens Subjected to Freezing," *Annual Book of ASTM Standards*, Vol. 4, No. 2, Concrete and Aggregate, pp.324-328.

Azarov, G.M., Maiorova, M.A., Oborina, M.A. and Belyakov, A.V. (1995), "Wollastonite Raw Materials and Their Applications," *Science for Ceramics Production*, Vol. 52, No. 9-10. pp.237-240.

Bager, D. H. and Sellevold E. J. (1986), "Ice Formation in Hardened Cement Paste, Part I – Room Temperature Cured Pastes with Variable Moisture Contents," *Cement and Concrete Research*, Vol. 16, pp.709-720.

Bager, D. H. and Sellevold E. J. (1986), "Ice Formation in Hardened Cement Paste, Part II – Drying and Resaturation on Room Temperature Cured Pastes," *Cement and Concrete Research*, Vol. 16, pp.835-844.

Bager, D. H. and Sellevold E. J. (1987), "Ice Formation in Hardened Cement Paste, Part III – Slow Resaturation of Room Temperature Cured Pastes," *Cement and Concrete Research*, Vol. 17, pp.1-11.

Balaguru, P. N. and Ramakrishnan, V. (1986), "Freeze-Thaw Durability of Fiber Reinforced Concrete," *ACI Journal*, Vol. 83, pp. 374-382.

Balaguru, P. N. and Shah, S. P. (1992), *Fiber-Reinforced Cement Composites*, McGraw-Hill, Inc. New York

Banthia, N., Pigeon, M. and Lachance, L. (1989), "Calorimetric Study of Freezable Water in Cement Paste," *Cement and Concrete Research*, Vol. 19, pp.939-950.

Beaudoin, J.J. (1982), "Fibre-Reinforced Concrete" *IRC Publications, CBD-223., National Research Council Canada*

Beaudoin, J.J. (1990), *Handbook of Fibre-Reinforced Concrete: Principles, Properties, Developments and Applications*, Noyes Publications, New Jersey.

Beaudoin, J.J., Catinaud, S. and Marchand, J. (2001), "Volume Stability of Calcium Hydroxide in Aggressive Solutions," *Cement and Concrete Research*, Vol. 31, pp.149-151.

Beaudoin, J.J. and Feldman, R.F. (1975), "A Study of Mechanical Properties of Autoclaved Calcium Silicate Systems," *Cement and Concrete Research*, Vol. 5, No. 2, pp.103-118.

Beaudoin, J.J., Gu, P. and Low, N. (1995), "Repair and Rehabilitation – A New Market for Wollastonite Micro-Fibres?," *Construction Canada*, Vol. 37, No. 5, pp. 48.

Beaudoin, J.J. and MacInnis, C. (1974), "The Mechanism of Frost Damage in Hardened Cement Paste," *Cement and Concrete Research*, Vol. 4, pp.139-147.

Beddoe, R.E. and Setzer, M.J. (1988), "A Low-Temperature DSC Investigation of Hardened Cement Paste Subjected to Chloride Action," *Cement and Concrete Research*, Vol.18, pp.249-256.

Brantervik, K. and Niklasson, G.A. (1991), "Circuit Models for Cement Based Materials Obtained from Impedance Spectroscopy," *Cement and Concrete Research*, Vol. 21, pp.496-508.

Cai, H. and Liu, X. (1998), "Freeze-Thaw Durability of Concrete: Ice Formation Process in Pores," *Cement and Concrete Research*, Vol. 28, No. 9, pp.1281-1287.

Copeland, L.E. (1956), "Specific Volume of Evaporable Water in Hardened Portland Cement Pastes," *Proceedings: Journal of American Concrete Institute*, Vol. 52, pp.863-874.

Copeland, L.E. and Hayes, J.C. (1956), "Porosity of Hardened Portland Cement Paste," *Proceedings: Journal of American Concrete Institute*, Vol. 52, pp.663.

Cormack, S.L., Macphee, D.E. and Sinclair, D.C. (1998), "An AC Impedance Spectroscopy Study of Hydrated Cement Pastes," *Advances in Cement Research*, 10, No 4, pp. 151-159.

Debenedetti, P. G. (1996), *Metastable Liquids: Concepts and Principles*, Princeton University, New Jersey

Defay, R., Prigogine, I., Bellemans, A. and Everett, D.H. (1966), *Surface Tension and Adsorption*, Wiley, New York.

Feldman, R.F. (1969), "Volume Change and Creep of Concrete" *IRC Publications, CBD-119., National Research Council Canada*

Feldman, R.F. and Beaudoin, J.J. (1991), "Pretreatment of Hardened Hydrated Cement Pastes for Mercury Intrusion Measurements," *Cement and Concrete Research*, Vol. 21, pp.297-308.

Feldman, R.F. and Sereda, P.J. (1969), "A Model for Hydrated Portland Cement Paste as Deduced from Sorption-Length Change and Mechanical Properties," *National Research Council Canada, Research Paper of the Division of Building Research*, No.400.

Feldman, R.F., Sereda, P.J. and Ramachandran, V.S. (1965), "A Study of Length Changes of Compacts of Portland Cement on Exposure to H_2O," *National Research Council Canada, Research Paper of the Division of Building Research*, No.248.

Fletcher, N. H. (1970), *The Chemical Physics of Ice*, Cambridge University Press, London, UK.

Gu, P., Xie, P. and Beaudoin, J.J. (1993), "Computer Simulation of Impedance Behaviour in Hydrating Portland Cement Systems," *Advances in Cement Research*, 5, Vol. 20, pp.171-176.

Gu, P., Xie, P. and Beaudoin, J.J. (1993), "Microstructural Characterization of the Transition Zone in Cement Systems by means of A.C. Impedance Spectroscopy," *Cement and Concrete Research*, Vol. 23, pp.581-591.

Gu, P., Xie, P., Beaudoin, J.J. and Brousseau, R. (1992), "A.C. Impedance Spectroscopy (I): A New Equivalent Circuit Model for Hydrated Portland Cement Paste," *Cement and Concrete Research*, Vol. 22, pp.833-840.

Gu, P., Xie, P., Beaudoin, J.J. and Brousseau, R. (1993), "A.C. Impedance Specroscopy (II): Microstructural Characterization of Hydrating Cement-Silica Fume Systems," *Cement and Concrete Research*, Vol. 23, pp.157-168.

Gu, P., Xie, P., Fu, Y. and Beaudoin, J.J. (1994), "A.C. Impedance Phenomena in Hydrating Cement Systems: Frequency Dispersion Angle and Pore Size Distribution," *Cement and Concrete Research*, Vol. 24, pp.86-88.

Gu, P., Xie, P., Fu, Y. and Beaudoin, J.J. (1994), "A.C. Impedance Phenomena in Hydrating Cement Systems: The Drying-Rewetting Process," *Cement and Concrete Research*, Vol. 24, pp.89-91.

Gu, P., Xu, Z., Xie, P. and Beaudoin, J.J. (1993), "Application of A.C. Impedance Techniques in Studies of Porous Cementitious Materials (I): Influence of Solid Phase and Pore Solution on High Frequency Resistance," *Cement and Concrete Research*, Vol. 23, pp.531-540.

Gu, P., Xu, Z., Xie, P. and Beaudoin, J.J. (1993), "An A.C. Impedance Spectroscopy Study of Micro-Cracking in Cement-Based Composites During Compressive Loading," *Cement and Concrete Research*, Vol. 23, pp.675-682.

Gu, P., Xu, Z., Xie, P., Beaudoin, J.J. and Low, N.M.P. (1993), "Impedance Studies of Wollastonite Micro-fibre-reinforced Cement Paste Systems," *Advances in Cement Research*, 5, No 18, pp. 87-92.

Hannant, D.J. (1978), *Fibre Cements and Fibre Concretes*, John Wiley & Sons, Chichester, U.K.

Hansen, T.C. (1966), "Notes from a Seminar on Structure and Properties of Concrete," *Department of Civil Engineering, Stanford University, Stanford, California*

Helmuth, R.A. (1960), "Capillary Size Restrictions on Ice Formation in Hardened Portland Cement Pastes," 4th International Symposium on Chemistry of Cement, Monograph 43, National Bureau of Standards, Vol. 2, pp.855-869.

Helmuth, R.A. (1961), "Dimensional Changes of Hardened Portland Cement Pastes Caused by Temperature Changes," *Highway and Research Board Proceedings*, Vol. 40, pp.315-336.

Helmuth, R. A. and Danica H. Turk (1966), "Elastic Moduli of Hardened Portland Cement and Tricalcium Silicate Pastes: Effect of Porosity, " *Symposium on Structure of Portland Cement Paste and Concrete*, Highway Research Board, National Research Council, Washington, D. C., pp.135-144.

Higuchi, K., (1968), "Properties of Substance Dispersed in Capillary Pores and its Structure, (I)," *Surface*, Vol. 6, No. 3, p.168. (Published in Japanese)

Hilling, W and Turnbull, D. (1956), "Theory of Crystal Growth in Undercooled Pure Liquids," Journal of Chemical Physics, Vol. 24, pp.914.

Hobbs, P. V. (1974), *Ice Physics*, Oxford University Press, London, UK.

Jacobsen, S., Sellevold, E. J. and Matala, S. (1996), "Frost Durability of High Strength Concrete: Effect of Internal Cracking on Ice Formation," *Cement and Concrete Research*, Vol. 26, No. 6, pp.919-931.

Kanno, H., Speedy, R.J. and Angell, C.A. (1975), "Supercooling of Water to -92°C.," *Science, 198:* pp.881.

Kobayashi, K. (1983), "Development of Fibre Reinforced Concrete in Japan," International Journal of Cement Composites and Lightweight Concrete, Vol. 5, No. 1, pp.27-40.

Koh, Y. and Kamada, E. (1975), "Frost Damage of Concrete and Pore Structure," Ceramics, 10 [10], pp.807. (Published in Japanese)

Lea, F.M. and Desch, C.H. (1935), *The Chemistry of Cement and Concrete*, Edward Arnold & Co., London, England

Litvan, G.G. (1966), "Phase Transitions of Adsorbates: Part 1. Specific Heat and Dimensional Changes of the Porous Glass and Water," *Canadian Journal of Chemistry*, Vol. 44, No. 22, pp.2617.

Litvan, G.G. (1972), "Phase Transitions of Adsorbates: III. Heat Effects and Dimensional Changes in Non-equilibrium Temperature Cycles," *Journal of Colloidal and Interface Science*, Vol. 38, No. 1, pp.75-83.

Litvan, G.G. (1972), "Phase Transitions of Adsorbates: IV. Mechanism of Frost Action in Hardened Cement Paste," *Journal of the American Ceramic Society*, Vol. 55, No. 1, pp.38-42.

Litvan, G.G. (1973), "Phase Transitions of Adsorbates: V. Aqueous Sodium Chloride Solutions Adsorbed of Porous Silica Glass," *Journal of Colloidal and Interface Science*, Vol. 45, No. 1, pp.154-169.

Litvan, G.G. (1975), "Phase Transitions of Adsorbates: VI. Effect of De-icing Agents on the Freezing of Cement Paste," *Journal of American Ceramic Society*, Vol. 58, pp.26-30.

Low, N.M.P. and Beaudoin, J.J., (1992), "Mechanical Properties of High Performance Cement Binders Reinforced with Wollastonite Micro-Fibres," *Cement and Concrete Research*, Vol. 22, pp.981-989.

Low, N.M.P. and Beaudoin, J.J., (1993), "The Effect of Wollastonite Micro-Fibre Aspect Ratio on Reinforcement of Portland Cement-Based Binders," *Cement and Concrete Research*, Vol. 23, pp.1467-1479.

Low, N.M.P. and Beaudoin, J.J., (1994), "The Flexural Toughness and Ductility of Portland Cement-Based Binders Reinforced with Wollastonite Micro-Fibres," *Cement and Concrete Research*, Vol. 24, pp.250-258.

Low, N.M.P. and Beaudoin, J.J., (1994), "Stability of Portland Cement-Based Binders Reinforced with Natural Wollastonite Micro-Fibres," *Cement and Concrete Research*, Vol. 24, pp.874-884.

Katsura, O. and Kameda, E. (1997), "A Mechanism of Frost Damage of Concrete under Supercooling," *Proceedings of the International RILEM Workshop on Frost Resistance of Concrete*, University of Essen, Published by E & FN Spon, London, UK.

McCarter, W. J. and Brousseau, R. (1990), "The A.C. Response of Hardened Cement Paste," *Cement and Concrete Research*, Vol.20, pp.891-900.

McCarter, W. J., Garvin, S. and Bouzid, N. (1988), "Impedance Measurements on Cement Paste," Journal of Materials Science Letters 7, pp.1056-1057.

Mehta, P.K. and Monteiro, P.J. (1993), "*Concrete: Structure, Properties and Materials,*" Prentice Hall, New Jersey.

Neville, A.M. (1995), *Properties of Concrete*, Pearson Education Limited, Harlow, UK.

Perron, S. and Beaudoin, J.J. (2002), "Freezing of Water in Portland Cement Paste – AC Impedance Spectroscopy Study," *Cement and Concrete Composites*, Vol. 24, pp.467-475.

Powers, T.C. (1945), "A Working Hypothesis for Further Studies on Frost Resistance of Concrete," *Portland Cement Association: Research and Development Laboratories, Bulletin 5*, pp. 245-272.

Powers, T.C. (1949), "The Air Requirement of the Frost Resistant Concrete," *Portland Cement Association: Research and Development Laboratories, Bulletin 33*, pp. 28.

Powers, T.C. (1954), "Voids Spacing as a Basis for Producing Air-Entrained Concrete," *Portland Cement Association: Research and Development Laboratories, Bulletin 49*, pp. 741-760.

Powers, T.C. (1956), "Resistance to Weathering-Freezing and Thawing," *Significance of Tests and Properties of Concrete and Concrete Aggregates,*" Special Technical Publications No. 169. Published by ASTM, pp.182-187.

Powers, T.C. (1958), "Physical Structure and Engineering Properties of Concrete," *Portland Cement Association: Research and Development Laboratories, Bulletin 39.*

Powers, T.C. (1958), "Structure and Physical Properties of Hardened Portland Cement Paste," *Journal of the American Ceramic Society,* Vol. 41, No. 1, pp.1-6.

Powers, T.C., Copeland, L. E., Hayes, J.C. and H. M. Mann (1954), "Permeability of Portland Cement Paste," *Portland Cement Association: Research and Development Laboratories, Bulletin 53.*

Powers, T.C., Copeland, L. E. and H. M. Mann (1959), "Capillary Continuity or Discontinuity in Cement Pastes," *Journal of the PCA Research & Development Laboratories, Bulletin 110,* Vol. 1, No. 2, pp.38-48.

Powers, T.C. and Helmuth, R.A. (1953), "Theory of Volume Changes in Hardened Portland Cement Paste during Freezing," *Portland Cement Association. Research and Development Laboratories, Bulletin;* No. 46, pp.285-297.

Ramachandran, V.S., Feldman, R.F. and Beaudoin, J.J. (1981), *Concrete Science,* Heyden & Son Ltd., London, UK.

Rammelt, U. and Reinhard, G. (1990), "On the Applicability of a Constant Phase Element (CPE) to the Estimation of Roughness of Solid Metal Electrodes," *Electrochimica Acta,* 35, pp.1045-1049.

Sellevold, E.J. (1980), "Ice Formation in Hardened Cement Paste," *Proceedings, Durability of Building Materials and Components,* Ottawa, Canada, Published by ASTM, Philadelphia, PA, pp.425-438.

Setzer, M.J. (1997), "Action of Frost and Deicing Chemicals – Basic Phenomena and Testing," *International Workshop in the Resistance of Concrete to Scaling Due to Freezing in the Presence of De-icing Salts,* Sainte-Foy, Quebec, Published by E & FN Spon, London, UK.

Sidebottom, E,W. and Litvan, G.G. (1971), "Phase Transitions of Adsorbates: Part 2. Vapour Pressure and Extension Isotherms of the Porous Glass and Water System Below 0°C," *Transactions of the Faraday Society,* No. 585, Vol. 67, Part 7, pp.2726-2736.

Sliwinska-Bartkowiak, M., Gras, J. and Sikorski, R. (1999), "Phase Transition in Pores: Experimental and Simulation Studies of Melting and Freezing," *American Ceramic Society,* 15, pp.6060-6069.

Soroka, I. (1979), *Portland Cement Paste and Concrete,* Macmillan Press LTD., London, UK.

Tanaka, H. (1997), "Phase Diagram for Supercooled Water and Liquid Transition," *Supercooled liquids : Advances and Novel Applications,* American Chemical Society, Washington, DC, Vol.7, pp. 233-245.

Taylor, H. F. W. (1964), *The Chemistry of Cements,* Academic Press Inc. Ltd., London, UK.

Verbeck, G. (1966), "Pore Structure," *Portland Cement Association. Research and Development Laboratories,* Bulletin 197, pp.211-219.

Virta, R. L. (1999), "Wollastonite," *US Geological Survey Mineral Yearbook*, pp.83.2-83.3.

Weast, R. C. (1968), *Handbook of Chemistry and Physics*, The Chemical Rubber Co. Ohio.

Xie, P. and Beaudoin, J.J. (1992), "Effects of Transition Zone Microstructure on Bond Strength of Aggregate-Portland Cement Paste Interfaces," *Cement and Concrete Research*, Vol. 22, pp. 23-26.

Xie, P., Gu, P., and Beaudoin, J.J. (1993), "Application of Electrical Conductivity Methods in Interfacial Cement Chemistry," *Advances in Cement Research*, 5, Vol. 17, pp. 41-45.

Xie, P., Gu, P., Fu, Y. and Beaudoin, J.J. (1994), "A.C. Impedance Phenomena In Hydrating Cement Systems: Detectivity of the High Frequency Arc," *Cement and Concrete Research*, Vol. 24, pp. 92-94.

Xie, P., Gu, P., Fu, Y. and Beaudoin, J.J. (1994), "A.C. Impedance Phenomena In Hydrating Cement Systems: Origin of the High Frequency Arc," *Cement and Concrete Research*, Vol. 24, No.4, pp. 704-706.

Xie, P., Gu, P., Xu, Z. and Beaudoin, J.J. (1993), "A Rationalized A.C. Impedance Model for Microstructural Characterization of Hydrating Cement Systems," *Cement and Concrete Research*, Vol. 23, pp.359-367.

Xu, Z., Gu, P., Xie, P. and Beaudoin, J.J. (1993), "Application of A.C. Impedance Techniques in Studies of Porous Cementitious Materials (II): Relationship between ACIS Behaviour and the Porous Microstructure," *Cement and Concrete Research*, Vol. 23, pp.853-862.

Xu, Z., Gu, P., Xie, P. and Beaudoin, J.J. (1993), "Application of A.C. Impedance Techniques in Studies of Porous Cementitious Materials (III): ACIS Behaviour of Very Low Porosity Cementitious Systems," *Cement and Concrete Research*, Vol. 23, pp.1007-1015.

Zhou, Y., Cohen, M. D. and Dolch, W. L. (1994), "Effect of External Loads on the Frost-Resistant Properties of Mortar with and without Silica Fume," *ACI Materials Journal*, Vol. 91, pp.595-601.